Aerosol-Cloud Interactions: A New Perspective in Precipitation Enhancement

by

Udaya Bhaskar Gunturu

M.Sc.(Tech.), Sri Venkateswara University, India (1996)
M.Tech., Sri Venkateswara University, India (2000)

Submitted to the Department of Earth, Atmospheric and Planetary Sciences
in partial fulfillment of the requirements for the degree of

Doctor of Philosophy

at the

MASSACHUSETTS INSTITUTE OF TECHNOLOGY

February 2010

Author .....
Department of Earth, Atmospheric and Planetary Sciences
January 29, 2009

Certified by .....
Ronald G Prinn
TEPCO Professor of Atmospheric Chemistry
Thesis Supervisor

Accepted by .....
Maria T. Zuber
E.A. Griswold Professor of Geophysics
Head, Department of Earth, Atmospheric & Planetary Sciences

Aerosol-Cloud Interactions: A New Perspective in Precipitation Enhancement

by

Udaya Bhaskar Gunturu

Submitted to the Department of Earth, Atmospheric and Planetary Sciences
on January 29, 2009, in partial fulfillment of the
requirements for the degree of
Doctor of Philosophy

Abstract

Increased industrialization and human activity modified the atmospheric aerosol composition and size-distribution during the last several decades. This has affected the structure and evolution of clouds, and precipitation from them. The processes and mechanisms by which clouds and precipitation are modified by changes in aerosol composition and size-distribution are very intricate. The objective of this thesis is to improve the understanding of the processes and mechanisms through which the changes in aerosol concentrations impact the evolution of deep convective clouds and precipitation formation. We develop a new coupled model in which a very detailed model of aerosol activation is coupled to a three-dimensional cloud resolving model. This coupled model can accurately represent different kinds of aerosol populations. This coupled model is used to investigate the impact of changing aerosol concentrations on the dynamics, microphysical evolution and precipitation formation in deep convective clouds.

We examine the theories of aerosol activation, and the representation of aerosol activation in cloud models. The limitations of the extant methods of representation of aerosol activation in cloud models are evaluated. Then we descibe the components of the coupled model – Modified Eulerian and Lagrangian Aerosol Model (MELAM) and the Cloud Resolving Model (CRM). The features of these two component models with respect to aersol activation and cloud formation are discussed.

The evaluation of the coupled model by simulation of a deep convertive event observed during the INDian Ocean EXperiment (INDOEX) by statistcal comparison of observed and simulated cloud fields shows that the coupled model can simulate deep convective events reasonably well.

We present a study of the senstivity of the model to initial thermodynamic conditions (CAPE). Different initial thermodynamic conditons sampled during the INDOEX are used to initialize the coupled model and, the structure and evolution of the deep convective event are discussed. The study sheds new light on the respone of deep convection to CAPE. It is found that when the atmosphere has moderate CAPE, the precipitation forming processes are very active and when the CAPE is

low or high, they are comparatively less efficient.

As the most important part of our study, we examine the response of deep convection to changing initial aerosol concentration. Different aerosol concentrations from those representing pristine to polluted atmospheres are considered. We look at the buoyancy of the cloud and the microphysical evolution. It is found that the dynamics and microphysics are tightly coupled and we infer that to understand aerosol-cloud interactions in deep convective clouds, both – dynamics and microphysics – and their interaction have to be taken into consideration.

Our results show that the response of a deep convective cloud to changing aerosol concentration is very different from the much well understood reponse of shallow clouds or small cumulus clouds. In general, increase in aerosol concentratin is seen to invigorate convection and lead to greater condensate. Although the cloud droplet size decreases, collision-coalescence is not completely inefficient. The precipitation in high aerosol regime is seen to occure in short spells of intense rain.

A very interesting anomalous response of deep convection to initial aerosol concentration is observed at intermediate aerosol concentrations. The cloud lifetime, and precipitation are seen to increase in this regime. A possible mechanism to explain this anomalous behavior is proposed and the available circumstantial support for the mechanism from extant observations is presented. It is proposed that the efficient collection of rain and cloud droplets by ice and graupel particles in the middle troposphere is primarily responsible for this increased cloud lifetime and precipitation.

Thesis Supervisor: Ronald G Prinn
Title: TEPCO Professor of Atmospheric Chemistry

Acknowledgments

The first person who comes to my mind when I complete this thesis is J.R. Kulkarni, Scientist, Indian Institute of Tropical Meteorology, Pune. He motivated and initiated me into Atmospheric Sciences. I constantly drew encouragement from him.

I am extremely grateful to Ron Prinn, my advisor, who has been a great support for me during all these years at MIT, particularly during my hard times. Meetings with him were full of fruitful discussions, and his suggestions always helped me in my research. I particularly appreciate the freedom Ron has given me in choosing my topic for thesis. I am deeply indebted to the other members of my thesis committee – Alan Plumb, Andrew Heymsfield and Chien Wang. Most of the skills I learnt in numerical modeling were from working with Chien. I greatly benefitted from the discussions with him time to time. Conversations with Andrew Heymsfield were sources of great insights into cloud microphysics. They really helped me analyze and understand the processes and mechanisms in cloud microphysics. The discussions I had with Alan Plumb during the committee meetings were very helpful. There is no doubt that without the great support of this great committee, this work would have not been possible.

I fondly cherish every moment I spent with Ian Fenty. He has been with me through my tough times and he is a great gift I got in Cambridge. My office mates at different times – Elke, Jason, Eunjee, Matt Rigby and Anita – have been extremely cooperative.

Mary had helped to a great extent in settling in Cambridge during the initial months. At later times too, she always had great concern and I acknowledge her help with a deep sense of gratitude. I express my thankfulness to Carol. She has been extremely helpful in all the administrative affairs.

My life away from home has been made lighter by Brahma, Deepika, Rajamohan and Raghavendra.

Lastly, I thank everyone at MIT for being of great help during all my years at MIT.

Dedicated to

My mother

My father

My brother, Sagar

J.R. Kulkarni

Ian Fenty

KrishnaMurthy mamayya

Contents

List of Figures

List of Tables

Chapter 1

Introduction

The continuous circulation of water between land, ocean and atmosphere is a chain of physical processes that sustains life on earth. The hydrological cycle is very complex and dynamic. The transfer of water from ocean to the atmosphere as clouds and from the atmosphere to the land surface as precipitation involves a wide range of physical and chemical processes which are sensitive to each other. Precipitation is the central mechanism for transport of water from the atmosphere to the Earth's surface. It also acts as a key link between the weather processes at different timescales and the response of the hydrological changes to weather processes. Precipitation patterns and changes in them have a very profound impact on the quality of life on the earth. Any change in the precipitation pattern can readily turn an agrarian economy from abundance to utter poverty. History is witness to the fact that many civilizations perished due to changes in precipitation patterns.

Although precipitation has direct consequences for life on earth in terms of availability of water, perturbations in temperature have received greater attention as a metric for global climate change. Precipitation varies in different time and space scales more than temperature does. It is affected by the atmospheric motions primarily. But the advances in research for the last five decades have shown beyond doubt that it is also affected by the microphysical processes associated with the atmospheric aerosols. Aerosols are the particles in the atmosphere which act as embryos for cloud droplets and so have a direct impact on cloud microphysics and hence precipitation.

Aerosol Effects on Clouds The United Nations Framework Convention on Climate Change (UNFCC) identified aerosols, cloud microphysical properties and precipitation as fundamental climate variables. The impacts of aerosol particles on cloud microphysical properties like the cloud droplet sizes and hence the radiation scattering properties of cloud droplet, have been confirmed [*Houghton et al.*, 2001].

Aerosols impact the reflective properties of clouds indirectly through their effect on cloud drop formation. The first indirect effect of aerosols on clouds' albedo is due to the reduction in size of cloud droplets with increasing aerosol concentrations. The second indirect effect concerns the suppression of precipitation due to the collision-coalescence process of rain formation becoming inefficient because of the smaller droplet size. The result is that the cloud becomes colloidally stable, lives longer and reflects the incoming solar radiation back into space for longer times. Because these climate effects have a direct bearing on the number concentration of cloud droplets, the central question in almost all these aerosol-cloud-radiation studies was – 'from a given population of aerosols, how many will turn into cloud droplets?'.

Previous discussion about the crucial role precipitation plays in our lives and the direct impact aerosols have on the microphysics of clouds let one surmise the sensitivity of precipitation to aerosols. Aerosol chemical composition, size distribution and number concentration have been observed to modulate the formation, structure of clouds and precipitation formation. *Hobbs et al.* [1970] observed an increase in precipitation up to 30% from warm clouds impacted by emissions from paper mills. Studies using MODIS and TRMM satellite data showed that clouds that clouds that were impacted by forest fires in the Amazon region, grew taller and increases in precipitation were also reported. Most of the observations and modeling studies of aerosol-cloud-precipitation interactions were in the context of stratocumulus and trade cumulus clouds for many years as the suppression of drizzle was seen as a signature of the indirect radiative effects on climate.

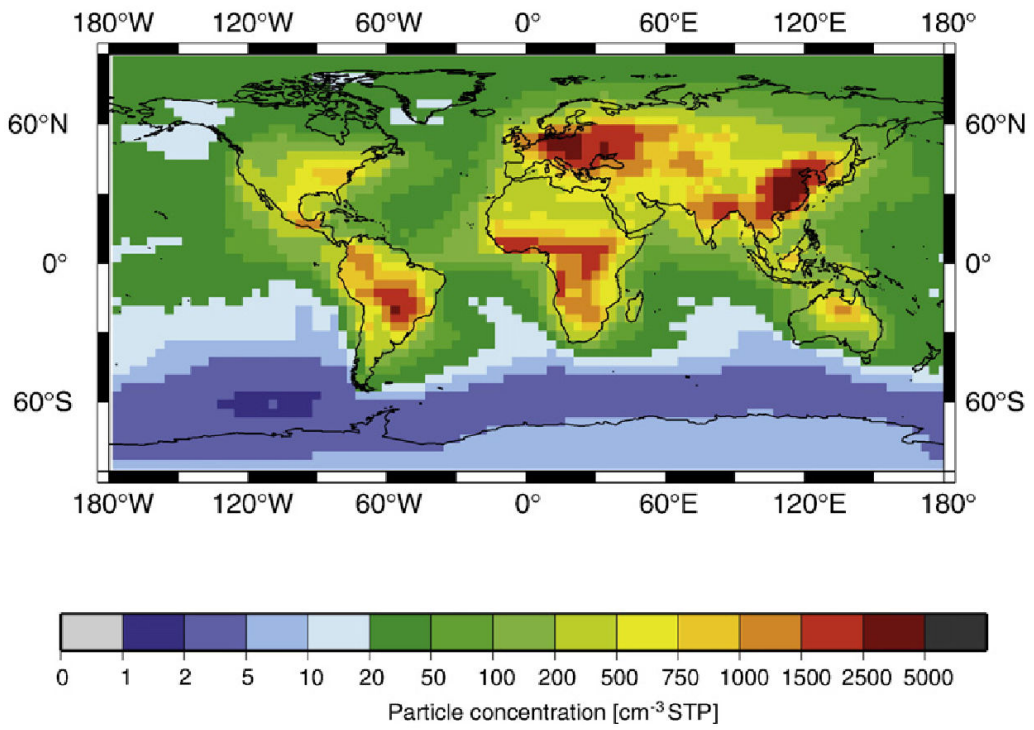

Figure 1-1: Climatological annual mean accumulation mode aerosol particle concentration from a 10-year integration. [*Lauer and Hendricks*, 2006]

1.1 Motivation for This Study

Due to increased human activity, the global aerosol content has been increasing [*Houghton et al.*, 2001]. Figure 1-1 shows the climatological annual means of accumulation mode aerosol particles [*Lauer and Hendricks*, 2006], which are potential cloud droplet embryos, from a 10-year integration. This figure shows that the concentrations of these particles are large in the continental atmospheres and most importantly in the tropical continental belt. Incidentally, high thick clouds or deep convective clouds are predominant in the tropical atmospheres. *Schumacher and Houze* [2003] have reported that 60% of the precipitation in the tropical region is convective in nature. Because this geographical belt is home to a large fraction of the world's population, any changes in precipitation patterns from these clouds, for instance due to aerosol effects, have serious ramifications. Thus, the study of sensitivity of precipitation from deep convective clouds to aerosols takes in the greatest importance.

1.2 Obstacles in Understanding

The crucial role of aerosols in modulating cloud macro-structure, microphysics and precipitation was identified as far back as fifty years. *Gunn and Phillips* [1957], *Squires* [1958], *Twomey and Warner* [1967] and *Warner and Twomey* [1967] pointed out that increased concentrations of cloud condensation nuclei from anthropogenic sources like industries and burning of sugarcane increased cloud droplet number concentration leading to enhanced colloidal stability of the cloud. Thus the precipitation efficiency (fraction of condensed water that falls to ground as rain [*Emanuel*, 1994]) of the cloud was reduced. It is well-established that cloud droplet concentration increases with CCN concentration. But the exact functional relationship remains elusive.

Twomey and Wojciechowski [1969] measured the CCN concentrations as a function of supersaturations in the atmosphere in a very comprehensive field campaign and parametrized the CCN concentrations with a simple power law:

$$N_{CCN} = N_0 s^k \tag{1.1}$$

where N_0 and k are parameters characteristic of the atmosphere in which the measurement is conducted. N_{CCN} is the activated CCN concentration at the supersaturation s.

This simple parametrization allowed simple analytic calculation of the number of activated particles and hence fueled considerable research in cloud physics using numerical models. But this parametrization does not take the chemical composition and size distribution of the aerosols into account. Thus, as our understanding of aerosol chemical and physical processes advanced, this parametrization stood in our way of advancing our understanding of the physical and chemical processes through which aerosols and clouds interact and consequently as to how precipitation is affected [*Houghton et al.*, 2001]. Further, the IPCC report urges the researchers to adopt activation (CCN becoming cloud droplets) methods that take the physico-chemical properties into account while computing this most important link in aerosol-cloud interactions.

Some researchers used the more physical approach based on Kohler theory of the behavior of a solution droplet in equilibrium with the ambient water vapor field [*Ekman et al.*, 2004a]. But *Nenes et al.* [2001] reported that this approach overestimated the cloud droplet concentration due to kinetic limitations of mass transfer between aerosols and ambient atmosphere as the aerosols grow by condensing water vapor from the ambient atmosphere.

Several researchers urged that the representation of cloud droplet formation from aerosols (called activation of aerosols) should be based on time-dependent calculation of mass transfer between aerosols and the ambient atmosphere. To achieve this goal, the aerosol activation model of *Steele* [2004], Modified Eulerian-Lagrangian Aerosol Model (MELAM), has been coupled with the cloud resolving model of *Wang and Chang* [1993]. MELAM computes the mass transfer to and from aerosols by solving a time-dependent diffusion equation while taking into account the chemical composition and size distribution of the aerosols. This coupled model is described in chapter 3.

Dynamics & Microphysics Most of the early researchers looked at the aerosol-cloud interaction as a problem involving only the microphysics of the cloud and the effects of aerosols on the microphysics.

But establishment of a causal relationship necessarily requires that other factors such as the kind of atmosphere in which the cloud evolves – maritime or continental – and the vertical profiles of moisture and static stability of the atmosphere be taken into account. Further, the response of cloud microphysics to aerosol changes during formation of the cloud impacts the dynamical structure of the cloud which in turn affects the microphysics. Thus, the study should take into account interplay between the dynamical fields in the cloud and microphysical evolution [*Khain et al.*, 2004, 2005].

1.3 Goals

Towards a study of aerosol-cloud-precipitation interactions in the context of deep convective clouds, the following are the objectives of this thesis.

1. Development of a coupled model in which the aerosol activation is computed taking into account the full aqueous chemistry and size distribution of the aerosols. Towards this goal, MELAM has been coupled to the cloud resolving model of *Wang and Chang* [1993] which computes the dynamical and microphysical evolution of the cloud.

2. Validation of this coupled model by simulating a deep convective event observed during the INDian Ocean EXperiment (INDOEX).

3. Studying the sensitivity of deep convection to initial thermodynamic condition. This study also helps in understanding the sensitivity of the coupled model to initial thermodynamic condition.

4. Studying the effect of increased aerosol concentrations on deep convection, particularly the interplay of dynamics and microphysics. To facilitate comparison of results with similar experiments by earlier researchers, this study looks at the response of a deep convective cloud to extreme aerosol concentrations – a low concentration representing pristine conditions and a high concentration representing polluted atmosphere.

5. As the figure 1-1 shows, the aerosol concentrations in the tropical atmosphere are typically between $100\,/\mathrm{cm}^3$ and $2000\,/\mathrm{cm}^3$. So, a study of the response of deep convection to this range of aerosol concentrations may shed new light on the physical processes in aerosol-deep convection interactions and precipitation formation in these clouds.

1.4 Outline of the Thesis

Chapter 2 of this thesis discusses aerosol activation in terms of Kohler equilibrium theory and the implications of the equilibrium assumption, the concept of cloud condensation nuclei, representation of aerosol activation in cloud models and their limitations, all of which point to the need for a new model. The chapter further discusses the known theory of precipitation formation processes to set the stage for the discussion in the subsequent chapters. The chapter reviews some of the most important observational and numerical modeling studies of aerosol-deep convection-precipitation interactions and the wealth of knowledge they have generated for furtherance of the cause.

Chapter 3 describes the aerosol activation model (MELAM), the cloud resolving model and the development of a coupled model.

Chapter 4 describes the data collection during INDOEX. This data is used to evaluate the model and also as initial conditions in the subsequent experiments.

Chapter 5 describes the simulation of a deep convective cloud observed with an aircraft during INDOEX. The observed mean properties of the cloud are summarized. The comparison of model results simulated cloud fields are compared with the observations at different vertical levels. The results of the statistical comparison are discussed.

Chapter 6 describes the sensitivity of the model to initial thermodynamic condition. This experiment can also be seen as the response of a deep convective cloud to the initial convective available potential energy (CAPE). The evolution of dynamical and microphysical fields are discussed as is their role in precipitation formation.

Chapter 7 describes the study of the effect of increased aerosol concentrations. This study is similar to most of the previous numerical studies in which a low and a high aerosol concentrations are used. The study looks at the evolution and interplay of buoyancy and precipitation.

Chapter 8 is about the response of deep convection and precipitation from deep convection to a range of aerosol concentrations. This study reveals that at the inter-

mediate concentrations, a new precipitation enhancement is observed. The mechanism of this enhancement is discussed using ice and liquid drop microphysics.

Chapter 9 concludes with a summary of these experiments and the most important findings with future perspectives to validate some of the findings of this work and advance the understanding of changes in precipitation formation brought about by aerosols.

Chapter 2

Aerosol-Cloud Interactions

2.1 Introduction

Aerosols that can absorb or adsorb water molecules from the ambient atmosphere are important for cloud formation. Since these aerosol particles act as embryos for the formation of cloud droplets, the number of cloud droplets that form is a function of the number of aerosols with affinity for water present in the atmosphere. Because the water-affinity of these aerosols depends on their chemical composition, the chemical composition of the aerosols becomes another important factor in cloud formation.

Further, the sizes of the cloud droplets that form also depend on the sizes of the aerosols. If the drops that form are smaller, precipitation formation via collision-coalescence is retarded, and the long living clouds reflect the incoming solar radiation longer. *Twomey* [1977] argued that increases in aerosol concentrations result in smaller cloud droplets that enhance the colloidal stability of the clouds leading to longer living clouds. Thus increased aerosol concentrations lead to cooling the atmosphere as less solar radiation reaches the ground. This is the aerosol indirect effect. But this effect is more relevant to the stratocumulus clouds which have longer life times, low updraft speeds and water contents.

The effects of aerosols on deep convective clouds may be very different from those expected from the above argument. Deep convective clouds have large water vapor concentrations, updraft speeds and also have shorter life times. Since this work is

about the impacts of aerosols on precipitation forming processes in deep convective clouds, and because deep convection has richer dynamics than drizzling clouds, the response of dynamics is also very important.

2.2 Aerosol Activation

Cloud droplets can not form in the natural atmosphere by spontaneous collision of water molecules and subsequent sticking together as the supersaturations required for this homogeneous nucleation of cloud droplets are several hundreds of percent which do not occur in the natural atmosphere. Rather, the cloud droplets form by heterogeneous nucleation in which the hydrophilic aerosols act as embryos.

Kohler described the theory of the behaviour of small solution droplets in a water vapor field. These small solution droplets are water drops in which a chemical salt like ammonium sulphate or sodium chloride is dissolved. The subsection 2.2.1 discusses the equilibrium behavior of pure water drops in a water vapor field and the subsection 2.2.2 discusses that of solution droplets in a water vapor field.

2.2.1 Kelvin Equation

Kelvin considered the phase equilibrium of pure water drop in a field of water vapor. This system consists of two components – air and water. So, this system has three degrees of freedom according to the phase rule. If the temperature and the total air pressure are held constant, the variations of water vapor pressure with the radius of the drop is expressed by [*Pruppacher and Klett*, 1998]

$$\frac{-2V_{w,0}}{T}\, d\left(\frac{\sigma_{w/a}}{a}\right) + R\, d\, ln a_v = 0 \tag{2.1}$$

where $V_{w,0}$ is the water vapor pressure in the ambient atmosphere, T is the temperature, $\sigma_{w/a}$ is the surface tension of water with respect to air, a is the radius of the water drop, R is the universal gas constant and a_v is the water activity of the drop.

If the air is assumed to behave as an ideal gas, then $a_v = \frac{e_{a,w}}{p}$ where $e_{a,w}$ is the

saturated vapor pressure of water vapor over the droplet surface and p is the total pressure.

With these assumptions and ignoring the compressibility of water, the above equation can be integrated to

$$\frac{e_{a,w}}{e_{sat,w}} = exp\left(\frac{2M_w\,\sigma_{w/a}}{RT\,\rho_w a}\right) \tag{2.2}$$

This is called the Kelvin equation. $e_{sat,w}$ is the equilibrium water vapor pressure over a bulk water surface, M_w is the molecular weight of water, and ρ_w is the density of water.It shows that the saturation vapor pressure over the surface of a water drop is larger than that over a flat surface, and the increase of saturation vapor pressure increases with decreasing radius of the drop. Since equilibrium is assumed, the saturation vapor pressure over the drop is equal to the partial pressure of water vapor in the atmosphere.

2.2.2 Equilibrium of a Solution Drop

Since the cloud droplets grow on soluble chemical particles, they are not pure water drops as assumed above, but are aqueous solution drops in which a soluble salt of mass equivalent to the dry aerosol particle is dissolved.

Two key assumptions in the investigation of this equilibrium behavior are:

1. The dissolved salt does not have vapor pressure of its own.

2. The mass of the salt in the drop remains constant.

The first assumption is usually true for all salts in the atmosphere as they are non-volatile. The second assumption is not strictly always valid. During the initial stages of cloud formation, the mass of the solute remains fairly constant but after the drops are formed, there are several mechanisms in which the amount of solute is changed. Dissolution of atmospheric gases into the drop and different scavenging mechanisms are examples of these processes.

This system has three components – air, water and the salt. So, according to the phase rule, it has four degrees of freedom. But assumption 2 above reduces one degree of freedom and hence, the system has three degrees of freedom. Further, the relation between the molar volumes provides the relation [*Pruppacher and Klett*, 1998]:

$$\frac{1}{x_w} = 1 + \frac{n_s}{n_w} = 1 + \frac{n_s v_w}{\frac{4\pi a^3}{3} - n_s v_s} \tag{2.3}$$

where v_s and v_w are the molar volumes of the salt and water; n_s and n_w are the number of moles of the salt and water in the drop and x_w is the mole fraction of water in the drop.

Now, the dependence of equilibrium vapor pressure $e_{a,w}$ on radius of the drop is given by [*Pruppacher and Klett*, 1998]

$$\frac{-2\, v_{w,0}}{RT}\; d\left(\frac{\sigma_{s/a}}{a}\right) + d\, ln e_{a,w} - d\, ln a_w = 0 \tag{2.4}$$

where $v_{w,0}$ is the partial molar volume of water in the droplet. Integrating this equation from a, $e_{a,w}$, a_w to $a \rightarrow \infty$, $e_{a,w} = e_{sat,w}$, $a_w = 1$ gives

$$\frac{e_{a,w}}{e_{sat,w}} = a_w\, exp\left(\frac{2M_w\, \sigma_{s/a}}{RT\rho_w a}\right) \tag{2.5}$$

where a_w = water activity of the drop.

For a pure drop, $a_w = 1$ and the equation reduces to the Kelvin law. For a flat surface, $a \rightarrow \infty$ and so,

$$\frac{e_{w,a}}{e_{sat,w}} = a_w \tag{2.6}$$

which is Rauolt's law which states that the equilibrium vapor pressure of any component in an ideal solution is proportional to its mole fraction in the solution.

Robinson and Stokes [1970] consider the mean activity coefficient $\gamma\pm$ and molality m and express the water activity of the drop a_w as

$$a_w = exp\left(\frac{-\nu\, \Phi_s m_s (M_w/M_s)}{(4\pi a^3/3)\rho_s'' - m_s}\right) \tag{2.7}$$

where ν is the total number of ions a salt dissociates into in the solution, Φ_s = molal osmotic coefficient of the salt in the solution, M_w and M_s are the molecular weights of water and the salt, m_w and m_s are the masses of water and salt in the drop, and a is the radius of the drop.

For very dilute solutions, equation becomes

$$lnS_{v,w} = \frac{A}{a} - \frac{B}{a^3} \tag{2.8}$$

where $A = \dfrac{2M_w\sigma_{w/a}}{RT\rho_w}$ and $B = \dfrac{3\nu m_s M_w}{4\pi M_w \rho_w}$.

If $\dfrac{e_{a,w}}{e_{sat,w}} \approx 1$, that is, near saturation,

$$S_{v,w} = 1 + \frac{A}{a} - \frac{B}{a^3} \tag{2.9}$$

This is the famous Kohler equation and it describes the equilibrium behavior of a solution droplet in a water vapor field.

The important assumptions that went into this description are:

1. The solution drop and the ambient water vapor field are in equilibrium.
2. The dissolved salt has no partial vapor pressure.
3. The mass of the salt remains constant in the drop.
4. The drop solution is very dilute, i.e., $m_s \ll m_w$.

Figure 2-1 shows the equilibrium behaviour described by the equation 2.9. The radii at which equilibrium vapor pressure is the maximum is called the critical radius and the corresponding vapor pressure is called the critical equilibrium vapor pressure.

The following are some of the important implications of the Kohler's theory described above.

1. To the left of the critical radius, the solution drop is in stable equilibrium with the ambient water vapor field. That is, if a small amount of water is added to the drop, it will attain an equilibrium vapor pressure larger than the vapor

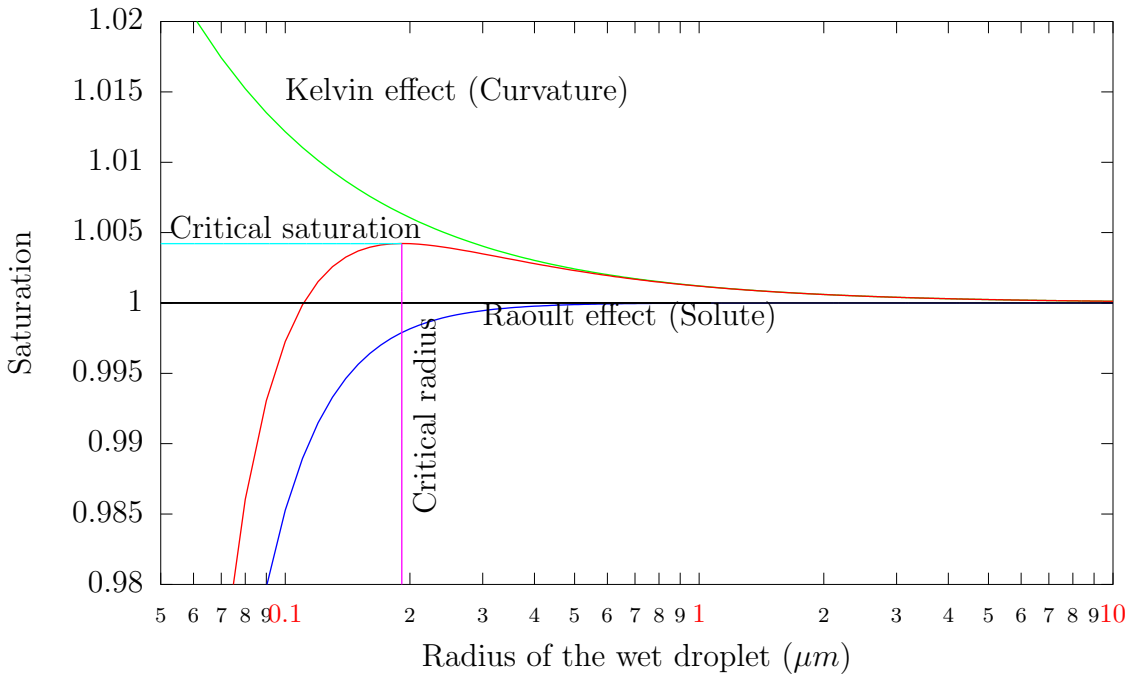

Figure 2-1: Equilibrium supersaturation over the surface of a droplet. The green curve is for a pure water droplet, the blue curve for a bulk solution surface and the red one for a solution droplet. The peak of the equilibrium curve shows the critical point.

pressure of the ambient atmosphere. So, the drop evaporates to return to its equilibrium value. Similarly, the drop returns to its equilibrium vapor pressure also when there is a small evaporation.

2. To the right of the critical radius, the solution drop is in unstable equilibrium. If it grew slightly, the equilibrium vapor pressure would be lower than the ambient. Thus, the ambient supersaturation is greater than the vapor pressure on the drop surface. That is, the growth is only limited by the supply of water vapor. Similarly, if the drop evaporates slightly, it will have a surface vapor pressure greater than the ambient vapor pressure and the drop evaporates further. As more water evaporates, the difference between the vapor pressure over the drop and that in the ambient atmosphere increases until it reaches the stable equilibrium point over on the Kohler curve.

   If the ambient vapor pressure exceeds the critical value on the Kohler curve,

there would be no feasible equilibrium size and the particle grows indefinitely [*Seinfeld and Pandis*, 1998].

A solution drop that has transitioned from the stable equilibrium on the left of the critical radius to the unstable equilibrium on the right is said to be activated and the drop grows indefinitely only limited by the supply of water vapor.

3. The Kohler equilibrium curves are different for droplets of different dry radius and different composition. Droplets with different compositions have different supersaturations and so, will be in the different regimes of equilibrium. This process of activation is central to the formation of cloud droplets as all of the subsequent processes in cloud evolution and precipitation have a direct bearing on the size and number of cloud droplets. This is the most important link in aerosol-cloud interactions. A subsequent section will discuss the representation of this process in models. The assumptions of Kohler theory would also be discussed with regard to their efficacy in describing aerosol activation.

2.2.3 The Concept of CCN

If we consider a population of aerosols in the atmosphere, a fraction of them which attain their critical radii in the ambient vapor field activate to become cloud droplets. This subset of aerosols that can potentially activate in a cloud are called cloud condensation nuclei. The entry for cloud condensation nuclei in the Glossary of Meteorology reads:

> **Cloud condensation nuclei** – (Abbreviated CCN) Hygroscopic aerosol particles that can serve as nuclei of atmospheric cloud droplets on which water condenses (activates) at supersaturations typical of atmospheric cloud formation (fraction of one to a few percent, depending on cloud type). Condensation of CCN need to be given in terms of a supersaturation spectrum covering the range of interest or at a specified supersaturation value

Twomey and Wojciechowski [1969] measured the CCN concentrations in various

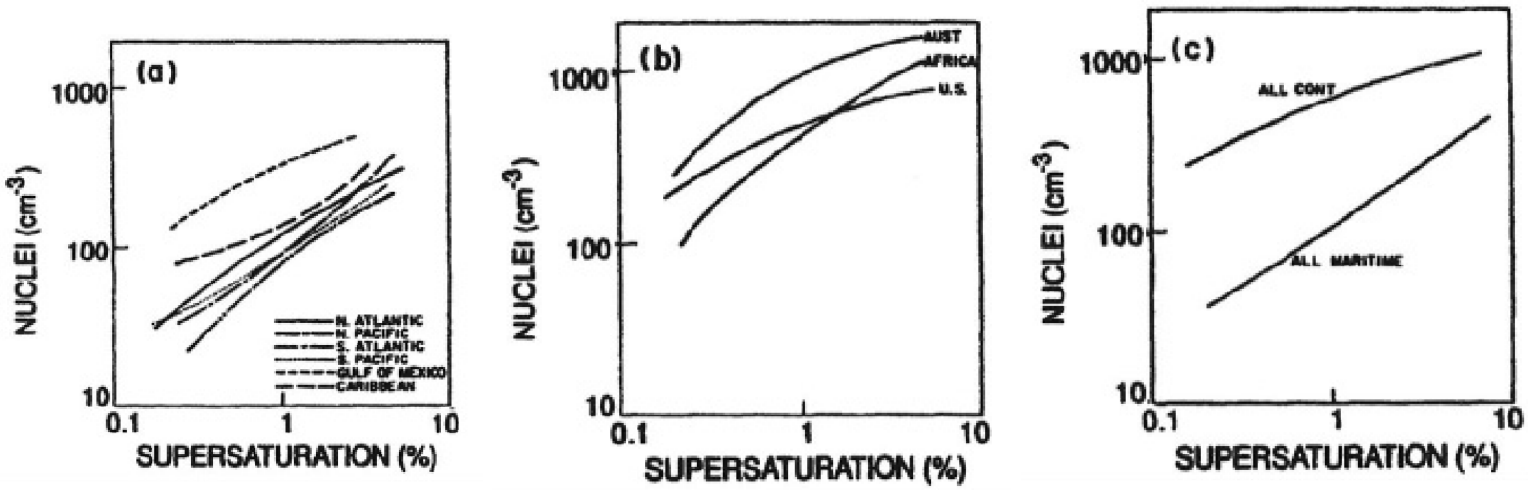

Figure 2-2: Global median CCN concentrations as a function of critical supersaturation measured by Twomey. (a). Marine (b). Continental (c). Global *Pruppacher and Klett* [1998]

atmospheres around the world in a very comprehensive study. Figure 2-2 shows the median world-wide concentrations in the marine and continental atmospheres and everywhere, as functions of supersaturation. From the figures, the following inferences can be drawn:

1. As supersaturation increases, the number of CCN increases.

2. The continental atmospheres have higher CCN numbers.

3. At supersaturations below 10%, the marine atmospheres have a few tens to a few hundred CCN per cubic centimeter whereas the continental atmosphere has a few hundred to a few thousand CCN per cubic centimeter.

Using these observations, Twomey parameterized the CCN concentrations as a function of the ambient supersaturation as :

$$N_{CCN} = Cs^k \tag{2.10}$$

where s is the supersaturation (%) and C and k are constants characteristic of the ambient atmosphere. This simple parameterization was immediately attractive for the whole cloud physics community. For modeling cloud formation, this idea of a distinct subset of the complex aerosol spectrum was very appealing. In fact, the concept served the cause of research in cloud physics very well. Much of the advancement in cloud physics during the last four decades is owing to this concept.

But as the understanding of aerosol physics and chemistry advanced and as the computational power increased many folds, the oversimplifications inherent in the concept of CCN became difficult to justify with the advances in the different aerosol processes [*Houghton et al.*, 2001]. The two most important of these oversimplifications that are mentioned boxed in the IPCC 2001 report are:

1. The measurements of CCN are strictly dependent on the thermodynamic setting forced upon the aerosol sample let in to the instrument. Those settings do not resemble the conditions in a cloud. There are many physical and chemical

processes that make the actual subset of the total aerosol population in a cloud [*Kulmala et al.*, 1996; *Seinfeld*, 1999].

2. The concentration of CCN at a particular supersaturation does not translate into an equivalent concentration of cloud droplets. Even the generally used statement that increase in aerosol concentration leads to increased cloud droplet concentration is not necessarily true. For instance, in marine atmospheres, there is a competition between ammonium sulphate aerosols and sea salt particles [*O'Dowd et al.*, 1999]. When the sulphate concentration is low, more sea salt aerosols deplete water faster and inhibit the activation of sulphate aerosols whereas when the sulphate aerosols are large in concentration, the sea salt particles add to the activated particles.

In view of the limitations of the idea of CCN and the uncertainties in their measurements, IPCC 2001 recommends the 'Condensational growth of size resolved atmospheric particles'. This approach is discussed in a later chapter in greater detail.

2.3 Representation of Aerosol activation in Numerical Models

Lohmann and Feichter [2005] describe the aerosol-cloud droplet closure or the relationship between aerosol particles and cloud droplets as the 'weakest point in the estimates of the aerosol indirect effects'.

Most of the cloud models use Twomey's formulation as described earlier because of the simple representation.

Another approach used to calculate CCN activation employed in some models is based on the theoretical framework developed by *Twomey* [1959]. In this approach, the maximum supersaturation $(S_{v,w})_{max}$ is computed as a function of vertical velocity W:

$$(S_{v,w})_{max} \leq C^{1/(k+2)} \left[\frac{6.9 \times 10^{-2} W^{3/2}}{k\beta\left(\frac{k}{2}, \frac{3}{2}\right)} \right]^{1/(k+2)} \tag{2.11}$$

where C and k are parameters. In this expression, W is in cm/sec, C is in cm^{-3}, and $(S_{v.w})_{max}$ is in percent. β is the beta function. The maximum activeable CCN concentration, N_{max}, at that updraft is given by

$$N_{max} \equiv C^{2/(k+2)} \left[\frac{6.9 \times 10^{-2} W^{3/2}}{k\beta\left(\frac{k}{2}, \frac{3}{2}\right)} \right]^{2/(k+2)} \tag{2.12}$$

Although this is an improvement over Twomey's power law, this parameterization also does not take the chemical composition and size distribution of aerosols into consideration.

The one notable exception is the use of Kohler formulation by *Ekman et al.* [2004a] in which she considers the chemical composition and size of the aerosol particles to activate using the Kohler formulation. Kohler formulation is advantageous and is efficient as it takes into account the chemical composition and size of the aerosol particles.

A parameterization had been developed by *Abdul-Razzak and Ghan* [2000] based on Kohler theory that can describe cloud droplet formation for multi-modal aerosol populations.

It is generally acknowledged that there are issues with Kohler theory. Revisiting the assumptions of Kohler theory, one of the assumptions is that the solution drops are in equilibrium with the ambient water vapor field. It implies that the mass transfer from the aerosols to the ambient atmosphere and nice-versa are instantaneous. But the assumption of instantaneous equilibration of all the aerosol particles to any changes in supersaturation leads to a problem with the large aerosol particles [*Chuang et al.*, 1997]. The water vapor absorbed by those large particles when they activate may be larger than the total water vapor available at that point in the atmosphere. But as *Nenes et al.* [2001] point out that, it does not have an impact on the number of aerosols activated.

But the assumption of equilibrium leads to a wrong estimation of the number of activated particles due to mass transfer limitations. *Chuang et al.* [1997] compared the time scale of particle growth under assumption of equilibrium and that for condensational growth and inferred that the aerosol particles that have their critical supersaturations less than a threshold value do not have sufficient time to grow to their critical size and hence can not activate. But these particles would be deemed activated under equilibrium assumption. Thus the equilibrium models consistently overestimate the number of cloud droplets.

Nenes et al. [2001] found that there are kinetic limitation mechanisms due to which particles smaller than the activated one are produced under the assumption of equilibrium. The following lines discuss these kinetic mechanisms with reference to the figure 2-3. The figure shows the typical cloud parcel and droplet equilibrium supersaturation profiles as a function of cloud depth as predicted by adiabatic parcel theory. The different equilibrium growth curves are for aerosol particles with different amount of solute dissolved in them. As the parcel supersaturation evolves (black curve), the equilibrium supersaturations of the different aerosol particles evolve too. According to Kohler theory, all the particles whose critical supersaturations are less than the maximum the parcel has will activate immediately.

But according to condensational growth theory, the time for which the particle encounters a supersaturation greater than its critical supersaturation is very important too. The aerosol must encounter such supersaturations long enough for the aerosol to grow to its critical size.

The four different scenarios shown in the illustration are discussed below.

1. The yellow curve represents an aerosol particle which activates at parcel supersaturation, s_{c3}.

   After activation, its equilibrium, its equilibrium supersaturation decreases and always remains less than the parcel supersaturation. Thus, this particle always remains activated.

2. The blue curve represents a large aerosol particle, that is, it has a large dry

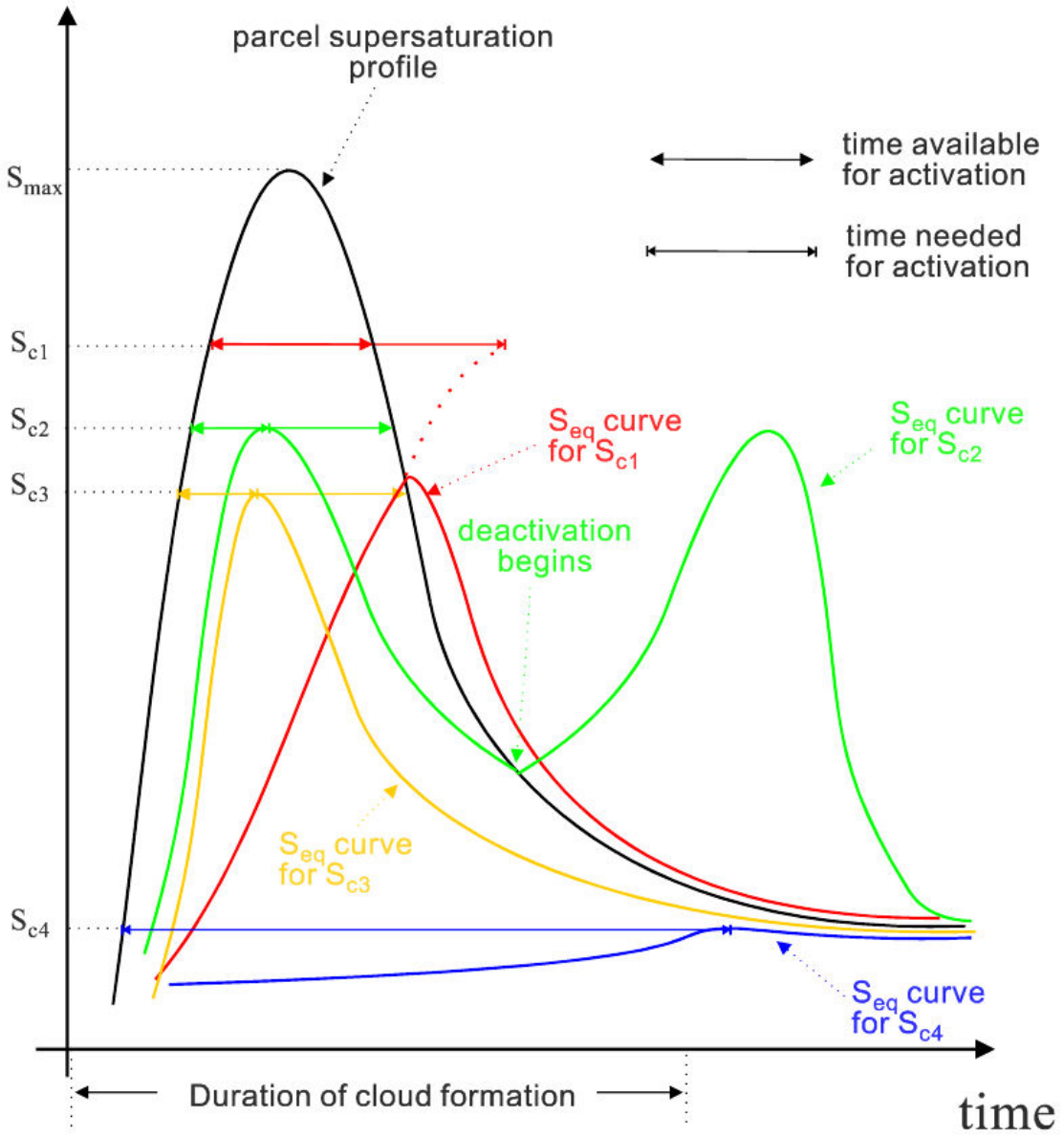

Figure 2-3: Schematic to illustrate kinetic limitations on mass transfer to aerosols. The curves represent supersaturations over the drop surface as the cloud parcel rises and hence as the parcel supersaturation evolves. The curves represent a particle with no kinetic limitations (yellow), inertial mechanism (blue), evaporation mechanism (red) and deactivation mechanism (green)
Nenes et al. [2001]

diameter. Thus, the critical supersaturation according to Kohler theory is low. These particles need very large times to reach equilibrium. But the particles are almost as large as other activated particles. So, those must be counted as

activated.

3. The red curve represents an aerosol particle with a high critical supersaturation s_{c1}. For this particle, the time for which the parcel supersaturation is sustained greater than the critical supersaturation of the particle (that is , $s > s_{c1}$ is not sufficient for the particle to grow to its critical size. Thus, this particle initially grows as long as $s > s_{c1}$ but when $s < s_{c1}$, it starts evaporating. This mechanism is called evaporation mechanism.

4. The green curve represents the aerosols which are activated initially but during the evolution of the parcel supersaturation s_{c2}, it becomes lower than the equilibrium supersaturation of the particle and the particle starts evaporating. Thus this droplet evaporates and the water vapor added to the ambient atmosphere allows the other particles to grow. *Nenes et al.* [2001] call this deactivation mechanism.

Their experiments showed that because of these kinetic limitations, the equilibrium assumption overpredicts the cloud droplet number by less than 10% for pristine marine aerosol and by more than 40% for continental aerosols.

Mass Redistribution A population of non-monodisperse aerosol particles can never be in equilibrium [*Colbeck*, 2008].If we consider two aerosol particles of different sizes, then the equilibrium vapor pressure over those particles is different because, by Kohler equilibrium theory, it depends on their sizes. So, in cases where the ambient supersaturation falls between the equilibrium supersaturations of these two particles, the smaller particle would evaporate while the larger one would grow. Thus, in a way, water molecules are transfered from the smaller drops to the larger one. This kind of redistribution mass can occur due to several effects – different amounts of salt in the two particles, different sizes, radiative cooling or heating of the drops. Although these effects are negligible for monodisperse aerosols, they become pronounced as the chemical composition and size distribution vary greatly.

2.3.1 Need for a New Model

To address some of the limitations discussed above and to accurately predict the cloud droplet number realistically, a new model to calculate aerosol activation at realistic water vapor concentrations in clouds, taking into consideration the aerosol composition and size distribution is needed. Modified Eulerian-Lagrangian Aerosol Model developed by *Steele* [2004]. MELAM computes activation using a condensation scheme which calculates the kinetic condensation rates and the growth of the aerosol particles is constrained by conserving the total water budget during condensation. This model is discussed in greater detail in the next chapter. This explicit computation of aerosol activation is expected to result in accurate prediction of cloud droplet number concentrations from aerosol concentration. At the same time, it is also expected to fulfil the demand of the aerosol-cloud research community that condensation growth of aerosols be used in cloud models to simulate aerosol activation [*Lohmann and Feichter*, 2005; *Seinfeld*, 1999; *Houghton et al.*, 2001].

2.4 Precipitation Formation

Precipitation-sized particles can not form in a cloud by condensation processes only [*Rogers and Yau*, 1989] . As the cloud droplets grow larger condensing water vapor, their rate of growth becomes low. Precipitation formation inevitably consists of a collection process in which the cloud droplets or the ice particles collide and coalesce to form a larger drop/particles. This section will discuss some of the important mechanisms involved in precipitation formation.

For a given amount of condensed water, the size of the smaller drops increases faster than that of the larger ones *Curry and Webster* [1999]. Figure 2-4 shows the growth rate of a drop by diffusion (condensation) and accretion processes. Below $\sim 20\,\mu$m radius, the growth of the drop is predominantly by diffusion and after $\sim 20\,\mu$m, it is by accretion. Accretion is the process in which the drops/particles collide and stick together to form a larger drop. This mechanism for liquid drops is also called collision-coalescence.

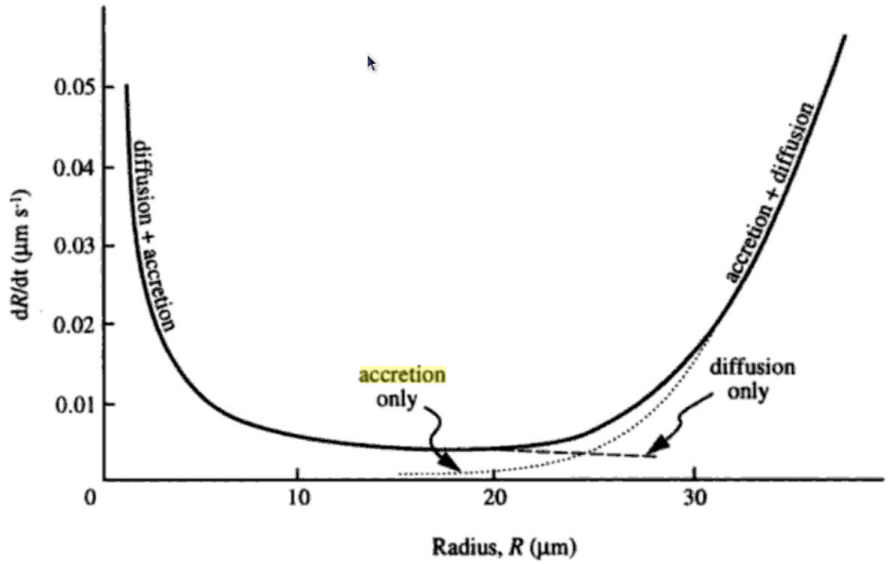

Figure 2-4: Droplet growth rate only by diffusion (dashed) and only by accretion (dotted). The solid curve represent the combined growth rate. Diffusional growth rate decreases with radius, while accretional growth rate increases with radius [*Curry and Webster*, 1999]

2.4.1 Collision-Coalescence

As the cloud drops grow to a radius of $\sim 20\,\mu$m, their terminal velocities are appreciable and they start falling and while doing that, collide with other cloud droplets in their path and a fraction of these collisions results in the two colliding droplets sticking together to form a larger drop. This mechanism of formation of larger drops is the single most important mechanism of formation of precipitation-sized drops in the warm ($> 0°C$) region of the atmosphere. This process also happens in the upper layers of the troposphere but has greater relevance in the lower warm region because the concentration of the cloud droplets is the greatest in that region. A drop of radius R that falls through a population of smaller droplets can collect droplets of radius r while sweeping out a volume per unit time given by

$$\pi(R+r)^2[u_T(R) - u_T(r)]n(r)E(R,r) \tag{2.13}$$

where $u_T(R)$ and $u_T(r)$ are the terminal velocities of the collector and collected particles; $n(r)$ is the particle size distribution and $E(R, r)$ is the coalescence efficiency. This expression shows that the efficiency of this process is greater when

1. $u_T(R) - u_T(r)$ is large: this is again an implication of the existence of some large drops as terminal velocities increase with the size of the drops.

2. the number concentration of the droplets $n(r)$ is large.

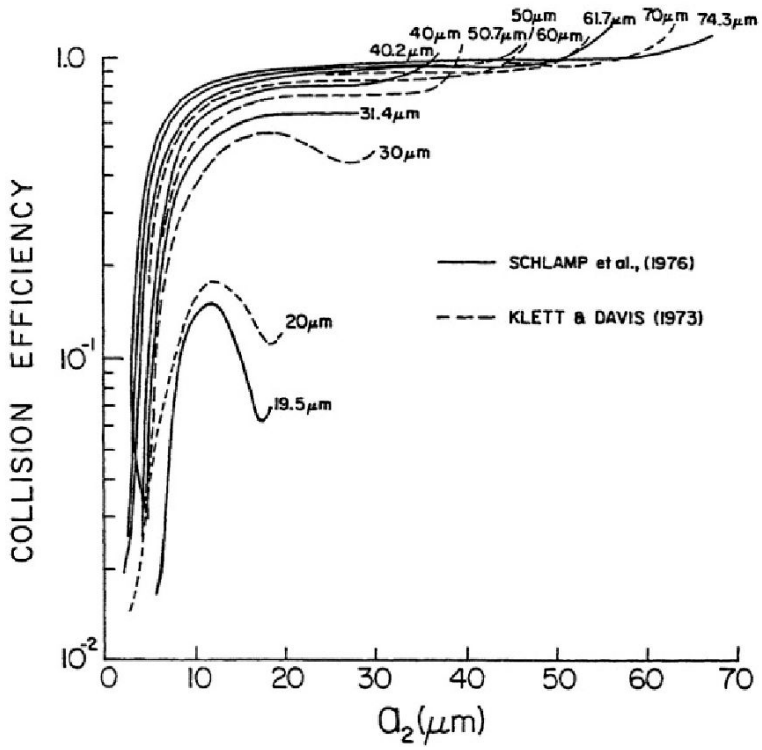

Figure 2-5: Computed collision efficiencies of spherical water drops in still air as a function of the radius of the collector drop radius (a_1) and the collected drop radius (a_2). Each curve is labeled with the collector drop radius. [*Pruppacher and Klett*, 1998]

Figure 2-5 [*Pruppacher and Klett*, 1998] shows the theoretically computed collision efficiencies as a function of drop sizes. This figure shows that as discussed earlier, the collision efficiency of the cloud drops is very low till the drops attain the size of $\sim 20\,\mu$m.

Figure 2-4 [*Curry and Webster*, 1999] shows the drop growth rates by diffusion and accretion (collision-coalescence) as a function of the drop radius. Droplets smaller than $10\,\mu$m grow efficiently by diffusion and those larger than $25\,\mu$m grow faster by accretion. There is a window between $10\,\mu$m and $25\,\mu$m where the growth by both processes is slow. For precipitation-sized particles to form, the larger drops have to grow $\sim 25\,\mu$m rapidly.

The following mechanisms have been proposed to bridge the gap between $\sim 10\,\mu$m and $\sim [25\,\mu$m so that there are some large drops which can start collision-coalescence [*Levin and Cotton*, 2008].

1. Presence of giant hygroscopic aerosols : This is the case usually in marine atmospheres where the giant sea salt aerosols turn collision-coalescence very efficient. This is also the basis for hygroscopic cloud seeding where giant aerosol particles at $2-5\,/\mathrm{cm}^3$ are introduced to accelerate collision-coalescence.

2. Turbulence effects on condensation : The inhomogeneous updrafts at cloud base create inhomogeneous supersaturations and the particle growths are different. Thus the cloud droplet size spectrum is broadened.

3. Turbulence effects on collision-coalescence : Turbulence can enhance the efficiency of collision-coalescence by

   - enhancing the collision efficiencies as the droplets accelerate in a turbulent flow rather than fall at their terminal velocities [*Koziol and Leighton*, 1996].
   - creating differential fall speeds of the drops [*Pinsky and Khain*, 1997b] *and*
   - increasing the droplet concentration due to spatial inhomogeneities [*Pinsky and Khain*, 1997a].

4. Radiative cooling of drops : Radiative cooling of drops lowers the surface temperature of the drops and the equilibrium vapor pressure of the drops is reduced due to the reduced temperature. Thus, the drops grow by diffusion. But this can happen when the cloud droplets are at the top of the cloud. So, this is not a very common process.

In summary, the marine warm-based (hence greater water vapor concentrations) are most efficient in precipitation formation. They also have sea salt aerosols which act as giant nuclei. Because of the large water vapor concentrations, they also have large condensate mass.

Formation of precipitation by collision-coalescence is very efficient also because the lagrangian time scales of the precipitation particles is short, that is, because they form closer to the ground, their evaporation is lower before they reach the ground. In the next subsection, precipitation formation by ice particle mechanisms is discussed in which the precipitation particles fall from greater heights and hence evaporation losses are compared to the precipitation from collision-coalescence.

2.4.2 Ice and Mixed Phase Processes

In deep convective clouds which reach heights of ten kilometers an more, nucleation of ice particles , their growth and their interaction with other ice and liquid particles leads to precipitation. The following lines describe some of the important mechanisms in ice growth that are relevant to deep convective clouds.

1. In a mixed phase region of a cloud, in which supercooled liquid drops are abundant, the atmosphere is almost saturated with respect to water. But since ice has a lower equilibrium saturation at the same temperature, the atmosphere is supersaturated with respect to ice. So, in such a situation, the ice particles grow by deposition of water vapor and as the atmosphere is under-saturated, the supercooled drops evaporate to bring the atmosphere to saturation again. Thus, the ice particles grow rapidly than liquid drops. This may lead to precipitation-sized particles.

2. Riming is the process in which ice particles collide with the liquid drops which then freeze. Riming can result in heavily rimed ice particles, graupel particles.If the atmospheric conditions are favourable – sufficient concentration of supercooled drops, sufficient cloud depth and sufficiently strong updrafts – hail stones can also form.

Ice particles can also collide with other ice particles to produce aggregates.

Borys et al. [2000, 2003] found that if the concentration of cloud droplets increases and hence their average size decreases, riming may be retarded due to the lower collection efficiency of cloud droplets by the ice particles. This result becomes very relevant in a subsequent chapter where the collection efficiencies of liquid drops by ice particles is studied. The different aspects of precipitation forming processes are discussed in subsequent chapters in the context of the relevant atmospheric conditions and pathways.

2.5 Previous Studies

Understanding the effect of aerosols on the structure, microphysics and precipitation has remained one of the focal area of research in atmospheric science for almost fifty years. In the initial years, the spearheading works of *Gunn and Phillips* [1957], *Squires* [1958], *Squires and Twomey* [1961], and *Warner and Twomey* [1967] pointed out that the increasing concentrations of cloud condensation nuclei from industrial sources increased cloud droplet concentration thus reducing the collision-coalescence efficiency leading to reduced precipitation efficiency and enhanced microphysical stability of clouds.

But one of the severe constraints on elucidating aerosol-cloud interactions in the sense of cause-and-effect relationships is the wide spectrum of aerosol composition, concentrations and a similarly diverse atmospheres in which the clouds evolve in terms of their characteristics like moisture content, stability and cloud types.

For instance, the boundary layer clouds are very sensitive to vertical profiles of moisture and stability [*Levin and Cotton*, 2008] but the deep convective clouds are less sensitive to small changes in moisture and temperature in the boundary layer but are very sensitive to the convergence of sensible and latent heat in the lower levels and to the stability profile.

In the following subsections, some of the previous attempts to understand the interactions between aerosols and clouds via observations and numerical modeling

are discussed.

2.5.1 Observations

Aerosol Activation

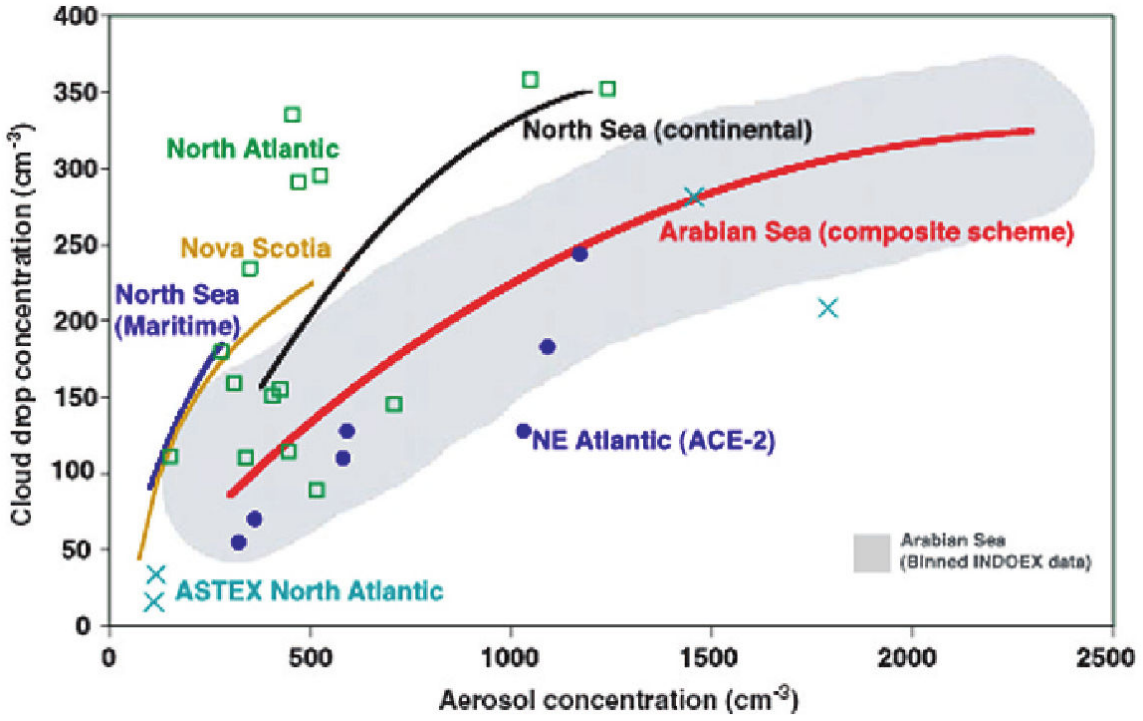

Figure 2-6: Aircraft measurements of cloud droplet number concentration increase with aerosol number increase in different atmospheres. The red line is from a theoretical fit of the INDOEX data for the Arabian Sea. [*Levin and Cotton*, 2008]

The most important link in aerosol-cloud interactions is the relationship between aerosol concentration and cloud droplet number concentration. Simultaneous aircraft measurements of CCN and cloud droplet concentrations have shown that largely irrespective of location, cloud droplet concentrations increased with CCN concentrations [*Leaitch et al.*, 1992; *Taylor and McHaffie*, 1994; *Chuang et al.*, 2000; *Ramanathan et al.*, 2001]. However the cloud droplet concentration tapers off with further increase in aerosol concentration as can be seen in the figure2-6 [*Levin and Cotton*, 2008]. The large variations in this figure are attributed to the following facts:

1. CCN are only the activable fraction of the total aerosol concentration and this fraction is dependent on the size distribution and chemical composition of aerosols.

2. Activation and hence cloud droplet concentration depends on the updraft speeds in the clouds. In the North Atlantic case in figure 2-6, a large fraction of the aerosols were activated whereas in the Arabian Sea case, the activated fraction is less. The North Atlantic case was a deep convective event where the updrafts were greater than $10\,\mathrm{ms}^{-1}$ [*Levin and Cotton*, 2008] where as in the Arabian Sea INDOEX case, the updrafts were small [AJ. Heymsfield, personal communication, December 22, 2008] and hence lower activations.

   Further, the total aerosol concentration also depends on the range of measurement. Although the particles smaller than $\sim 10-20\,\mathrm{nm}$ contribute to the total aerosol concentration, they cannot be easily activated.

   McFiggans et al. [2005] concluded that observations of CCN activation can be seen in the right perspective with a comprehensive understanding of the particle sizes, chemical composition, mixing state, and surface coating. It also has to be noted that the vertical velocities in the actual clouds are not uniform in space and time. The subsequent processes after cloud droplet formation like mixing with entrained air, coalescence and precipitation affect the observed cloud droplet number concentrations.

Cloud microphysics

As discussed earlier, *Twomey and Warner* [1967] and *Warner and Twomey* [1967] observed that smoke particles from sugarcane fires enhanced the cloud droplet concentrations and reduced the cloud droplet size. They reasoned that these two factors together retard the growth of rain drops by collision-coalescence.

The most comprehensive observational study of aerosol impact on cloud microphysics and precipitation development has been the aircraft and ground-based observational campaign in the Amazon region *Andreae et al.* [2004]. This study has

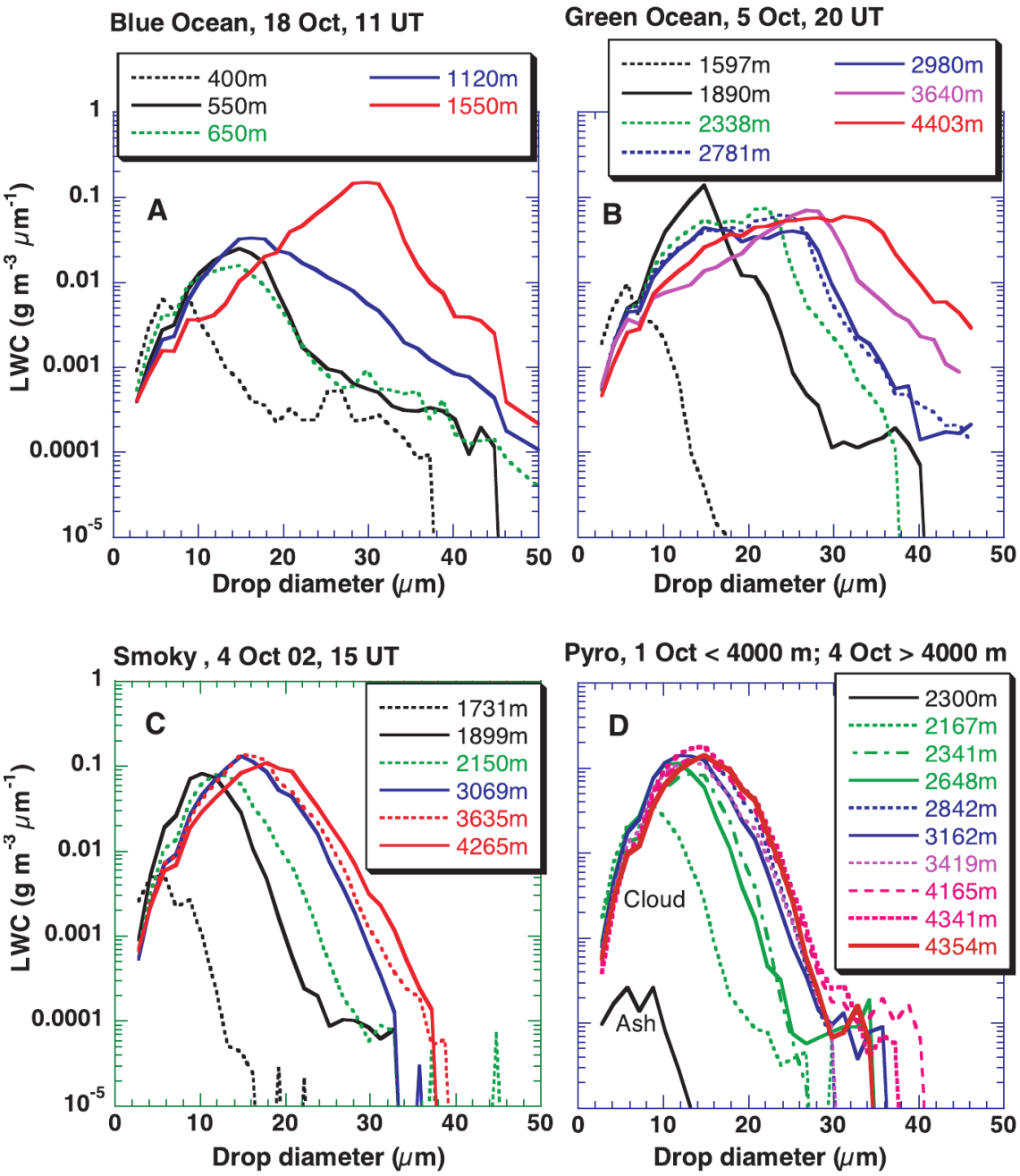

Figure 2-7: The drop size distributions at different altitudes in a number of Amazonian clouds. The drop size distribution is broadened in the 'blue ocean' and 'green ocean' situations. The drop size distributions in the case of 'smoky clouds' and 'pyro-clouds' are narrow. [*Andreae et al.*, 2004].

great relevance to the present thesis because this stands out as the only observational campaign to study aerosol effects on precipitation from deep convective clouds. The observations were categorized into four classes of clouds:

1. Maritime shallow clouds : These clouds had low CCN concentrations so, cloud droplets in low concentrations and there were a few larger drops. These clouds were shallow. These clouds were termed 'Blue Ocean'. Figure 2-7 shows these clouds in the top left panel. The widening of the drop size distribution with height shows that precipitation formed efficiently.

2. Pristine continental clouds : These are the clouds observed inland in the western Amazon in the pristine atmospheres. These were observed in the rainy season. These clouds had low CCN concentrations as CCN were scavenged by rain. Thus even though they developed in continental conditions, they had CCN concentrations characteristic of maritime atmospheres. So, *Andreae et al.* [2004] called them 'Green Ocean'.

3. Smoky clouds : The high CCN concentrations from smoke from fires in the dry season persisted in the atmosphere because of the lack of rain which could scavenge them. The authors found that these high CCN concentrations resulted in high concentrations of cloud droplets hence the narrower drop size distribution in the lower left panel in the figure 2-7. Because of the narrow size distribution, collision-coalescence was inefficient and the drops continued growing condensation to higher altitudes. It was inferred that ice could form in these clouds. These were deep convective clouds which produced lightning, hail and heavy precipitation.

4. Pyro-clouds : These clouds ingested smoke and heat from biomass fires. The high concentrations of CCN produced large concentrations small drops. Thus warm rain was suppressed. The rain probe did not measure any rain drops although the clouds were very deep.

Vertical Profiles of Droplet Effective Radius

Rosenfeld and Lensky [1998] used satellite observations to retrieve the vertical profiles of effective radius of cloud droplets. They assumed that the different similar in structure – same cloud base heights and similar droplet growth. *Freud et al.* [2005] validated this assumption by in-situ aircraft measurements. Based on the cloud top heights and the cloud top temperatures, they found that the cloud droplet effective radius increases as the depth of the cloud increases and, in continental clouds with higher cloud droplet concentrations, the growth of the particles is slower than in the maritime ones which have lower droplet concentrations.

This technique was used by several researchers to study the impact of different aerosol populations on convective clouds [*Rosenfeld*, 1999; *Rosenfeld et al.*, 2001, 2002; *Rudich et al.*, 2002, 2003; *Koren et al.*, 2005; *Fromm et al.*, 2006].

Largely, these studies are in agreement with in-situ measurements. *Rosenfeld et al.* [2001] reported that precipitation particles were found when the droplet effective radius was greater than $14\mu m$.

Koren et al. [2005] analyzed convective clouds and detected systematic impacts of pollution, desert dust and biomass burning aerosols on the development. Cloud droplet sizes were decreased by $\sim 20\%$ in the high aerosol cases. They also found that increase in aerosol concentrations resulted in taller clouds and higher cloud cover. These results were simulated by [*Khain et al.*, 2005; *Teller and Levin*, 2006].

Effect on Precipitation

Most of the aerosol-cloud interaction research for the past five decades dealt with the effects of aerosols on cloud formation and microphysics. Although some studies looked at the formation and development of precipitation embryos, measurement of precipitation reaching the ground still remains a challenge.

Warner [1968] studied the effects of sugarcane smoke on rainfall but remained inconclusive. *Hobbs et al.* [1970] observed an increase of $\sim 30\%$ in rainfall from warm clouds impacted by pollution from paper mills. Many researchers reported increase

in precipitation from areas downwind of paper mills. This observation also led to the technique of precipitation enhancement using hygroscopic particles to broaden the cloud droplet spectrum.

In a recent study, *Lin et al.* [2006] looked at the effects of forest fires on precipitation from convective clouds in the dry season in the Amazon. They reported increased cloud depths and precipitation. They reasoned that the convection was invigorated resulting in great ice particle formation and growth.

Since measurement of precipitation that reaches ground is still an obstacle, the theory of effect of aerosols on precipitation is still incomplete.

2.5.2 Aerosol Effects on Clouds : Numerical Modeling Studies

Most of the aerosol-cloud interactions studies until recently looked mostly at the effect of aerosol concentration on cloud droplet size hence on the scattered radiation. Since deep convective clouds usually have very reflecting anvils as tops, they are they are not very susceptible to changes in cloud droplet radius. Also because the life times of small cumulus and deep convective clouds are not as large as those of stratocumulus clouds, changes in their scattering properties are not very important.

But because deep convective clouds create heavy precipitation, changes in their precipitation characteristics are important. As a result, almost all of the studies of aerosol effects on these clouds concern their precipitation formation characteristics. This subsection would discuss some of the important studies in this context. As discussed in the subsection [representation], most of these studies use Twomey parameterization for aerosol activation.

[***Khain et al.*, 2005**] *Khain et al.* [2005] used the Hebrew university Cloud Model to study the various microphysical processes in precipitation formation in deep convective clouds. The model uses spectral (bin) microphysics to compute the cloud microphysics. They used the atmospheric conditions measured by *Rosenfeld and Woodley* [2000] during cloud observations in Texas. The atmosphere was assumed

to be of continental character and they considered maritime aerosol concentration ($100\,/\mathrm{cm}^3$) and continental ($1260\,/\mathrm{cm}^3$).

The simulations showed that increased aerosol concentrations resulted in smaller cloud droplets and ice particles. Because the atmosphere was considered to be continental, it was largely dry in the upper layers. As a result of increased aerosol concentrations, both precipitation and precipitation efficiency decreased. They reasoned that as the precipitation particles fell through the dry air, they evaporated and hence the decrease in precipitation and precipitation efficiency.

[***Khain et al.*, 2004**] *Khain et al.* [2004] used the Hebrew University Cloud model described above to conduct comprehensive simulations of aerosol effects on the microphysical and dynamical structure and evolution deep convective clouds forming in continental thermodynamics conditions. They used the initial atmospheric conditions measured by during observations of deep convective events in Texas by *Rosenfeld and Woodley* [2000].

Their experiments showed that aerosol concentrations have a crucial effect on both warm and mixed phase precipitation. When the CCN concentrations (hence droplet) are low, diffusion growth led to formation of sufficiently large cloud droplets for collision-coalescence to be triggered. The rain drops fell down or were frozen in the upper cold layers of the atmosphere and graupel particles were larger. As a result, the precipitation from both collision-coalescence and mixed phase processes formed efficiently.

The accumulated rain in their experiments showed a monotonic decrease with increasing aerosol concentrations. They consider it the main conclusion of their study. Increased aerosol concentration led to stronger cloud updrafts. Thus the altitude of precipitation formation is elevated and the size of the precipitation particles decreased. Since the particles fell from higher altitude and because of their small sizes have lower terminal velocities, they have longer lagrangian times of fall and hence more evaporation. Thus the coupling of microphysics and dynamics leads to precipitation suppression.

[***Khain et al.*, 2005]** *Khain et al.* [2005] studied some of the mechanisms through which aerosol concentrations affected cloud microphysics, dynamics and precipitation. The model used was the same as the one mentioned above. The aerosol concentrations considered were 100 /cm^3 and 1260 /cm^3 as in the above cases. They considered two different atmospheric conditions: a maritime one and a continental one.

In the continental conditions, increasing aerosol concentration from $100/cm^3$ to $1260/cm^3$ led to delayed and decreased precipitation. The cloud water content and rain water content in the high aerosol case are higher than those in the $100/cm^3$ case. But the conversion of these water contents into precipitation was inefficient. They inferred that the low precipitation efficiency meant that the greater growth of droplets by condensation led to significant release of latent heat. Similarly, the deposition of ice particles and freezing of droplets contributed to heating. And this heat released was largely neutralized by the absorption of heat in drop evaporation and ice sublimation and melting.

In the maritime conditions where the air has greater moisture content, they found that increased aerosol concentration may lead to increased precipitation if the evaporation losses are small. Thus while studying the effect of aerosol concentrations on deep convection, it is important to keep the atmospheric conditions in view to gain the right perspective.

[***Wang*, 2005]** Most of the numerical modeling studies of aerosol impacts on clouds in general, and deep convective clouds in particular, conspicuously consist of a low aerosol concentration case and a high concentration case. Perhaps, the researchers believed that the effect could be discernible. This study stands out as a comprehensive look at a range of aerosol concentrations.

This study uses a cloud resolving model to simulate a tropical deep convective event observed during the CEPEX in 1993. It is a maritime cloud with CCN concentrations increasing from 50 /cm^3 to 6000 /cm^3.

Wang reports that the ratio of cloud droplet concentration to the initial CCN concentration decreases with increasing CCN concentration up to 2000 /cm^3 and the

ratio is constant for further increase in CCN concentration. In general, the convection is invigorated due to increased latent heat due to the increase in cloud droplet number concentration. The total precipitation monotonically increases with aerosol concentration due to greater content and number density of ice and graupel particles.

One result that is at variance with other studies is that the precipitation efficiency increases with CCN concentrations and after about 1500 /cm^3, it saturates. Most other studies found that the precipitation efficiency decreases with CCN concentration. It is possible that this result is valid for the kind of atmosphere considered and the assumptions in the model.

The study notes that most of the effects saturate after a CCN concentration, roughly varying as the logarithm of the CCN concentration.

[***van den Heever and Cotton*, 2007]** *van den Heever and Cotton* [2007] used the Regional Atmospheric Modeling System to study the effect of urban aerosol concentrations on deep convective clouds developing over urban areas. She considered two CCN concentrations 1200 /cm^3 and 2000 /cm^3 which are representative of rural and urban atmospheres. They were measured during METROMEX. The simulated storm had a CAPE of 1500 J/Kg.

Their results results showed that once a deep convective storm develops, the aerosols modulate the dynamics and microphysics. As CCN concentrations changed from rural to urban, the formation of cloud and rain water was delayed. The liquid and ice condensates were less and precipitation decreased.

But when a few giant nuclei were added, the clouds lasted longer and precipitation was enhanced too. Further, the ice and liquid water contents were higher.

Thus, the author finds it difficult to categorically conclude the impacts of urban enhanced CCN and giant CCN on downwind convection and precipitation.

[***Fan et al.*, 2007]** *Fan et al.* [2007] used the Hebrew university cloud model to simulate a deep convective event observed on 24th August, 2000 in Houston, Texas.

This study reports that increased activated particles resulted in longer cloud life

time, larger cloud sizes, formation of secondary clouds and the precipitation was enhanced.

[***Teller and Levin*, 2006**] *Teller and Levin* [2006] used a 2D-cloud model to study the effect of aerosol concentration on cloud droplet growth processes and precipitation. They considered the aerosol concentrations 100, 300, 600, 900 and 1370 per cubic centimeter.

Their results showed that as the aerosol concentrations increased from 100 /cm^3 to 1370 /cm^3 precipitation was suppressed and the initiation was also delayed. Also, the introduction of giant CCN enhanced the total precipitation on the ground in polluted clouds but the cleaner clouds did not respond to giant CCN. The introduction of giant CCN increased graupel content and the rainfall was enhanced. Although giant CCN caused more rain, the increase in rain due to giant CCN was very small compared to the reduction in precipitation due to increase in CCN.

Chapter 3

The Models

3.1 MELAM

The dependence of activation of aerosols on their composition and mixing state is, as discussed in the previous chapters, is the biggest puzzle in understanding aerosol-cloud interactions [*Berg et al.*, 1998; *Crumeyrolle et al.*, 2008; *Lohmann and Feichter*, 2005; *McFiggans et al.*, 2005; *Nenes and Seinfeld*, 2003]. Mixed Eulerian-Lagrangian Aerosol Model of *Steele* [2004] is the most sophisticated aerosol model for simulating aerosol activation and cloud formation. The next few subsections describe the representation of aerosols, the thermodynamic state of aerosols, equilibrium and non-equilibrium, and dissolution of gases. Unlike all the other models used by the research community, MELAM can accurately model activation of very complex aerosol populations. It was used to accurately model the sensitivity of aerosol activation to aerosol mixing state, complex composition, and multiple aerosol populations. Although the author's intended goal is to use the model to develop parameterizations for use in global climate models, I consider the challenge of coupling it with a cloud resolving model to run the two models interactively.

The thermodynamic state of an aerosol consists of its characteristics like ionic strength, density, water activity, extent of dissolution of electrolyte, pH and the surface tension of the particle. MELAM tracks all these characteristics of the aerosol explicitly.

The inputs to MELAM are the aerosol composition, distribution and mixing state. The output of MELAM consists of information on aerosol activation, the chemical state of the aerosols, their size distribution, and the state of cloud droplets.

Other models in the literature parameterize both the inputs and output. The identification of the activating aerosols from a given aerosol population is the essential pointer to the impact of aerosols on clouds [*Conant et al.*, 2004].

The next few subsections describe the important structural features of MELAM that are relevant to the present work.

3.1.1 Aerosol Size Distribution

Aerosol sizes range over several orders of magnitude and composition is also as diverse as their sources or method of formation. Aerosols are usually represented using bulk, moment-based, continuous, modal or sectional methods in models describing aerosol physics [*Steele*, 2004]. In sectional representation, the mass and number concentration of aerosols in each size bin are tracked [*Jacobson*, 1999]. MELAM allows to represent aerosols in size bins. Multiple sectional distributions may be used. MELAM assumes the whole aerosol population to be distributed in a log-normal distribution whose geometric mean radius and geometric standard deviation are prescribed as model parameters.

3.1.2 Aerosol Thermodynamics

The electrolytic salts present in aerosols dissolve in the solvent – water – in an aerosol and dissociate into their constituent ions. The resultant properties of the solution determine the nature of its equilibrium, equilibrium water content, surface tension, density, pH and the rates of transfer of gases into and out of the particle. MELAM computes the equilibrium state of the aerosol particles taking into consideration the chemical composition and size of the particles. The atmosphere is assumed to be sufficiently humid ($RH > 60\%$) for the electrolytes to be in a dissolved state. The equilibrium constant of dissociation of the electrolyte, K_{eq}, in a generalized, non-ideal

solution may be determined as a function of the thermodynamic activity of each of the chemical species involved as [*Tester and Modell*, 1997]:

$$K_{eq}(T) = \prod_x a_x^{k_x \nu_x} \tag{3.1}$$

where a_x is the thermodynamic activity of species x, $k_x = \pm 1$ according to whether species x is a product (+1) or a reactant (-1), ν_x is a stoichiometric coefficient, and K_{eq} is the equilibrium constant which is a function of temperature.

The activity of an undissociated electrolyte is its molality (m_x). The activity of a dissociated electrolyte is corrected for its non-ideality as

$$a_{ij} = \mathbf{m_i}^{\nu_\mathbf{i}} \mathbf{m_j}^{\nu_\mathbf{j}} \gamma_{\mathbf{ij}}^{\nu_\mathbf{i}+\nu_\mathbf{j}} \tag{3.2}$$

where a_{ij} is the activity of the dissociated electrolyte, $\mathbf{m_i}$ and $\mathbf{m_j}$ are the molalities of the cation and the anion, ν_i and ν_j are the stoichiometric coefficients, and γ_{ij} is the mean activity coefficient. γ_{ij} is a function of the total ionic strength of the ions in solution. There are a number of theoretical frameworks for computing the mean activity coefficient γ_{ij}. MELAM uses the Kusik-Meissner parameterization which is very accurate [*Kusik and Meissner*, 1978].

MELAM uses a mass-flux model that computes the condensation rates and the growth of aerosols is constrained by conservation of water in gas and aerosol phases together. For subsaturated atmospheres, MELAM uses the equilibrium method by direct integration of the Gibbs-Duhem equation [*Steele*, 2004]. Several studies showed that the equilibrium method is more accurate than the condensational growth method when the relative humidity is much below saturation [*Ferron and Soderholm*, 1990; *Resch*, 1995]. Further, the equilibration model is also used to initially equilibrate the dry aerosols to the ambient atmosphere. In this case, the ambient atmosphere is considered to be an infinite reservoir of water vapor. The particle surface tension is calculated using Gibbs dividing surface formulation [*Li and Lu*, 2001]. Aerosol density is calculated using a simple parameterization developed by *Resch* [1995].

3.1.3 Gas-Aerosol Transfer

The center piece of MELAM is the condensation scheme. In computing condensation rates to or from aerosols, the composition and mixing state are important because they are essential to resolve the competition for activation [*Gillani et al.*, 1995]. If there are aerosols of different composition and mixing state, then due to the competition, the relative rates of condensation on to different aerosols are important to correctly predict cloud droplet concentration [*Chuang et al.*, 1997]. The challenge in calculating the condensation rates in the case of a complex aerosol population is the evaluation of the saturation ratio which is affected by the composition of the droplet, curvature of the droplet surface (hence size), radiative effects and hydrophilic nature of the insoluble cores, if present [*Colbeck*, 2008].

MELAM computes the gas-aerosol transfer of species by two methods. One is the equilibrium approach discussed earlier.

In the second method, the Fick's law of diffusion is used in which gradient of vapor density between the ambient atmosphere and the particle surface drives condensation. For condensation of water vapor, the difference between the ambient relative humidity and the modified saturation ratio (ratio of equilibrium vapor pressure over the drop to the equilibrium vapor pressure over a flat surface of pure water) drives the flux of water vapor into or out of the solution droplet.

The Diffusion-Limited Growth Model

MELAM assumes that the condensation or adsorption of water vapor on to a droplet is limited by diffusion and uses Fick's law of diffusion as discussed above . For a quasi-stationary condensational flux on to or away from a droplet, the Fickian theory of diffusion. The theory was modified by *Maxwell* [1990] and *Langmuir* [1918] by integrating the diffusion equations under suitable conditions to derive the following simplified equation:

$$\frac{dm_{a,i}}{dt} = 4\pi r_a D_i \left[\rho_{v,i}(\infty) - \rho_{v,a}(r)\right] \tag{3.3}$$

Here, $m_{a,i}$ is the mass of component i in the particle, r_a is the radius of the particle, $\rho_{v,i}$ and $\rho_{v,a}$ are the molecular concentrations of the vapor phase in the ambient atmosphere and on the surface of the droplet, and D_i is the molecular diffusion coefficient of vapor i in air.

But this model overestimates the growth of small aerosol particles [*Pruppacher and Klett*, 1998]. This happens because for particles with sizes comparable to their mean free path, the assumption of ideal gas behavior breaks down and the vapor density in moist air is not continuous right up to the drop surface [*Fukuta and Walter*, 1970; *Pruppacher and Klett*, 1998].

When D_i is corrected for non-ideal behavior and time dependence, the model agrees well with measurements [*Jacobson*, 1999; *Gorbunov and Hamilton*, 1997; *Gorbunov et al.*, 1998; *Pruppacher and Klett*, 1998; *Ansari and Pandis*, 2000].

Condensation of water vapor at the surface of the drop causes warming due to release of latent heat. *Fitzgerald* [1972] found that this results in a temperature gradient and hence conduction of heat away from the drop. Correction for the aforementioned effects gives the following equation for the mass flux form of the growth equation:

$$\frac{dm_i}{dt} = 4\pi r_a D_i'(P_i - P_{a,i,s}) \left[\frac{D_i' L_i P_{a,i,s}}{k_d' T} \left(\frac{L_i M_i}{R^* T} - 1 \right) + \frac{R^* T}{M_i} \right]^{-1} \tag{3.4}$$

Here, k_d' is the corrected thermal conductivity of dry air, R^* is the gas constant, T is the temperature, L_i is the latent heat of condensation of component i, D_i' is the corrected molecular diffusion coefficient, $m_{a,i}$ is the mass of component i in the particle, P_i is the ambient partial pressure of the condensing gas, $P_{a,i,s}$ is the saturation vapor pressure of vapor i at the surface of the particle, and M_i is the molecular mass.

Using the equation of state, and assuming a rate constant k_i, the mass transfer rate can be cast into an ordinary differential equation:

$$\frac{dc_i}{dt} = k_i(C_i - C_{a,i}) \tag{3.5}$$

where c_i is the water molecule concentration in the aerosol phase, C_i and $C_{a,i}$ are the water molecule concentration in the ambient atmosphere and the effective saturation

water molecule concentration just above the drop surface. $C_{a,i}$ can be assumed to be a product of a dimensionless equilibrium saturation ratio of the particle-specific near-surface concentration to the saturation concentration over a flat interface of an equivalent solution, and the equilibrium concentration over a bulk surface of an equivalent solution. The rate constant is determined to be [*Jacobson*, 1999]

$$k_i = 4\pi r_a D_i' \left[\frac{D_i' L_i M_i S_{a,i} C_{s,i}}{k_d T} \left(\frac{L_i M_i}{R^* T} - 1 \right) + 1 \right]^{-1} \tag{3.6}$$

Further, the molecular diffusion coefficient D_i is corrected for collisional geometry, sticking probability and ventilation effects [*Steele*, 2004]. Thus, the mass transfer equation becomes:

$$\frac{dC_w}{dt} = k_w C_{s,w} (RH - S') \tag{3.7}$$

where C_w = aerosol water content, k_w = effective condensation rate constant, $C_{s,w}$ = saturation water vapor concentration with respect to a flat interface with liquid water at the local pressure, RH = relative humidity of the ambient atmosphere and S' = supersaturation correction.

This equation is used to solve diffusion of water vapor into the droplet.

Activation According to Kohler theory, if the droplet radius is larger than its critical radius, the droplet is deemed to be activated. But in such a formulation of condensation as above, this activation criterion leads to problems like varying surface tension with changing electrolyte molalities. MELAM defines an aerosol as activated if $\frac{dS'}{dr}$ is negative. In other words, growth is favoured over evaporation as radius increases.

3.2 Cloud Resolving Model

The cloud resolving model that has been used to compute the cloud microphysics and dynamical fields was developed by *Wang and Chang* [1993]. It has three important modules – a cloud physics module, a cloud chemistry module, and a microphysics

module. The model has a non-hydrostatic, pseudo-elastic, and multi-dimensional framework. The cloud physics module together with the microphysics module computes fields like winds, temperature, air pressure and air density. Prognostic microphysical quantities include bulk mass mixing ratios of four different hydrometeors – cloud droplets, rain drops, ice crystals and graupel – and also their number concentrations.

The model divides each variable into a grid-scale contribution and a subgrid-scale contribution. This division is used to derive the equations of motion. The model assumes a hydrostatic and horizontally homogeneous reference atmosphere.

3.2.1 The Cloud Physics Module

This module is based on the dynamical frame work developed by *Klemp and Wilhelmson* [1978]. It assumes pseudo-elastic continuity equation.

As mentioned above, all variables are divided in to a grid-scale and a subgrid-scale contribution:

$$F = \overline{F} + F' \tag{3.8}$$

where $\overline{F}$ is the grid-scale contribution and F' is the subgrid-scale contribution. The grid-scale contribution is further divided into a base state, F_0, which is horizontally homogeneous and the deviation from the base state, f:

$$\overline{F} = F_o + f \tag{3.9}$$

Continuity Equation The pseudo-elastic continuity equation is

$$\frac{\partial \pi}{\partial t} = \frac{c^2}{C_p \theta_{v_0}^2 \rho_0} \frac{\partial \rho_0 \theta_{v_0} u_j}{\partial x_j} \qquad j = 1, 2, 3 \tag{3.10}$$

where t is time, x_j is the spatial coordinate, u_j is the wind speed component along the jth coordinate axis; $c^2 = \frac{C_p}{C_v} R_d \pi_0 \theta_{v_0}$ where c is the speed of sound and π is the deviation of the non-dimensional pressure from the initial unperturbed state Π_0, C_p and C_v are the specific heats of dry air at constant pressure and volume. R_d is the

gas constant for dry air, ρ is the air density, θ_v is the virtual potential temperature. The non-dimensional pressure (Exner function) is defined as

$$\Pi = \left(\frac{P}{P_0}\right)^{R_d/C_p}. \tag{3.11}$$

Momentum equation The momentum equations are derived from the primitive equations in which the Coriolis terms are neglected and they are non-hydrostatic:

$$\begin{aligned}\frac{1}{\rho}\frac{\partial}{\partial t}(\rho u_j) + \frac{1}{\rho}u_i\frac{\partial}{\partial x_j}(\rho u_j) + u_i\frac{\partial u_j}{\partial x_j} = & - C_p\theta_{v0}\frac{\partial \pi}{\partial t} \\ & + \left[\frac{\theta}{\theta_0} - 1 - Q_T + 0.61(Q_v - Q_{v_0})\right] g\delta_{i3} \\ & + E_{u_i} \qquad i,j = 1.2.3\end{aligned} \tag{3.12}$$

Here, the second term on the right hand side is the buoyancy. ρ is the density of moist air, θ is the potential temperature, Q_T is the condensate drag, Q_v is the mass mixing ratio of water vapor, and $(Q_v - Q_{v_0})$ is the buoyancy due to water vapor perturbations. $\dfrac{\theta}{\theta_0}$ is the buoyancy change due to temperature changes. E_{u_i} is the contribution of all the subgrid-scale process to u_i. θ is the potential temperature. g is the acceleration due to gravity and δ is the delta function.

Thermodynamic Equation CRM uses the ice-liquid potential temperature defined by *Tripoli and Cotton* [1981] which is conserved under phase changes in the cloud. In terms of the conserved ice-liquid potential temperature, θ_{il}, the thermodynamic equation is

$$\begin{aligned}\frac{1}{\rho}\frac{\partial}{\partial t}(\rho\theta_{il}) + \frac{1}{\rho}u_j\frac{\partial}{\partial x_j}(\rho\theta_{il}) + \rho\theta_{il}\frac{\partial u_j}{\partial x_j} = & \frac{\theta_{il}^2}{\theta}\left[\frac{L_{lv}P_l + L_{iv}P_i}{c_p Max(T, 253)}\right] \\ & + E_\theta \qquad j = 1,2,3\end{aligned} \tag{3.13}$$

where T is the temperature, L_{lv} and L_{iv} are the latent heats of condensation and sublimation, E_θ is the subgrid-scale contribution to θ_{il}. P_l and P_i are the liquid phase

and ice phase precipitations. The first term on the right shows that the amount of latent heat is the latent heat of the amount of precipitation that leaves the atmosphere as liquid or ice.

Continuity Equations for Hydrometeors The continuity equations for the different hydrometeors consist of different equations for their bulk mass mixing ratios and their number concentrations:

$$\frac{1}{\rho}\frac{\partial}{\partial t}(\rho Q) + \frac{1}{\rho}u_j\frac{\partial}{\partial x_j}(\rho Q) + \rho Q\frac{\partial u_j}{\partial x_j} - \frac{1}{\rho}\frac{\partial \rho V_t Q}{\partial x_3} = S + E_Q \tag{3.14}$$

for mixing ratios (Q) and

$$\frac{1}{\rho}\frac{\partial}{\partial t}(\rho N) + \frac{1}{\rho}u_j\frac{\partial}{\partial x_j}(\rho N) + \rho N\frac{\partial u_j}{\partial x_j} - \frac{1}{\rho}\frac{\partial \rho V_t N}{\partial x_3} = S + E_N \tag{3.15}$$

for the number concentrations (N).

Here, S is the source or sink of the quantities, V_t is the terminal velocity of precipitating particles. The Es are the subgrid-scale contributions.

The model can be run in a warm mode when there are no ice processes and a cold version in which ice and mixed phase processes are allowed. Since the present study concerns deep convection, the cold version is used allowing for ice and mixed phase processes.

3.2.2 Microphysics

CRM calculates the transformation rates between different microphysical entities using a two-moment bulk scheme. Twenty six microphysical processes of transformations between the different hydrometeors are computed. In this scheme, every hydrometeor category has a distinct size spectrum represented by

$$dN = N_0 D^b e^{-\lambda D} dD \tag{3.16}$$

where D is the diameter of the hydrometeor, and N_0 and λ are two parameters that can be deduced as explicit functions of the bulk mass mixing ratio Q and number concentration N. This moment scheme was found to be more accurate [*Srivastava*, 1978; *Shiino*, 1983].

Empirically the mass and diameter of a hydrometeor are related as

$$M = A_m D^{\alpha} \tag{3.17}$$

where M is the mass and D is the diameter of the hydrometeor. A_m and α are coefficients [*Mason*, 1971]. The terminal velocity of the hydrometeors is parameterized as

$$V = A_v D^{\beta} \tag{3.18}$$

where A_v and β are coefficients. The values or expressions for N_0, λ, b, α and β for hydrometeor category are listed by *Wang and Chang* [1993].

3.2.3 Subgrid-scale Terms

CRM uses a first order closure scheme to treat the subgrid-scale terms and to close the basic equations. This scheme is based on the *Klaassen and Clark* [1985] scheme. But unlike *Klaassen and Clark* [1985], CRM uses different methods to compute the Richardson number under saturated and unsaturated conditions.

3.2.4 Boundary Conditions

Since the solution of a modeling system for a cloud has fast spreading waves, adopting a suitable lateral boundary condition is a daunting task. CRM uses the scheme developed by *Miller and Thorpe* [1981].

A ten-level 'sponge' boundary condition is used at the top of the domain to absorb the reflected waves. The vertical velocity at the top of the domain and at the bottom is zero. These boundary conditions were found to be quite stable in all the experiments done.

The cloud resolving model had been used to conduct sensitivity experiments with the data from CCOPE project [*Knight*, 1982]. Further, the model had been used successfully in several studies [*Wang*, 2004, 2005; *Ekman et al.*, 2004a,b; *Wang and Prinn*, 2003, 1998; *Engström et al.*, 2008].

3.3 The Coupled Model

The following lines describe the coupling between the two models and their interaction.

1. MELAM is an aerosol model which consists of a sectional representation of aerosols at a point. To couple MELAM with the cloud resolving model to run both the models interactively, an instance of MELAM is created at each grid point of CRM.

2. MELAM samples the aerosol particles at the grid point in a log-normal distribution, equilibrates to the ambient atmosphere and then populates the size bins with these equilibrated aerosol particles.

3. The aerosol concentrations, composition, mixing state and distribution are initially considered to be horizontally homogeneous, but varying in the vertical. So, a vertical profile of aerosols is equilibrated to the ambient atmosphere at that level and distributed into different size bins according to their sizes as described above.

4. The CRM domain is initialized with this vertical profile of aerosol size bins. Each bin has the different mean aerosol particles attached to it.

5. MELAM uses moving-center sectional distribution. In this representation, the bin edges are fixed and the mass concentration and chemical composition of each bin are tracked. The contents of each bin are represented by one aerosol particle whose aerosol characteristics like mass concentration, radius, chemical composition are representative of the whole aerosol population in the bin. As

the mean aerosol particle grows or shrinks, its radius changes. If the radius increases due to growth such that the radius is greater than the right bin edge, all the aerosols in the bin are moved to the adjacent right bin.

Since the bin edges are fixed, advection is simplified. The advection scheme extant in CRM is used to advect aerosol particles in the CRM domain.

6. After each advection cycle, the aerosol bin characteristics are recalculated.

7. For condensation, temperature, pressure and water vapor mixing ration of the ambient atmosphere at each grid point are passed from CRM to MELAM and MELAM computes condensational growth of the aerosol particles based on the saturation state of the grid point. If the local atmosphere at the grid point has a relative humidity less than 98%, MELAM uses the equilibration approach to grow or shrink the particles. If the relative humidity is greater than 98%, time-dependent diffusion equation is solved.

8. After each condensation cycle at each grid point, the bins are tested for activation and the concentration of activated particles are passed to CRM as newly activated cloud droplets and their mass as the mass of the newly activated cloud particles. Further condensational growth of the cloud droplets is computed by CRM.

In a deep convective cloud, a wide range of saturations are created by the different moistening and drying processes. And also, the large extent of a deep convective cloud creates vastly different saturation states. Some of the difficulties when the equilibration routine in MELAM failed to converge are described below.

- One of the difficulties in using MELAM interactively with CRM was that in downdrafts or subsaturated regions, the equilibration routine in MELAM dries the particles and in doing so, tries to remove more water from the aerosol than the amount of water the aerosol had.

- While being advected, the aerosols moved to regions which had less water vapor than the aerosol water contents but the aerosols had higher water activity and

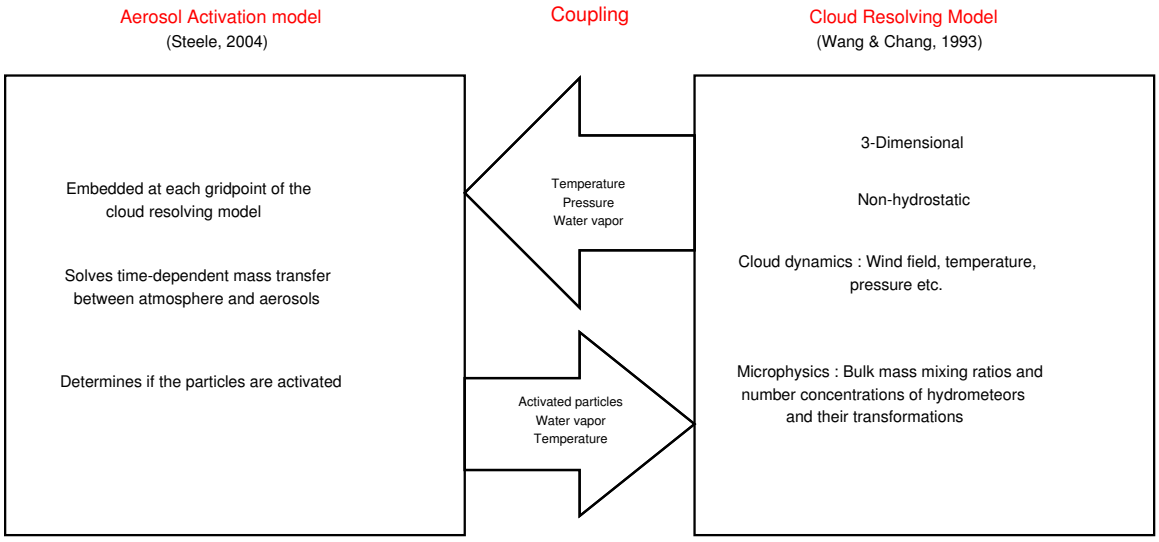

Figure 3-1: Schematic of the coupled model.

were leeching water and the equilibrium routine tried to diffuse more water than the atmosphere had. This was observed particularly in the upper layers of the troposphere where the water vapor concentrations are very less.

To remedy this non-convergence, the equilibration routine in MELAM was rewritten.

The schematic 3-1 shows the models MELAM and CRM and the nature of the coupling between them. At each time step temperature, pressure and water vapor mixing ratio are passed to MELAM for computing condensation and after condensation, the number of activated particles, changed water vapor mixing ratio and temperature corrected for the latent heat release due to condensation are passed back to CRM.

Several runs of the model with different aerosol concentrations and atmospheric conditions showed that the condensation and advection processes in the coupled model are stable. The model is used to study the impact of aerosols on deep convective clouds as described in subsequent chapters

Chapter 4

Data

4.1 INDOEX

The INDian Ocean EXperiment was a consorted observational campaign to measure the impact of aerosols transported from the south Asian region into the equatorial region where these aerosols are lifted up into the upper atmosphere and are processed in different ways [*Ramanathan et al.*, 2001]. The study included model simulations to understand the impact of these aerosols of varied composition on the clouds in the tropical and mainly equatorial region. The campaign consisted of measurements using satellites, research ships, aircraft, surface stations, and balloons. The campaign lasted from January to March in 1999.

Qn March 18th, 1999, the research aircraft C-130 was used to measure the microphysics of several clouds and traversed a deep convective cloud [*Heymsfield and McFarquhar*, 2001] at the location shown in the figure 4-1 at about 0915 UTC. The aircraft spiraled from about 4000 m down to about 500 m. The figure also shows the location of the soundings taken from the different places. The times and date of the soundings are shown in parenthesis at the place.

Some of the instruments aboard the aircraft were

- FSSP-100 particle detector
- OAP-260X particle counter.

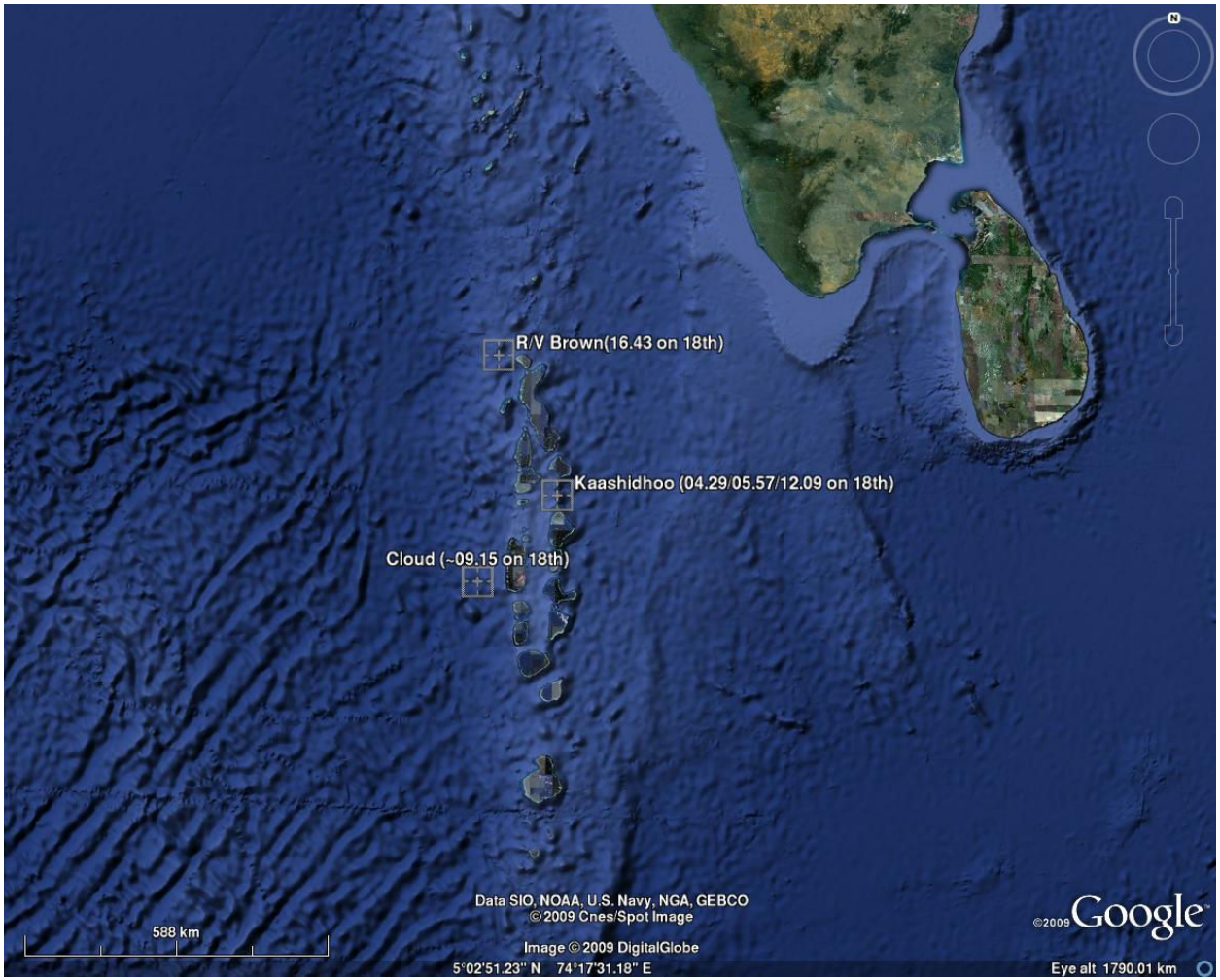

Figure 4-1: The geographical location of the observed deep convective cloud on March 18, 1999 during the INDOEX Intensive Field Campaign. Locations of R/V Ronald Brown and Kaashidhoo Climatological Observatory are also shown. The time of observation of the cloud is shown in paranthesis. Similarly, the times at which atmospheric sounding weretaken from Kaashidhoo Climatological Observatory and R/V Ronald Brown are also shown.

- TSI condensation nuclei counter
- Winds were measured with flow meters
- Cold CN counter

The geographic coverage of the campaign was from $25°N$ to $25°S$ and $50°E$ to $100°E$.

4.2 Aerosol Distributions

The aerosol distribution data was collected by using an Optical Particle counter aboard the NCAR C-130 research aircraft.

The aerosols are passed in to a laser illuminated volume and the intensity of the light scattered by the particles is estimated to find the size of the aerosol particles. A solid state detector detects the scattered light.

The sampled air is sometimes heated to 150C to evaporate sulfuric acid and to 380C to evaporate ammonium sulfate. When heated to 380C the refractory material remaining is usually dust, sea salt and soot.

In the present experiment, all the aerosols are assumed to be ammonium sulfate. So, the distributions of the *unheated* aerosols are considered.

The data is given as the $\frac{dN}{dlogD}$ in each size range and the sizes are divided into 263 size bins.

Since the cloud was entered at about 0915 UTC, the aerosol distributions in the boundary layer, *unheated*, and adjacent to the location of the cloud are averaged to obtain the mean aerosol distribution before the cloud formation. The logarithmic mean and standard deviation and the total aerosol concentration which are required to use as input for the coupled-aerosol-activation-cloud-resolving-model are derived from the averaged aerosol size distribution. The mean total concentration is found to be about 631 cm^{-1} and this conforms well with the boundary layer condensation nuclei concentration just outside the cloud as measured by the aircraft.

The geometric mean diameter of the aerosol distribution is found to be 0.24 micrometers. And the geometric standard deviation is found to be 1.32 micrometers.

When this distribution is used to simulate the deep convective cloud, all the aerosols are assumed to be ammonium sulfate.

4.3 Microphysical Data

Cloud microphysical data were collected on the NCAR C-130 aircraft [*Heymsfield and McFarquhar*, 2001; *McFarquhar and Heymsfield*, 2001]. Details of the instrumentation used and the data processing are available from data processing are available from *Research Aviation Facility, NCAR-Earth Observing Laboratory* [2002].

The data from the Forward Scattering Spectrometer Probe (FSSP) is combined to obtain the size distribution of cloud droplets, covering the diameter range from 3 to 50 micrometers. The FSSP is an instrument developed for measuring cloud droplet size. The sensor is developed for the study of microphysical processes like nucleation and growth of cloud droplets through condensation and coalescence. A He-Ne laser beam is shone in a small volume and cloudy air is let into this volume. The size of the particles is detected by measuring the intensity of the light scattered by the cloud droplets and using Mie scattering to relate intensity to drop size. The droplets are distributed in to 15 size bins. The size bins are equidistantly distributed from 3 microns to 47 microns with a bin width of 3 microns.

Larger droplets were measured using an OAP-260X particle counter which has 60 channels from 40 microns to 620 micron with an interval of 10 microns. This measures the larger drops which are drizzle or rain drops. The winds were measured using a flow meter fitted to the radome on the aircraft. PMS King hot wire liquid water probes were used to measure the liquid water content. Most of the data used in an experiment in this thesis to simulate the cloud traversed on 18th March, 1999, called research flight 14, were recorded at 10Hz or 25Hz. Then the data were postprocessed to generate one second averages for most of the variables.

Chapter 5

Simulation of a Deep Convective Event

Because of the complexity of the aerosol activation physics and chemistry, the coupled model simulations are only approximations to the real world processes. To gain confidence in the results of model simulations, comparison of model simulation results with observations of an observed deep convective cloud is the only way to examine whether the predictions of the model can reflect the true nature of the physical and chemical processes.

On March 18th 1999, during the INDOEX Intense Field Campaign, the NCAR C-130 research aircraft flew through a deep convective cloud. The figure 4-1 shows the location of the cloud. The aircraft entered the cloud at a height of about 4000 m and spiralled down in the cloud making almost horizontal passes. As described in the chapter 4, the aircraft was fitted with a huge array of instruments for measuring several dynamical and microphysical fields of clouds.

5.1 Meteorological conditions

Verver et al. [2001] describe the prevailing meteorological conditions during the Indian Ocean Experiment in 1999. The following aspects of the atmosphere corroborate the fact that the atmosphere was conducive for deep convection.

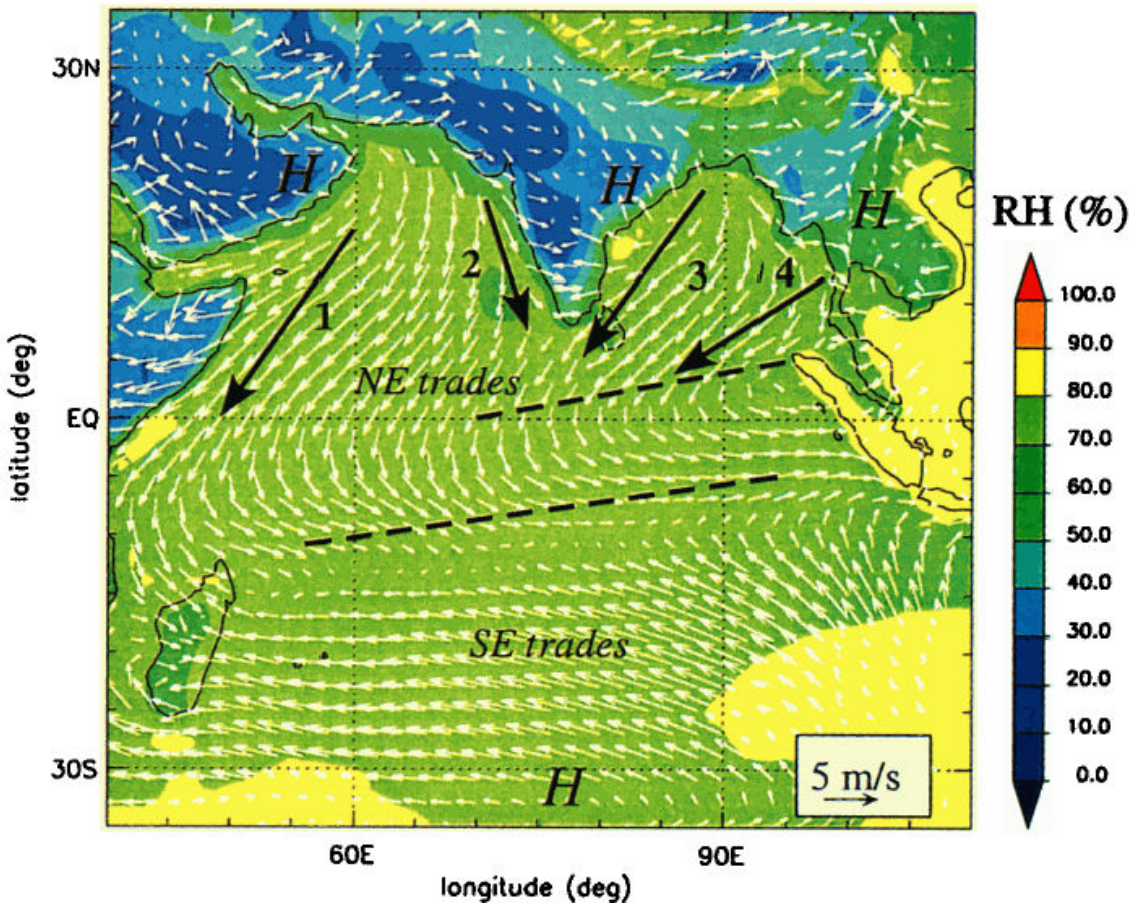

Figure 5-1: ECMWF wind (arrows) and relative humidity (RH, colors) at 1000 hPa; February climatology (1900-1999). Large arrows numbered 1 to 4 indicate the main flow channels. The two dashed lines indicate the location of the two near-equatorial convergence zones. [*Verver et al.*, 2001]

5.1.1 Monsoon circulations

Climatologically, at this time of the year, the Northeast monsoon winds bring the continental air to the equatorial Indian Ocean region. Figure 5-1 shows the February climatological wind and relative humidity in the region.

The flow from Southeast Asia is blocked by Sumatra and enters the eastern equatorial Indian Ocean in a cyclonic flow just north of the equator.

The warm waters of the South East Arabian Sea, the Bay of Bengal and the Sumatra region, in association with the cyclonic low-level North-East trade winds between 70° and 100° E trigger organized oceanic convection in this region.

Also, there are two convergence zones in the INDOEX region. The first is in the Northern Hemisphere along 2° - 5° N which is usually less intense and a second one in the southern Hemisphere. Both these convergence zones are characterized by cyclonic vorticity.

In the convergence zone in the Northern Hemisphere, the wind changes direction from Northeast to Northwest near the equator.

5.1.2 Sea Surface Temperature and ITCZ

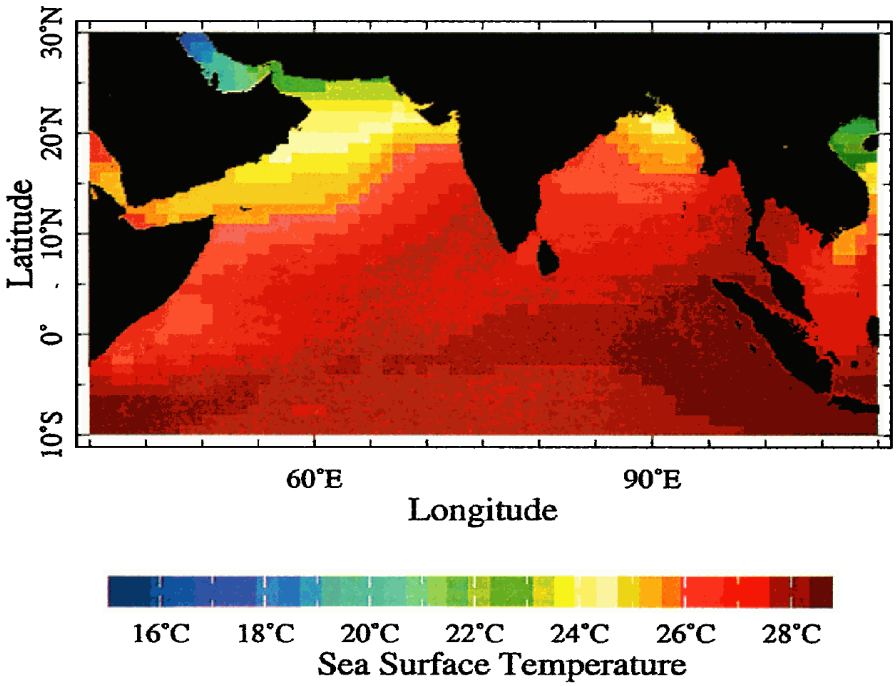

Figure 5-2: Climatological mean sea surface temperatures over the INDOEX region [*Reynolds and Smith*, 1994]

The boundary layer air in tropical marine atmospheres is moistened by the evaporation from the warm sea surface. Sea surface temperature is an important control on the evaporation from the sea surface. Sea surface temperature greater than $27°C$ is a necessary condition for organized convection. But it is not sufficient. Large-scale convergence is another important control on tropical deep convection [*Bjerknes*, 1969; *Graham et al.*, 1987; *K. and Chang*, 1987].

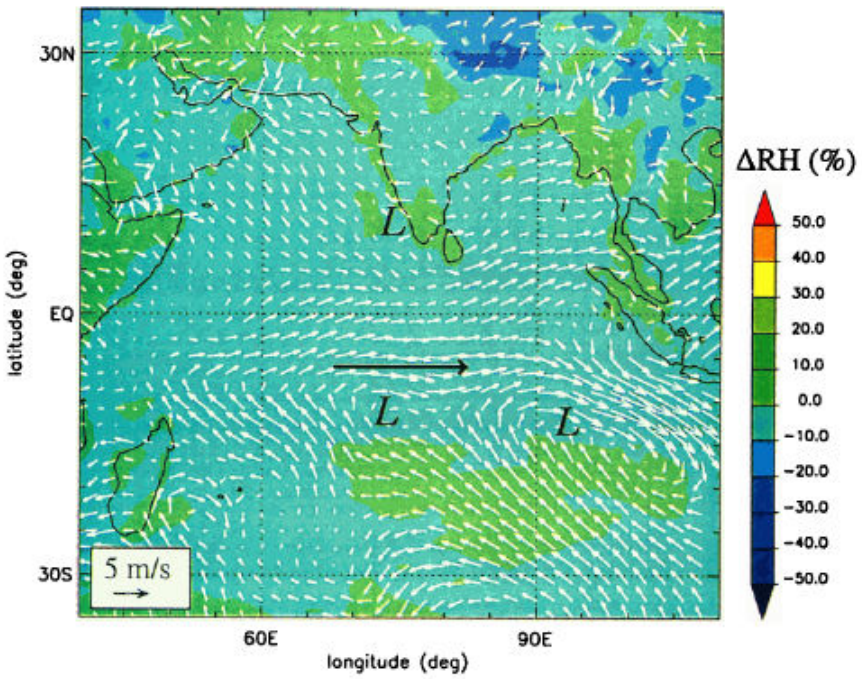

Figure 5-3: Wind (white arrows) and relative humidity (filled contours) perturbations to climatological means in March 1999 at 1000 hPa from ECMWF analyses. [*Verver et al.*, 2001]

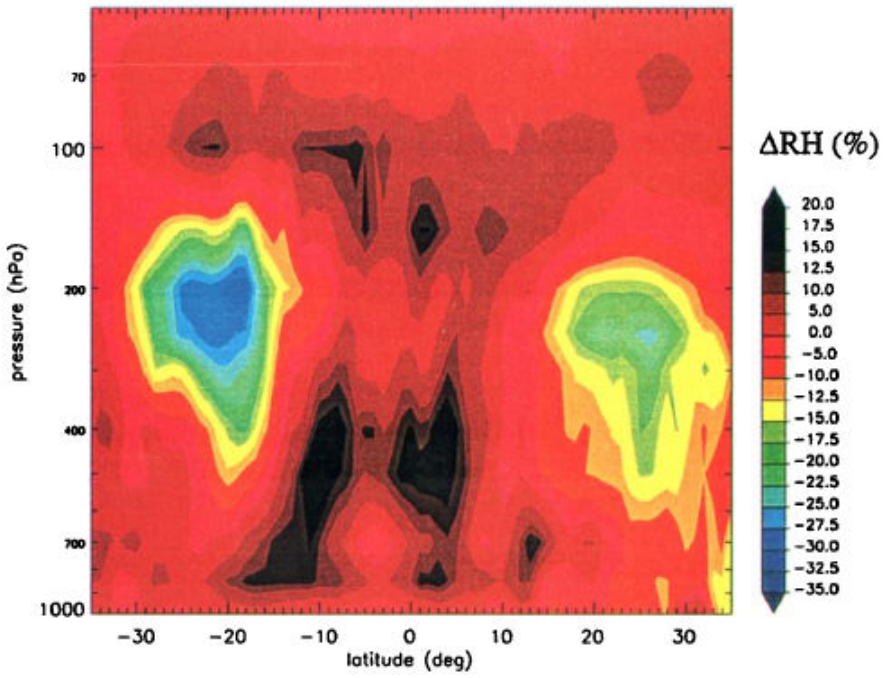

Figure 5-4: Relative humidity perturbation to climatological mean relative humidity cross sections at 75° E for March 1999 from ECMWF analyses [*Verver et al.*, 2001]

From the sea surface temperature plot shown in 5-2, this region shows temperatures above the threshold ($27°C$) throughout the year. And also, the tropical convergence zone is a region of low level moisture convergence. Hence, this region is amenable for deep convection.

5.1.3 Convergence

During March 1999, the low level winds show an anomalous center of cyclonic circulation in the Southeast Arabian Sea and the Male region (70° and $75°E$) and a cyclonic shear zone in the Bay of Bengal. These indicate convergence in the northern intertropical convergence zone stronger than normal with anomalously high convective activity [figure 5-3].

The relative humidity anomalies at $75°E$ shown in the figure 5-4 also point to convergence in the low levels during March 1999.

5.2 Initial Conditions

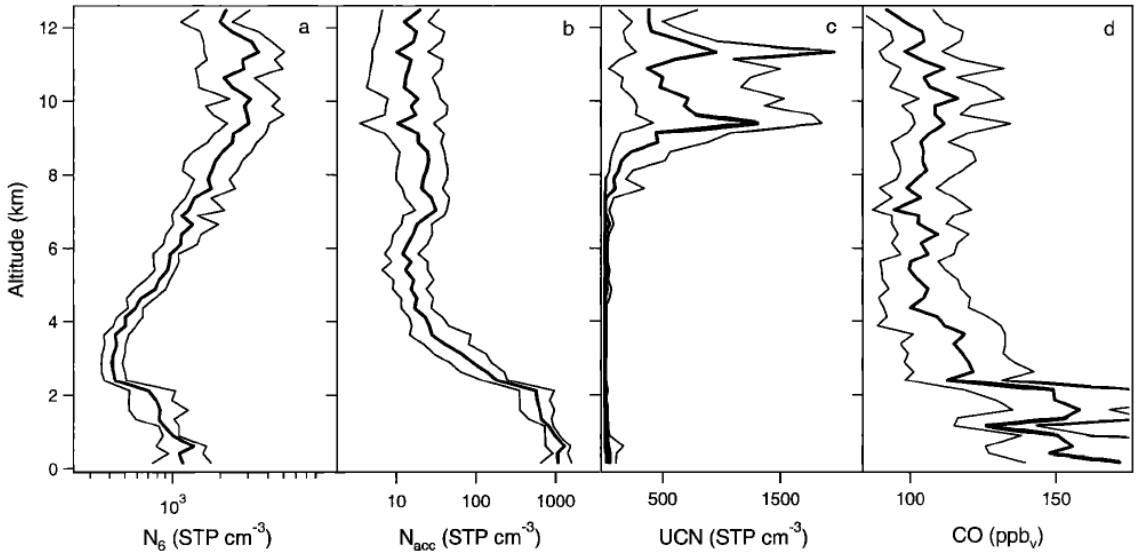

Figure 5-5: Median altitude profiles of (a) submicron, (b) accumulation and (c) ultrafine particle number concentrations measured during INDOEX. The thin lines show the 25th and 75th percentiles [*de Reus et al.*, 2001]

5.2.1 Aerosol Profile

Vertical profile of aerosol concentration has a determining effect on the evolution of a cloud [*Andrews et al.*, 2004; *Adhikari et al.*, 2005], particularly in the context of processes like in-cloud nucleation and cloud processing of aerosols.

Some of the previous aerosol-cloud interaction modeling studies assumed a homogeneous aerosol concentration in the whole domain [*Wang*, 2004, 2005]. This would result in larger concentrations of aerosols in the upper layers of the atmosphere. Some studies considered a vertical profile that is a function of air density [*Ekman et al.*, 2004a].

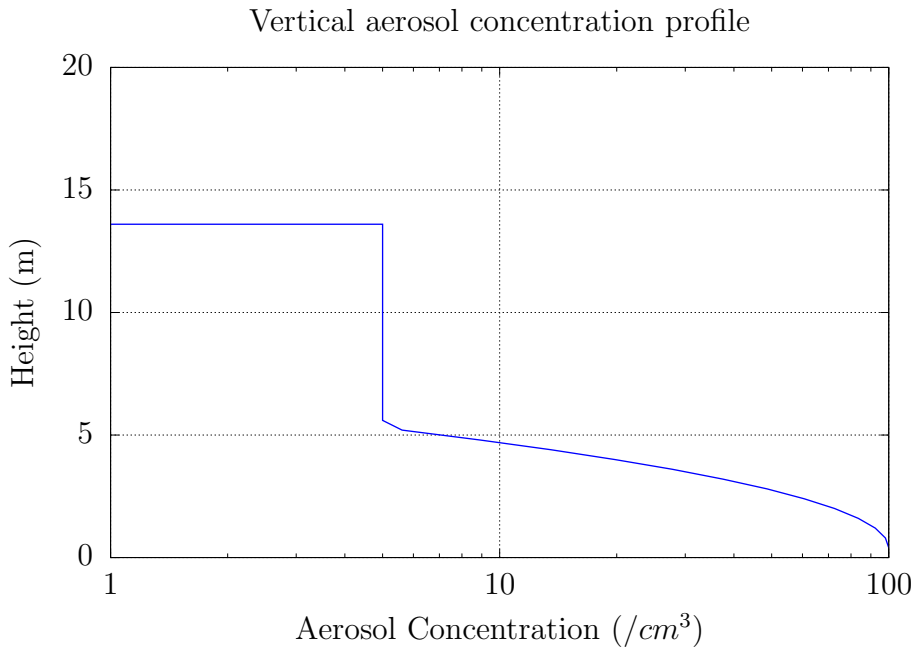

Figure 5-6: The vertical aerosol profile used in the model simulations. This profile is created so as to resemble the observed accumulation mode vertical aerosol profile shown in figure 5-5

Figure 5-5 shows the mean vertical profile of aerosol number concentration [*de Reus et al.*, 2001]. There is a maximum in the boundary layer and decreases rapidly with increasing altitude to a low value at 3.5 Km. For a realistic representation of aerosol profile, this profile is replicated and a Gaussian profile resembling this observed profile is considered. This profile shown in the figure 5-6 is used for all the experiments

in this thesis. The profile is scaled proportional to the aerosol concentration in each case.

5.2.2 Initial Thermodynamic Condition

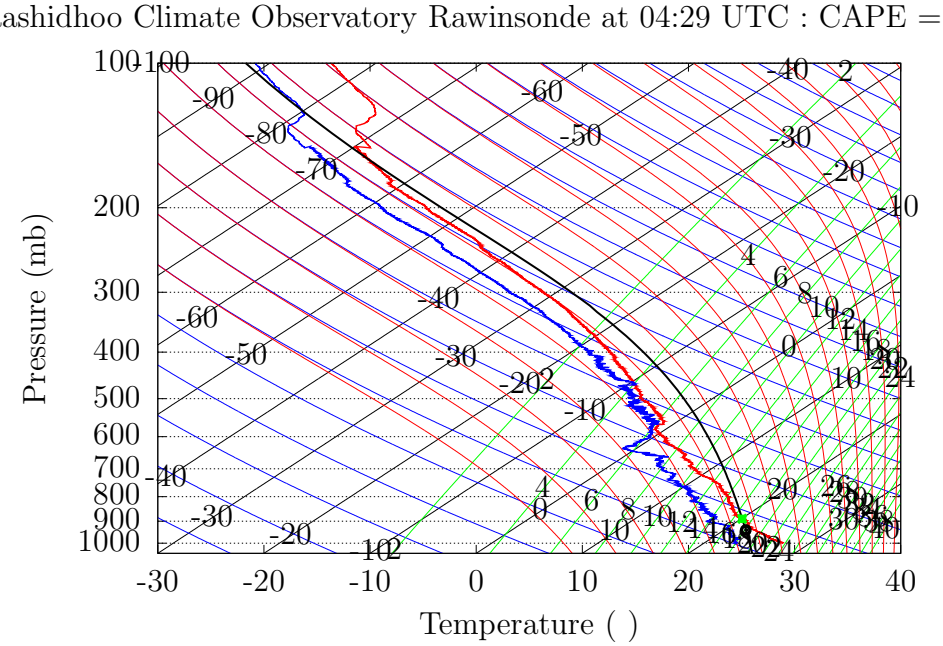

Figure 5-7: SkewT-logP plot of the atmospheric sounding taken at Kaashidhoo Climate Observatory at 04:29 UTC. This sounding has a CAPE of $\sim$ 1200 J/K. The sounding is denoted as ka0429.

On 18th March 1999, when the deep convective event was observed during the INDOEX Intense Field Campaign, a few atmospheric soundings were taken from different platforms close to the cloud. The one nearest in time and space was the one taken from Kaashidhoo Climatological Observatory at 05.57UTC. The cloud was observed at around 09.15 UTC. Usually, dropsondes are used to sound the atmosphere from aircrafts but for that particular research flight, RF14, no sondes were dropped.

The coupled aerosol-activation-cloud-resolving model is initialized with the initial thermodynamic condition of the atmosphere consisting of the vertical profile of temperature, pressure, water vapor and zonal and meridional winds.

Table 5.1: Model configuration

Dimensions	3
Basic time step	5 seconds
Vertical boundary condition	Rigid lid
Domain	dx = 2000 m dy = 2000 m dz = 400 m
Grid Points	60 50 50
Initial met fields	R/V Brown sounding
Convection initiation	One bulb
Aerosol bins	5
Salt bins	0
Aerosols	$(NH_4)_2SO_4$
Vertical aerosol profile	based on profile observed during INDOEX

The skewT-logP plot shown in figure 6-2 shows the vertical profile of temperature(red line) and dew point (blue line) as a proxy for water vapor mixing ratio. The black dot is the lifting condensation level and the green dot is the level of free convection. The black line is the moist adiabat through the lifting condensation level. This sounding profile has a convective available potential energy of 1200 J/Kg.

This atmospheric sounding is used as an initial thermodynamic condition to initialize the coupled model.

5.3 Model Configuration

Table 5.1 shows the configuration of the model used for simulating the deep convective cloud. The model was run in three dimensions with a basic time step of 5 seconds. The domain size is 120 Km in the zonal, 120 Km in the meridional and 20 Km in the vertical directions. The grid cell size is 2 Km in both the horizontal directions and 400 m in the vertical directions. So, there are 60 grid points in the zonal direction and 50 in the meridional and vertical directions.

As discussed in the subsection 5.2.2 the meteorological fields are initialized using the atmospheric sounding taken at the Kaashidhoo Climatological Observatory on 18th March 1999 at 04.29 UTC during the INDOEX.

Convection was initialized using a Gaussian bulb of perturbation in potential temperature and water vapor. The initial aerosols were distributed into five bins in the aerosol activation module. The aerosols were assumed to be ammonium sulphate. The vertical profile of aerosols is as shown in the figure 5-6.

5.4 Assumptions

1. The glossary of meteorology defines a cloud as a visible mass of water or ice particles. In the context of this thesis, a cloud is defined as the set of points in space with liquid water content greater than 0.01 g/m^3. Further, King probe which measures liquid water content, has resolution of 0.01 g/m^3. So, it is reasonable to assume that the estimates of microphysical parameters with lower threshold than 0.01 g/m^3 are not very accurate. The mean quantities in this study are computed as the mean of the quantities at these cloudy points.

2. The region around the point of maximum vertical velocity is assumed to be the convective core of the cloud. The distance of each point on the trajectory of the aircraft from a vertical axis drawn at this point of maximum vertical velocity is shown in the figure 5-8.

3. In the model, the cloud microphysics module assumes an gamma distribution for the diameters of the different hydrometeor classes as discussed in the subsection 3.2.2 :

$$dN = N_0 D^b e^{-\lambda D} dD \tag{5.1}$$

4. The cloud droplet concentration was measured using the FSSP-100 probe which measures droplets in the diameter range $2 - 47\,\mu$m. The cloud water contained in the cloud droplets in this range is found by integrating the water content of the drops in each diameter interval.

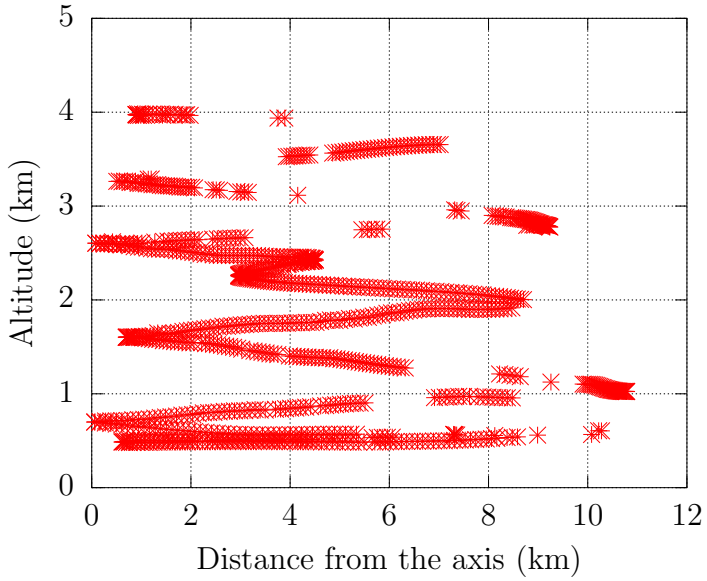

Figure 5-8: The radial distance from the axis of the core. See figs 5-10 and 5-11

Similarly, raindrop (larger drops) concentration was measured using an Optical Particle Counter. The size range of these raindrops as measured by the Optical Particle Counter is $80 - 320\,\mu$m.

So, the size distribution in the model is integrated from $2 - 47\,\mu$m to find the cloud droplet concentration and from $100 - 320\,\mu$m to find the raindrop concentration.

It is to be noted that the distributional parameters – b, λ and N_0 – are different for cloud droplets and raindrops [*Wang and Chang*, 1993].

5. Further, for better statistical comparison of the distributions, the points with concentrations of cloud droplets less than one particle per cubic centimeter and raindrop concentration less than one particle per liter of air are filtered.

6. The instruments FSSP-100 and the Optical Particle Counter count spuriously when larger drops (sometimes precipitation sized particles) splash on the probe of the instruments and breakup. To filter these spurious observations, an upper cut off of 500/L is imposed on the raindrop concentration and 25 g/m^3 on the liquid water computed from the FSSP-100 and the Optical Particle Counter.

Similar filters are applied to those cloud fields in the simulated cloud too.

5.5 Statistical Comparison of the Cloud Fields

5.5.1 Normal Practice

Numerical models have to be validated for their ability to realistically simulate the processes and phenomena under assumed conditions they are built to model. Then they provide confidence to simulate and study hypothetical situations and phenomena.

Towards this end, the simulation results of an event, for instance, a cloud are compared with observations of natural clouds.

One of the fundamental difficulties in such comparison is that convection varies greatly spatially and temporally. The inhomogeneous atmospheric stratification and the boundary layer water vapor flux into the cloud are huge sources of these variations in convection [*Rogers and Yau*, 1989]. These variabilities are very difficult to measure and also to model. So, it is appropriate to compare model results with observations using statistical methods.

As a general comment, *Rogers and Yau* [1989] stress that cloud modeling is still a developing technique and there are uncertainties about the robustness of the boundary conditions, initialization schemes and parameterizations. So, one can not assume too greater confidence or discouragement from a particular comparison of model results and observations.

Several researchers used different approaches to compare cloud model simulations to observations. *Guan et al.* [2001] chose to interpolate the model results to observation times and *Guan et al.* [2002] sampled the observations toward the model's spatial resolution. *Vaillancourt et al.* [2003] tried not to change the model or observation data. They eliminated the instances when the model completely misrepresented the observations and when it did well, they compared point to point, although it is a severe test when the errors and uncertainties in the initial conditions, parameteriza-

tions are kept in view.

The most common method of comparison is comparing snapshots in time and space.

In the present context,

1. the observations are very sparse in time. In fact, only one deep convective cloud was sampled.

2. the observations are abundant in the limited aircraft track.

3. the model results are limited in space and time compared to the observations.

5.5.2 Organization of the Data into Altitude Levels

Figure 5-9 shows the trajectory of the aircraft in the (longitude, latitude, altitude) space. The figures 5-10 and 5-11 show the same trajectory in (longitude, altitude) and (latitude, altitude) spaces. From these figures, it is clear that the aircraft entered the cloud at an altitude of about 4200 m and spiralled down to reach the boundary layer at 500 m. During this traverse, the aircraft measured horizontal profiles in the cloud.

In these figures, the assumptions listed in the section 5.4 are considered (implied).

Following assumption 2, an axis is assumed at the point of maximum vertical velocity. The longitude and latitude of this point are (72.231° E,3.588° N). If we draw a vertical line through this point, the result is the red line in the figures 5-11, 5-10. The figure 5-10 shows that the longitudinal extent of the cloud is about 0.1 longitudes wide, that is, about 11 km wide. Similarly, the red line in the figure 5-11 shows the axis passing through the point of maximum vertical velocity. Figure 5-11 shows that the cloud is 0.1 degrees of latitudes wide, that is about 10 km wide.

Figure 5-8 shows the radial distance of the different points on the aircraft trajectory from the axis drawn at (0,0). This figure shows that the girth of the cloud is about 10 km and at an altitude of 3-4 km, it is about 7 km. The aircraft, as can be seen in figure 5-8, makes passes and reaches the 'axis' as defined above at the heights

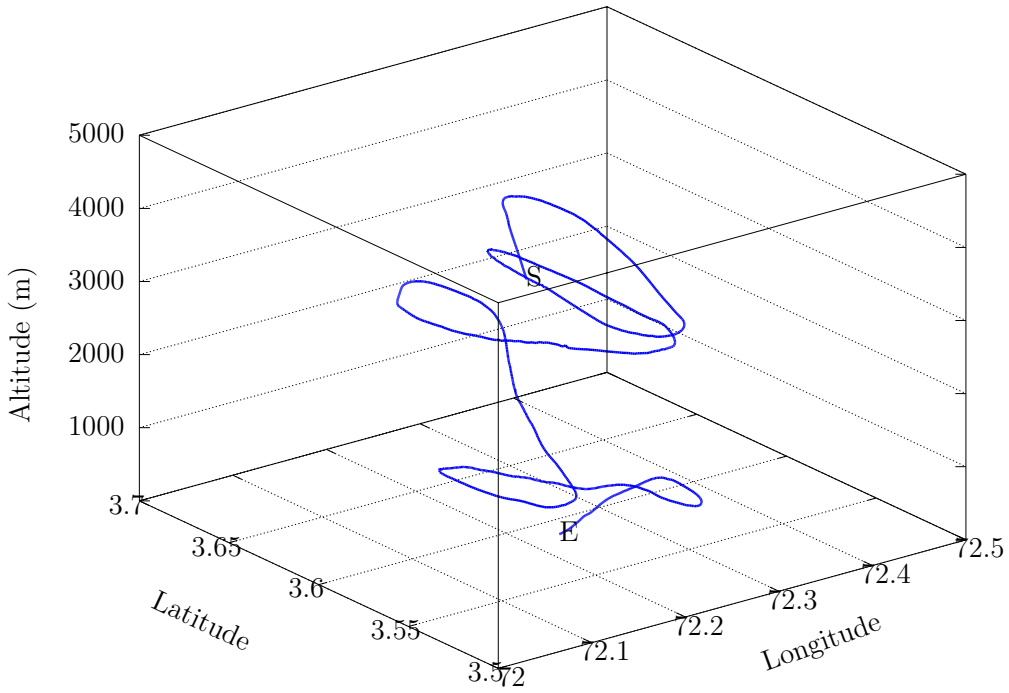

Figure 5-9: 3D trajectory of the aircraft inside the cloud. The aircraft enters the cloud at the start of the trajectory (blue curve) indicated by 'S' and leaves the cloud at $\sim 400\,\mathrm{m}$ at the point denoted by 'E'.

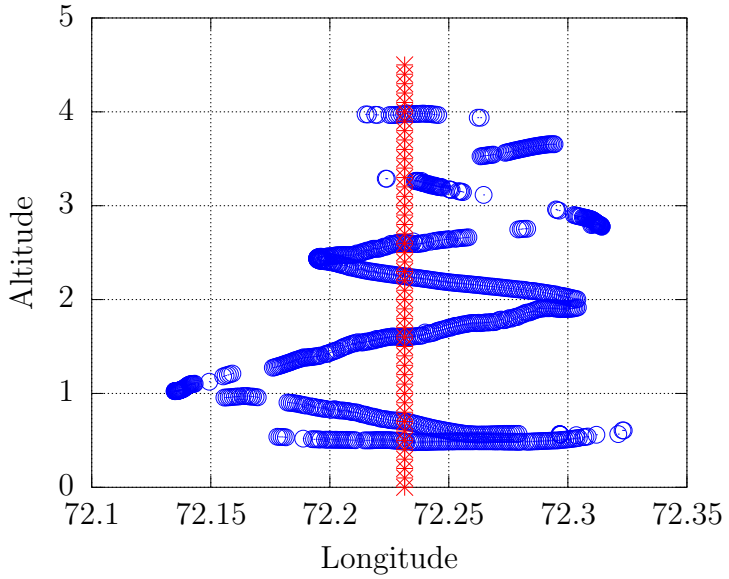

Figure 5-10: The cloudy points (with liquid water $> 0.01\,\mathrm{g/m^3}$) in the trajectory of the aircraft in the (longitude-altitude) space. The red vertical line shows an imaginary vertical axis through the point of maximum vertical velocity. The red line is assumed to coincide with the axis *convective* core of the cloud.

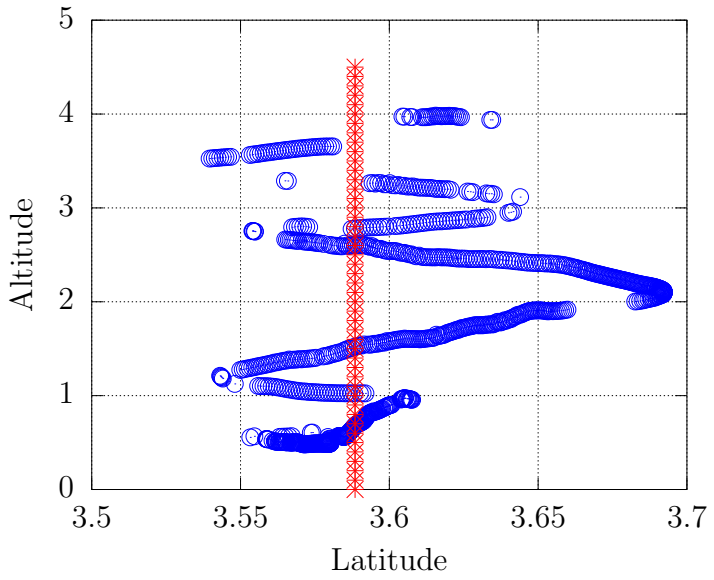

Figure 5-11: The convective core in the Latitude-Altitude space. (See in figure 5-10)

Aircraft altitude	Model altitude
m	m
400–1000	800
1200–2000	1600
2400–2800	2600
3000–3500	3200
3600–4200	4000

Table 5.2: Table of aircraft altitudes and the corresponding model altitudes for comparison. Aircraft altitudes are continuous and the model has discrete levels

800, 1600, 2600, 3200, 4000 m. The next subsection will discuss the mean properties of the observed at these cloud altitudes. For the purpose, the points in the altitude ranges in the following table are considered for the corresponding height level.

The model results will also be sampled at these heights for comparing model results and observations.

5.5.3 Mean Properties of the Cloud

Size The aircraft which measured this observed cloud entered the cloud at an altitude of about 4200 m and spiraled down to reach the boundary layer at ∼500 m. During this traverse, the aircraft made almost horizontal passes in the cloud.

Following the assumption 2 in the section 5.4, a vertical axis is assumed at the point of maximum vertical velocity within the cloudy region and the normal distance of each point on the trajectory of the aircraft from this vertical axis is shown in the figure 5-8. This plot shows that the horizontal diameter of the cloud is ∼ 20 Km.

Vertical Velocity The figure 5-12 is the vertical profile of vertical velocity observed by the aircraft. It shows that the convective activity as measured by vertical velocity is greater in the levels 1.5 km and above. The heights at which there is large variability correspond to the heights of horizontal passes listed in the table 5.2. Particularly, the updrafts and downdrafts at the 2600 m height are the largest (updraft 14 m/s and

downdraft $\sim 6m/s$).

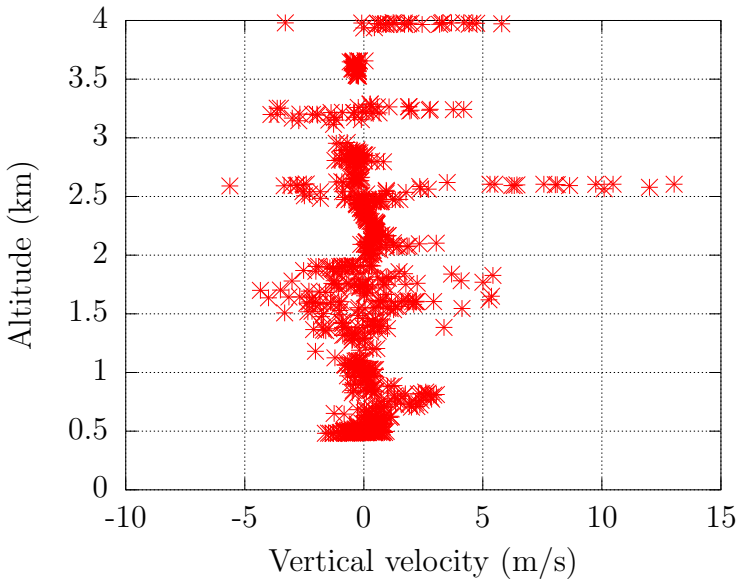

Figure 5-12: Vertical profile of vertical velocity in the lower 4 Km of the domain. The stars show the vertical velocity at the 'cloudy' points.

The distribution of vertical velocity at the different height levels in the table 5.2 are shown in the figure 5-13. There are greater updrafts and downdrafts at $\sim 2600m$.

Cloud Droplet Concentration The figure 5-14 shows the vertical profile of cloud droplet concentrations as measured by the FSSP-100 probe which measures cloud droplets in the diameter range $2 - 47\mu m$. The concentrations decrease from the higher levels to the lower ones. Large concentrations in the lower two levels (~ 800 m and ~ 1600 m) are due to

- possibly secondary cloud formation and the consequent new activations of aerosols or
- the counting error by the spectrometer probe when larger precipitation-sized particles (drizzle drops) splash on the probe and the spectrometer counts the broken drops. This phenomenon of miscounting the large drops as multiple small drops is documented in 'FSSP-100 manual'[1]. If it were new activations,

[1] `http://www.eol.ucar.edu/raf/Bulletins/B24/fssp100.html`

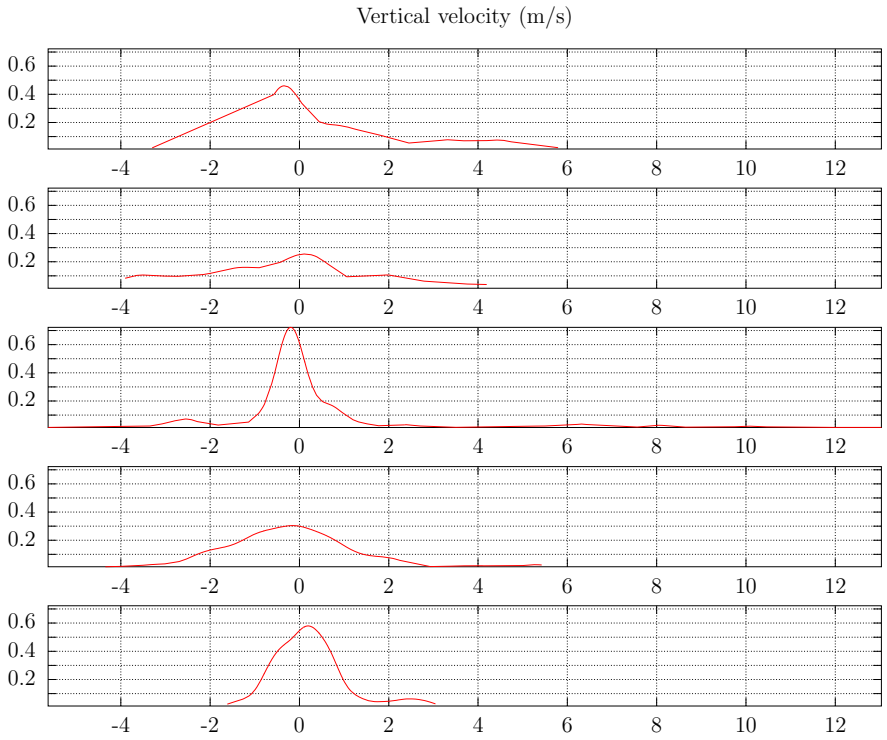

Figure 5-13: Distribution of vertical velocity at each level simulated by the model.

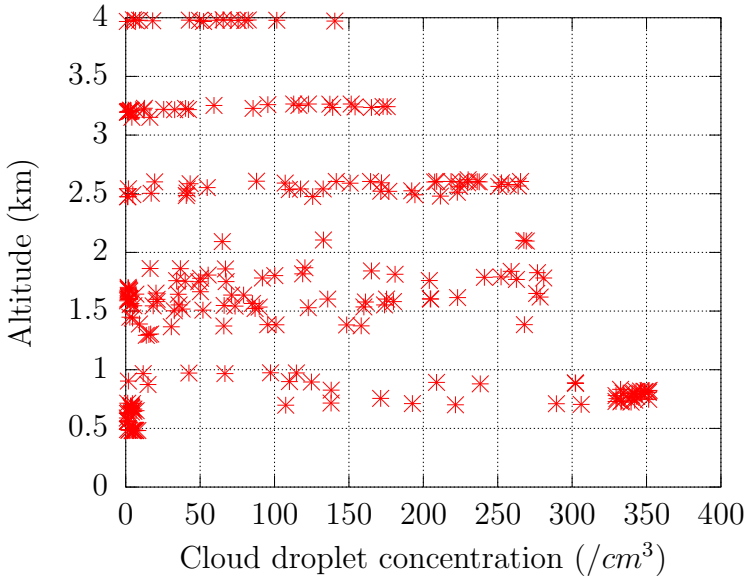

Figure 5-14: Observed vertical profile of cloud droplet concentration. The concentrations decrease with height.

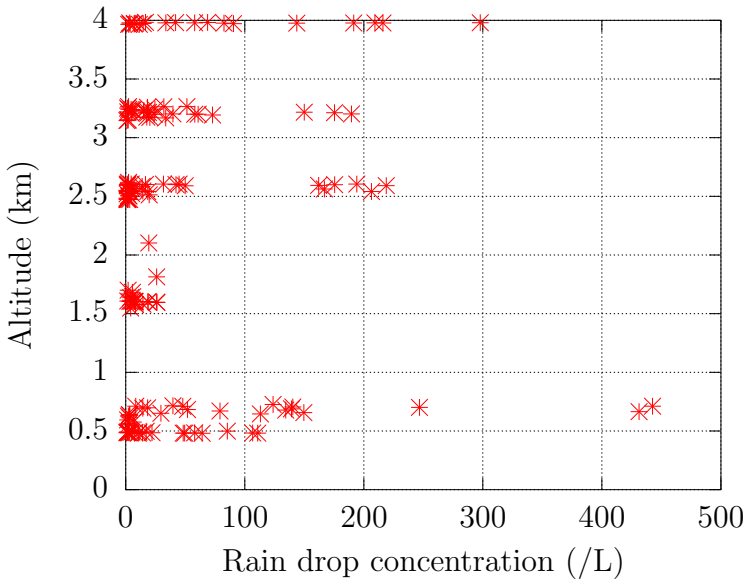

Figure 5-15: Observed vertical profile of raindrop concentration. The concentrations increase with altitude because the cloud droplets have favourable size for collision-coalescence as altitude increases.

the most probable level is at $\sim 2600m$ where the updrafts are considerably large which result in faster cooling and hence greater supersaturations.

Raindrop Concentration Figure 5-15 is the vertical profile of raindrop concentrations a measured by Optical Particle Counter which measures raindrops in the range $40\,\mu m$ to $620\,\mu m$. The concentration decreases from higher levels to lower ones except the lowest ones in which it records huge values of concentrations of raindrops.

Heymsfield (Personal communication, May 15, 2009) estimated the age of the cloud when the aircraft entered the cloud at an altitude of $\sim$ 4200 m to be about 40 minutes and the cloud had a well-formed anvil by then. He was aboard the aircraft.

The cloud droplet concentration and the raindrop concentration profiles, when considered together, point to secondary cloud formation as speculated above in 'cloud droplet concentration', when new cloud droplets are formed by activation at lower levels and hence greater concentration at the lower levels and the concentration decreases with altitude and collision-coalescence produces greater concentration of raindrops at

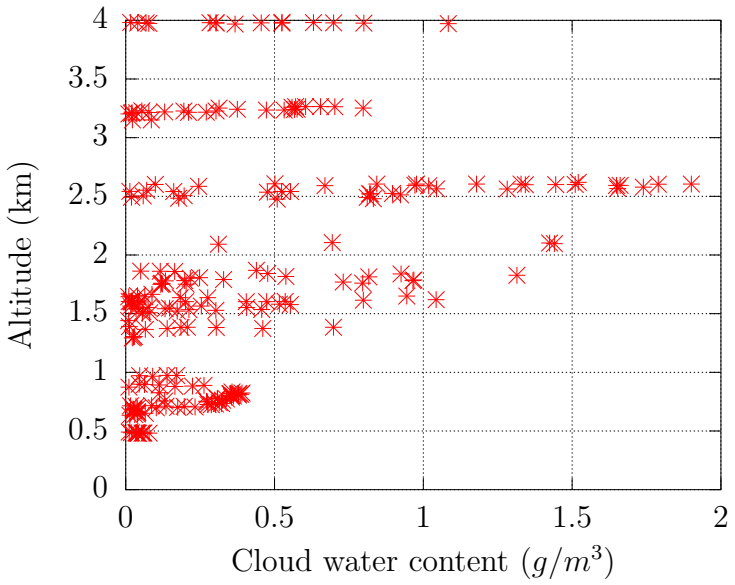

Figure 5-16: Observed vertical profile of cloud water content. The cloud droplets are larger as altitude increases, so, they have greater water content.

the higher levels and as the altitude decreases the process becomes inefficient as the cloud droplet diameter decreases towards lower altitudes as is evident from the plot 5-21.

Cloud and Rain Water Contents The vertical profile of cloud water content, shown in figure 5-16, increases from the lower levels upwards as the cloud droplet concentration [figure 5-14] increase and as the cloud droplets are efficiently converted into raindrops in the upper layers as discussed above. The vertical profile of rain water, shown in the figure 5-17, increases from the level of $\sim 3200m$ and up. And also, as the cloud droplets which are formed in the lower levels are advected in the vertical wind, they condense more water and grow to larger sizes. Thus the cloud water content in the upper layers is greater. But because of efficient collision-coalescence, the cloud water content in the top there levels is less than that in the next two levels.

The liquid water content shown in the plot 5-18 was measured by King probe. King probe measures the liquid water content by measuring the electric power spend in evaporating the intercepted liquid droplets/drops. Thus, it measures the water

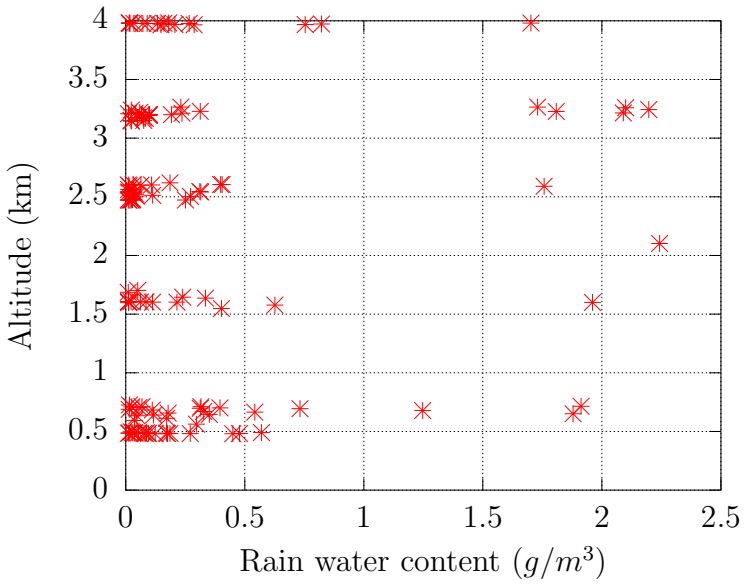

Figure 5-17: Observed vertical profile of rain water content

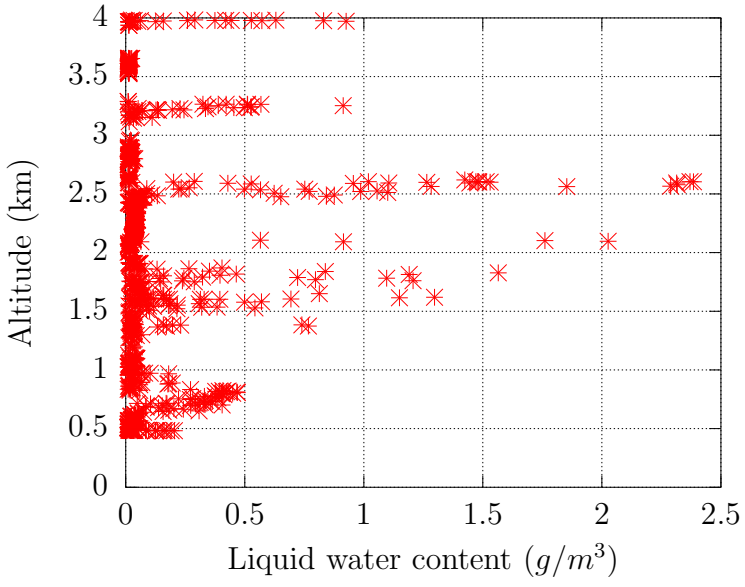

Figure 5-18: Observed vertical profile of total water content

content of the whole size spectrum of cloud droplets and raindrops where as, the cloud water content and rain water content are the water contents in the drop size ranges measured by FSSP-100 and OPC (refer to those in the data).

There is a mismatch between the rain water inferred from integration of the drop size spectrum from the optical practice counter and the total liquid water measured by King probe in the lower levels.

Cloud and raindrop Sizes Cloud droplet diameters increase from lower levels to upper levels as shown in figure 5-19. The aerosols are activated in the lower levels and as these cloud droplets are lofted by the updrafts condense water vapor because of raised supersaturations due to adiabatic cooling.

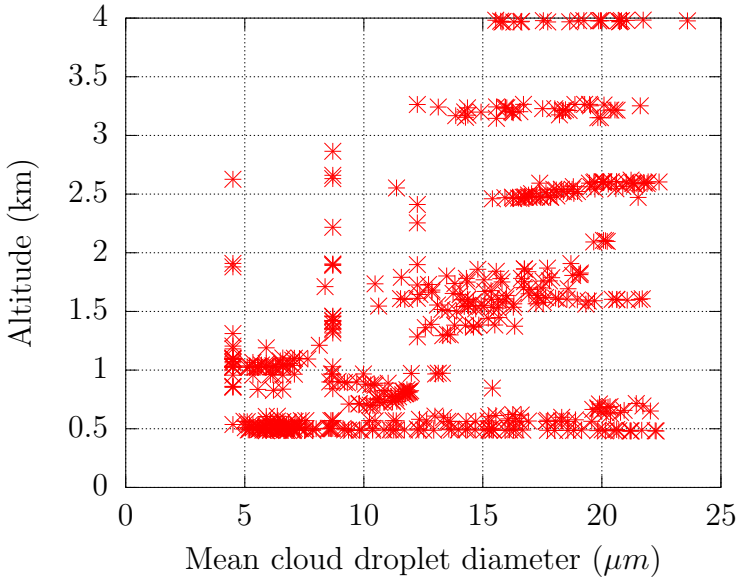

Figure 5-19: Observed vertical profile of cloud droplets diameter. Cloud droplet diameter increases with altitude.

Figures 5-21 and 5-22 show the kernel density smoothed size distributions at the five levels discussed in the table 5.2. The histogram of cloud and raindrop diameters are smoothed using a Gaussian kernel [*Wilks*, 2006]. The plot shows the normalized frequency distribution of the cloud and raindrop diameters at each height level.

They show that the cloud droplet diameter distributions shift towards larger diameters with height. But the raindrop diameters increase from top level to the lower

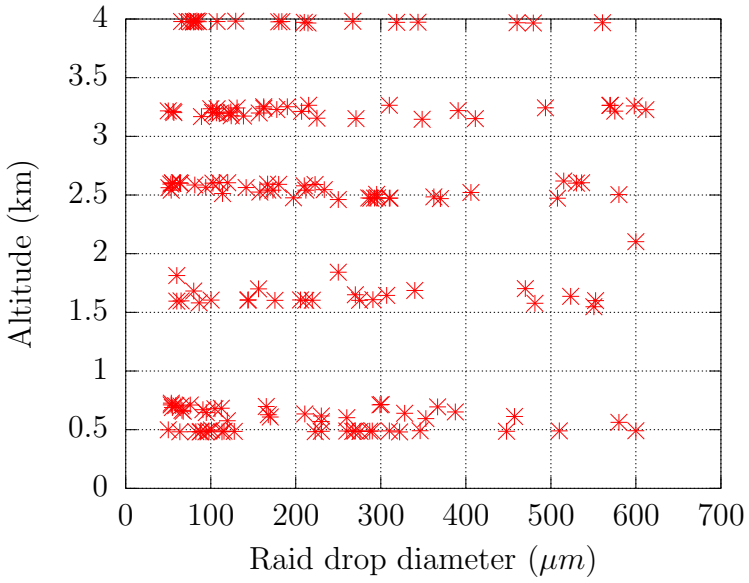

Figure 5-20: Observed vertical profile of raindrop diameter

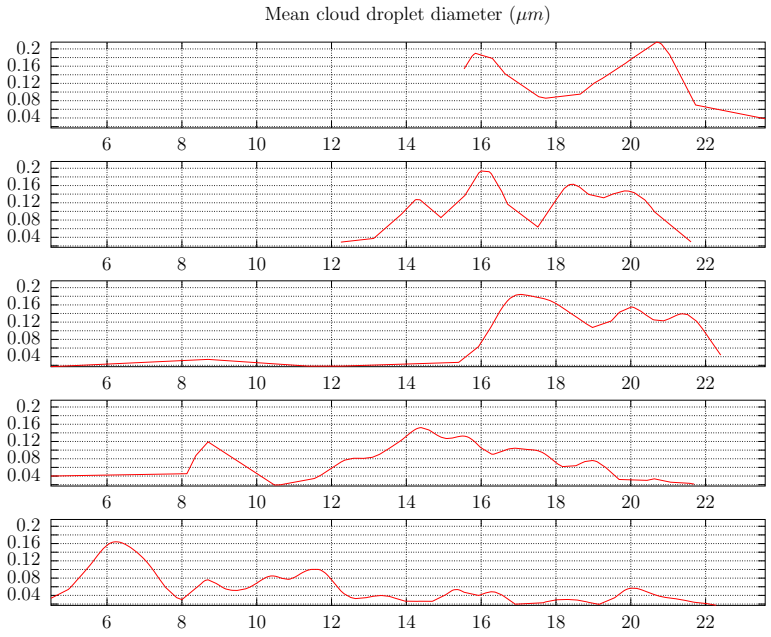

Figure 5-21: Distribution of cloud droplet diameter at each level. Cloud dropletdiameter decreases with altitude.

ones as they collect other drops while falling. The cloud droplets form at the lower levels and the raindrops form at the higher levels. The cloud droplets are lofted up by the updrafts and the raindrops fall due to larger terminal velocities. So, these observations are helpful to consolidate some of the theoretically known facts about cloud and raindrop formation and growth.

5.5.4 Sampling of the Model Results

In view of the constraints discussed in subsection 5.5.1, a straight point-to-point comparison of the simulated cloud fields and the observations is not possible. But still, an attempt is made to sample the model data so that the aircraft trajectory is simulated in space and time.

In addition to the assumptions in the section 5.4, the following filters are used to sample the model data to reflect the same data quality control and the aircraft trajectory as for the observations.

1. The mean cloud droplet and raindrop diameters are computed from the size (diameter) distributions of cloud droplets and raindrops integrated respectively in the ranges $2 - 47\mu m$ and $40 - 620\mu m$ as these are the measurement ranges of the FSSP-100 and the Optical Particle Counter.

2. To correspond to the heights of horizontal passes as in the table 5.2, the corresponding height levels are chosen from the model domain as shown in the table 5.3

   The modelled values at each level in the table are combined for each cloud field. For this purpose, at each height level, the grid points 25 to 35 in x (zonal) and 21 to 29 in y (meridional) direction are considered.

3. The aircraft did not observe thee different levels simultaneously. It entered the cloud at $\sim 4200m$ and spiralled down the cloud. It took about 22 minutes for observing this cloud.

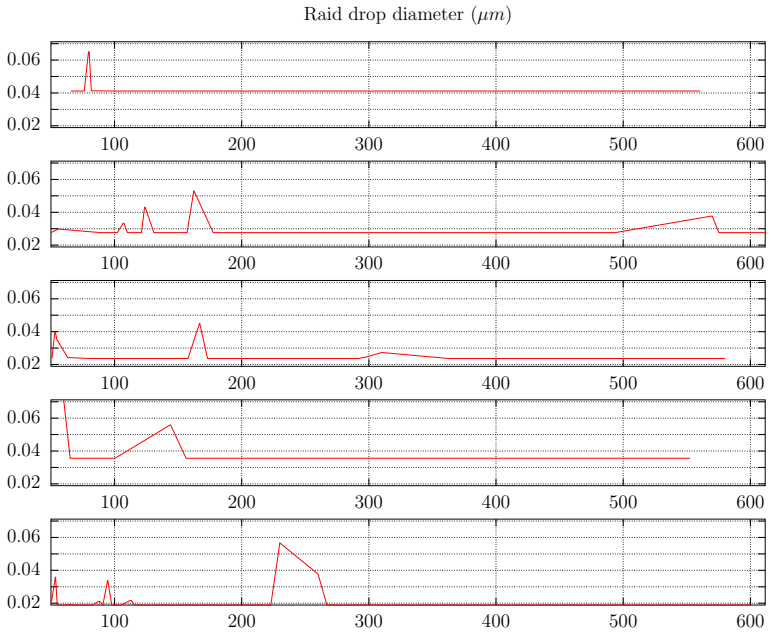

Figure 5-22: Distribution of raindrop diameter at each level

Aircraft altitude (m)	Model altitude (m)
400–1000	800
1200–2000	1600
2400– 2800	2400 & 2800
3000–3500	3200
3600–4200	4000

Table 5.3: Correspondence between aircraft and model altitudes

Levels	Time steps
5	23:26
4	26:28
3	28:31
2	32:34
1	35:37

Table 5.4: Levels and the model time steps chosen as the average times during which those levels are traversed

Further, from visual observation of the cloud from the aircraft, the age of the cloud was inferred to be about 40 minutes (Heymsfield A.J., personal communication, May 15, 2009) and also, there was a well-formed anvil.

The quantities of observed and modeled cloud fields at each height level were computed and the mean square difference between the quantiles of observations and model results at each of the levels are calculated at each model time step. These plots show that the mean square distance between the quantiles of observations and model results is a minimum between the 20th and 37th time steps, that is, from 40th minute to 70th minute of the evolution of the cloud. So, based on these mean square quantile difference plots, earlier time steps are used for higher levels and the levels are gradually translated in time. That is, the time steps shown in the table 5.4 are used. It is hoped that the time steps and the levels chosen as described would represent the trajectory of the aircraft sufficiently well.

5.5.5 Statistical Test

Because of the arbitrariness of the aircraft trajectory and the randomness of cloud motions in space and time, it is very difficult to find the underlying theoretical distribution of the observation samples. Further, the sample sizes of the model results and the observations are also not constant. So, a non-parametric test which is ro-

bust to sample size is an apt one to assess the confidence of simulating the observed cloud. The null hypothesis assumed for the test is that the observations and model simulated cloud field values come from the same underlying distribution. To test this hypothesis, one of the more robust non-parametric tests is the Mann-Whitney U test (also called Mann-Whitney-Wilcoxon rank-sum test).

The assumptions of the test are :

1. the observations and model simulated results are independent and also, the data points in the observations and model results, individually are independent. This is true because the measurement of cloud fields at one point in the aircraft trajectory does not depend on the measurement at any other point. Similarly, the cloud fields data at different points in the model domain can be assumed to be largely independent.

2. The observations and model simulated results are numerically comparable, that is, if a datum O from observations and a datum M from model results are chosen, one can determine if O>M or O<M or O=M.

3. The variances of the observations and model results samples at each level are approximately equal.

Computation The test statistic of this test is usually represented by U. The following sequence of steps elucidates the computation of U. For an illustration, I consider the vertical velocity W at level 5. For the purpose of illustration, let the sample of observations be wobs5 and the sample of the model results be wmod5.

1. Consider between wobs5 and wmod5, the sample with the lower sample size, for instance, wobs5.

2. Considering each data value in wobs5, count the number of data values in the other sample, wmod5, that are smaller than it.

3. The total of the counts for all data values in sample wobs5 is the test statistic U. Thus the test statistic U is not a function of the data values themselves, but

Levels →	1	2	3	4	5
Vertical Velocity	0.00	0.53	0.27	0.59	0.35
Cloud droplet concentration	0.69	0.62	0.59	0.94	0.09
raindrop concentration	0.00	0.24	0.61	0.00	0.00
Cloud water content	0.12	0.44	0.00	0.08	0.00
Rain water content	0.00	0.99	0.24	0.71	0.56
Cloud drop diameter	0.17	0.03	0.04	0.73	0.58
raindrop diameter	0.24	0.00	0.00	0.01	0.66

Table 5.5: p-values of the Mann-Whitney test for the observations and model results

their ranks within the sample data values that are pooled.

The null distribution of the Mann-Whitney test statistic U is approximately Gaussian [*Wilks*, 2006] with

$$\text{Mean} = \mu_U = \frac{n_1}{n_2} \tag{5.2}$$

and

$$\text{Standard deviation} = \sigma_U = \frac{n_1 n_2 (n_1 + n_2 + 1)^{\frac{1}{2}}}{12} \tag{5.3}$$

where $n_1 = n_{wobs5}$ and $n_2 = n_{wmod5}$ are the sample sizes of the observation and model results. Within this Gaussian distribution, the standard Gaussian value corresponding to the observed test statistic U is determined. The p-values are determined in the present experiment at a confidence level of 95%. Table 5.5 shows the p-values determined and those with the grey background show the non-rejection of the null hypothesis with a confidence greater than 95%, that is the p-value is greater than 0.05. The null hypothesis is : *the observations and model simulated values of the particular cloud field at the particular height level come from the same underlying distribution.*

5.5.6 Discussion

Table 5.5 shows the p-values of Mann-Whitney U test for observations and model simulation values of some important cloud fields. Some key inferences that can be drawn from the table are:

1. The observed vertical velocity at the upper four levels is well-correlated with the simulated ones.

2. In spite of the severity of the comparison, in which the observations and model results are compared at each level for having the same underlying distribution, at several levels, several of the chosen cloud fields compare well. This is significant.

3. We see from the table that the cloud water content and drop sizes do not match very well.

4. The cloud droplet number concentration which is simulated reasonably well is a measure of how well the processes leading to activation included in the aerosol activation model model the activation number.

   This test shows that the aerosol activation model simulates the cloud droplet number reasonably well.

5. This table also shows that when the updraft speeds are simulated well, the aerosol activation model simulates the cloud droplet concentration fairly well.

6. To enhance the confidence in the statistical comparison, I performed a permutation test on the observations and model results at the five different levels using Monte-Carlo method to resample from the observations and model results. The test corroborates the results in table 5.5.

7. The sum of mean square distance between quantiles of observations and the model simulated cloud fields show a decreasing trend and a valley between 40 minutes and 74 minutes of cloud evolution in the model which also confirms the results of the comparison.

Some of the possible reasons for the differences between the observations and model simulation are:

- Measurement errors: As discussed earlier, the probes FSSP-100 and OPC, in the event of drizzle or rain overcount the drop concentration.
- The uncertainty in the choice of model grid points to simulate the aircraft trajectory
- The different sample sizes for some of the variables
- Location, size and strength of the perturbation bubble used to initiate convection in the model
- An initial thermodynamic condition 120 km away from the location of the cloud and about 4 hours ahead in time.

These difficulties call for a thorough observation of a deep convective cloud starting from its formation through its evolution.

Chapter 6

Sensitivity of the Model to Initial Thermodynamic Condition

The structure and evolution of a deep convective cloud are strong functions of the wind shear and static stability of the atmosphere [*Houze*, 1993]. The convective available potential energy is a very important measure of the stability of the atmosphere. It is also well known that the aerosol concentration and composition impact the evolution of the cloud during the initial stages [*Rosenfeld et al.*, 2008]. The wind has a greater impact during the later stage of evolution of the cloud, particularly when the cloud has grown to higher altitudes. The present study is restricted to the interaction between aerosols and the initial thermodynamic condition of the atmosphere. The convective available potential energy is given by [*Houze*, 1993]

$$CAPE = g \int_{z_{LFC}}^{z_E} \frac{\theta_z - \bar{\theta_z}}{\bar{\theta_z}} dz \tag{6.1}$$

where θ is the potential temperature of a parcel of air lifted from $z = 0$ to $z = z$ adiabatically, that is, the parcel air does not mix with the ambient atmosphere.

From $z = 0$, the parcel rises dry-adiabatically and once it is saturated, further rise is moist-adiabatic, that is, the equivalent potential temperature is conserved. The level of free convection, z_{LFC}, is the height at which the air parcel is warmer than the ambient atmosphere and the equilibrium level, z_E, is the lowest height where the

potential temperature of the parcel is just the same as that of the ambient atmosphere and hence the parcel is not buoyant any more.

Larger CAPE values mean stronger convection and stronger updraft speeds leading to greater supersaturations. As a consequence, more water vapor is condensed.

Most of the previous studies/experiments in aerosol-cloud-precipitation looked at the impact of change in aerosol concentration. But, as discussed above, the cloud formation and evolution strongly depend on the initial thermodynamic condition. So, it is imperative that the effect of the initial thermodynamic condition on the cloud is assessed in the context of the model used to serve not only as as sensitivity study but also to provide an understanding of the impact on the physical process and mechanisms involved in aerosol-cloud interactions and precipitation formation. Towards this objective, the present section looks at the impact of the initial thermodynamic condition of the atmosphere on a deep convective cloud.

As an air parcel rises, supersaturations are produced due to adiabatic cooling. Then, the rate of change of the saturation ratio is

$$\frac{dS}{dt} = Aw - B\frac{dw_l}{dt} \tag{6.2}$$

where w is the vertical velocity and $\frac{dw_l}{dt}$ is the rate of formation of liquid water. The first term on the right hand side, Aw, represents the growth of supersaturations due to adiabatic cooling and the second term represents the quenching of supersaturation by condensation processes. A and B are coefficients given by [*Rogers and Yau*, 1989]:

$$A = \frac{1}{T}\left(\frac{L_{lv}g}{R_v C_p T} - \frac{g}{R_d}\right) \tag{6.3}$$

and

$$B = \rho_a\left(\frac{R_v T}{\varepsilon e_s(T)} + \frac{\varepsilon L_{lv}^2}{pTC_p}\right. \tag{6.4}$$

where T is the temperature of the parcel, L_{lv} is the latent heat of condensation of water vapor, g is the acceleration due to gravity, R_v is the gas constant for moist air, C_p is the specific heat at constant pressure, R_d is the gas constant for dry air,

Case	CAPE (J/kg)
ka0557	670
ka0429	1200
b1643	1800
ka1209	2700

Table 6.1: CAPEs of the different atmospheric soundings used for the sensitivity study

p is the pressure, ϵ is the ratio of gas constants for dry air and water vapor, and e_s is the saturation vapor pressure at the temperature T. So, the rate of formation of supersaturations in the initial stages of cloud formation when the condensation rates are small are given by

$$\frac{dS}{dt} = \frac{1}{T}(\frac{L_{lv}g}{R_v C_p T} - \frac{g}{R_d})w \tag{6.5}$$

Clearly, $\frac{dS}{dt}$ depends on T to the first order. Here w is dynamically generated due to the condensation of water vapor. Before condensation of water vapor can occur, the vertical velocities resulting from the instability of the atmosphere are important. The atmosphere in some regions of the Indian Ocean during INDOEX did not have sufficient initial vertical velocities and so, the rates of supersaturation generation were very low and hence the activation of aerosols was less less even though those regions had large CCN concentrations(Heymsfield A.J, personal communication, May 15, 2009).

The initial thermodynamic conditions for this study are taken from the INDOEX Intensive Field Campaign. Atmospheric soundings were taken from different platforms like ships, aircrafts and balloons. On 18th March, 1999, the soundings shown in figures 6-1,6-2,6-3,6-4 were taken from the different platforms. The soundings **ka0429**, **ka0557**, **ka1209** were taken at the Kaashidhoo Climatological Observatory at 04:29, 05:57 and 12:09 UTC. The fourth sounding **b1643** was taken from the research vessel Ronald V Brown at 16:43 UTC. Many of the soundings taken on that day were not continuous in height. These four soundings were mostly continuous.

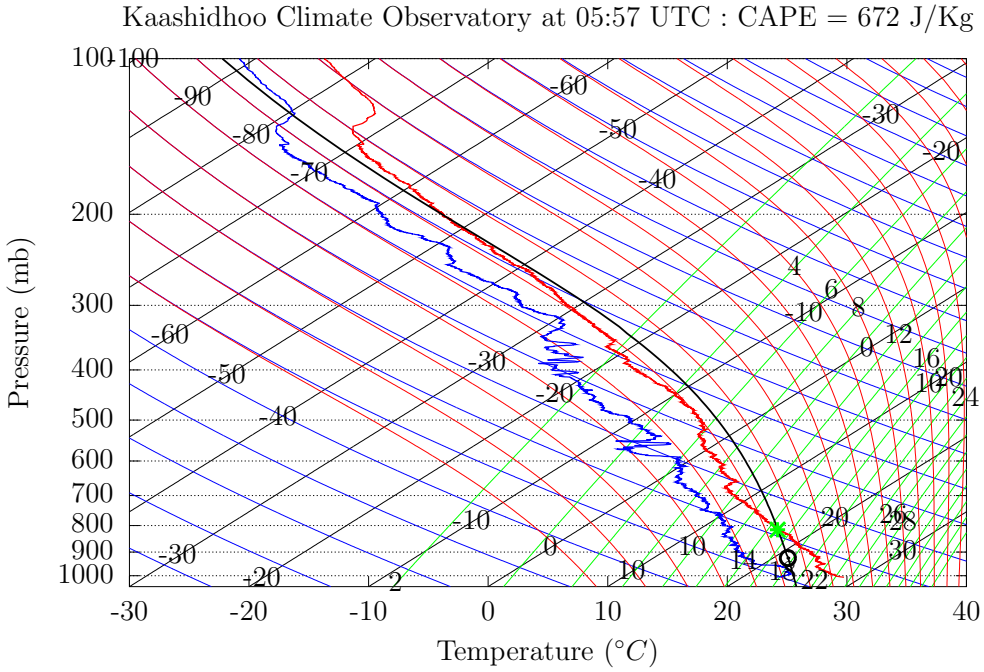

Figure 6-1: SkewT-logP plot of the atmospheric sounding taken at Kaashidhoo Climate Observatory at 05:57 UTC. This sounding has a CAPE of $\sim$ 670 J/K. The sounding is denoted as **ka0557**.

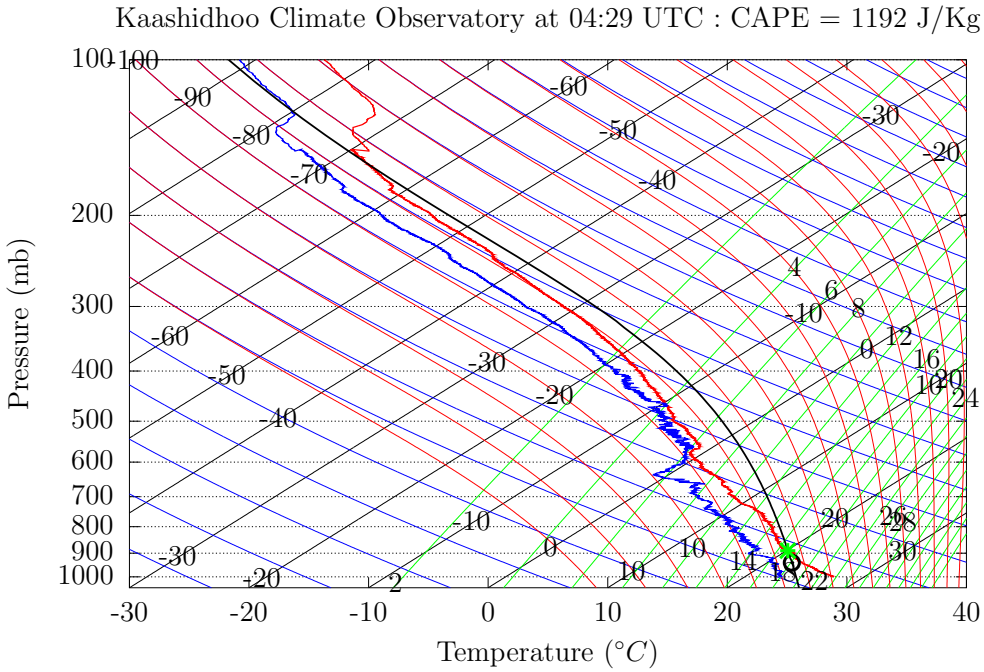

Figure 6-2: SkewT-logP plot of the atmospheric sounding taken at Kaashidhoo Climate Observatory at 04:29 UTC. This sounding has a CAPE of $\sim$ 1200 J/K. The sounding is denoted as **ka0429**.

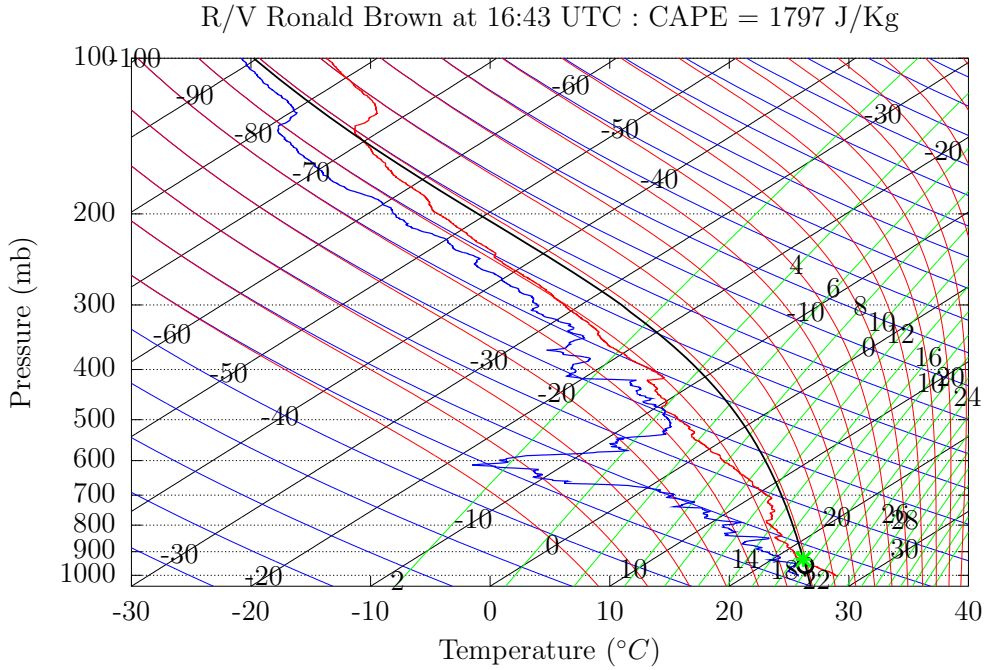

Figure 6-3: SkewT-logP plot of the atmospheric sounding taken from R/V Ron Brown at 16:43 UTC. This sounding has a CAPE of $\sim 1800\,\mathrm{J/K}$. The sounding is denoted as **b1643**.

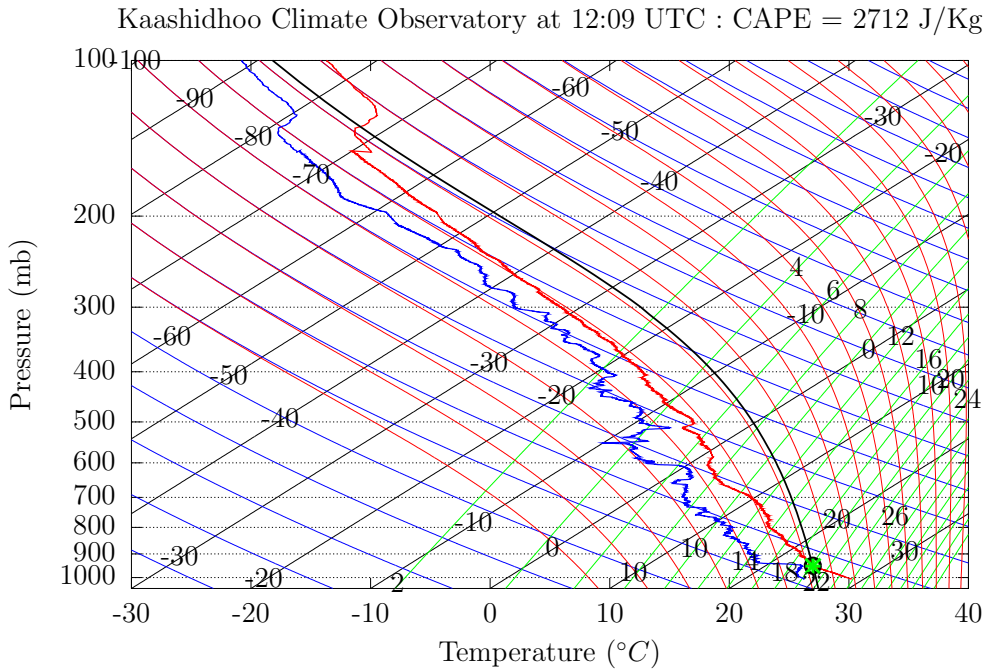

Figure 6-4: SkewT-logP plot of the atmospheric sounding taken at Kaashidhoo Climate Observatory at 12:09 UTC. This sounding has a CAPE of $\sim 2700\,\mathrm{J/K}$. The sounding is denoted as **ka1209**.

To isolate the effect of initial thermodynamic sounding, the background zonal and meridional wind profile and wind shear are kept the same.

The four atmospheric soundings used in this study have progressively increasing convective available potential energy as listed in the table 6.1. A CAPE value of 600 J/Kg is associated with small cumulonimbus clouds, 1200 J/Kg with tall cumulonimbus clouds, 1800 J/Kg with a moderate thunderstorm and 2700 J/Kg with a huge thunderstorm. Thus these four soundings help understand the role of the initial atmospheric structure in building the thunderstorm.

The updraft and downdraft speeds depend on the CAPE of the environment. High CAPE values produce intense updrafts. An intense updraft usually produces an intense downdraft since an intense updraft condenses more moisture and this condensate exerts drag on the vertical motions and decreases the buoyancy. Also, large updraft speeds increase entrainment of dry air from the ambient atmosphere causing cooling and downdrafts.

The figures 6-1, 6-2, 6-3, 6-4 show the skewT-logP plots of the four soundings considered in this study. The sounding **b1643** has a layer of dry air overlying the relatively moist boundary layer with the consequence that there is an added instability in the atmosphere.

6.1 Model Configuration

The model parameters for these runs are shown in the table 6.2. The simulations are all three dimensional with a basic time step of 5 seconds. The domain is $120\,\mathrm{Km} \times 120\,\mathrm{Km} \times 20\,\mathrm{Km}$ and has $60 \times 30 \times 50$ grid points in the zonal, meridional and vertical directions.

The thermodynamic structure of the atmosphere was initialized with the atmospheric soundings discussed above. Convection was initiated using a Gaussian bulb of temperature and water vapor perturbation centered at (30,15,3) grid point. The aerosols were assumed to be composed of only ammonium sulphate and are distributed into five size bins. The vertical aerosol profile is a scaled version of figure 5-6.

Dimensions	3
Basic time step	5 seconds
Vertical boundary condition	Rigid lid
Domain	dx = 2000 m dy = 2000 m dz = 400 m
Grid Points	60 30 50
Initial met fields	R/V Brown sounding
Convection initiation	One bulb
Aerosol bins	5
Salt bins	0
Aerosols	$(NH_4)_2SO_4$
Vertical aerosol profile	based on profile observed during INDOEX

Table 6.2: Model configuration for studying the sensitivity of a deep convective cloud to initial thermodynamic condition.

6.2 Results & Discussion

In the following discussion, I present the dynamical and microphysical structure of the four clouds simulated with different initial thermodynamic condition of the atmosphere but same aerosol concentration, composition and distribution. In these experiments, the mean values refer to the mean over the cloud area as defined in the previous chapter unless defined otherwise.

Vertical Velocity The initial thermodynamic condition has a determining effect on the structure and evolution of a deep convective cloud. The maximum vertical velocity is empirically related to the convective available potential energy as [*Emanuel*, 1994]

$$W_{max} = \sqrt{CAPE}\,\mathrm{m/s} \tag{6.6}$$

So, it is expected that vertical velocity increases with CAPE.

Figure 6-5 shows the mean vertical velocity averaged over the cloudy domain. For the four different cases, the vertical velocities are almost similar during the initial 20

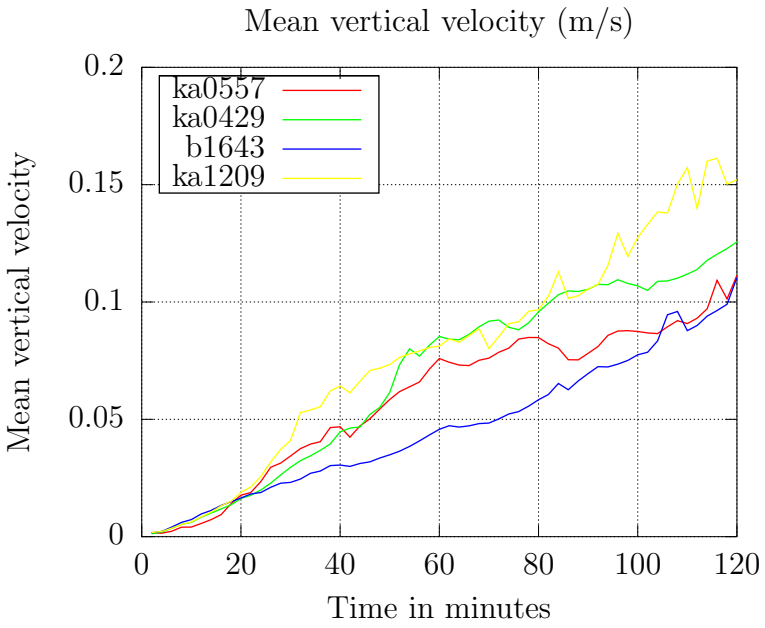

Figure 6-5: Mean vertical velocities in the simulation of the sensitivity of the deep convective cloud to CAPE

minutes. The mean vertical velocities start diverging after the initial precipitation which is a consequence of collision-coalescence. The differences in collision-coalescence efficiencies in the different cases result in the different evolutions of the clouds. The mean vertical velocity increases with CAPE except for the **b1643** case (CAPE = 1800 J/Kg) which has the lowest mean vertical velocity among all the cases in spite of having a higher CAPE. It has the largest maximum velocity and not the **ka1209** (CAPE = 2700 J/Kg) case. This is a consequence of the microphysics as will be seen in the subsequent sections.

6.2.1 Buoyancy

The buoyancy in a cloud is given by

$$B = g(\frac{T^*}{T_o} - -\frac{p^*}{p_o} + 0.61q_v^* - q_H) \tag{6.7}$$

where$B$ is the buoyancy, g is the acceleration due to gravity, T_o and p_o are initial temperature and pressure, p^* and q_v^* are the perturbations in pressure and water vapor mixing ratio from the initial values and q_H is the instantaneous total condensate

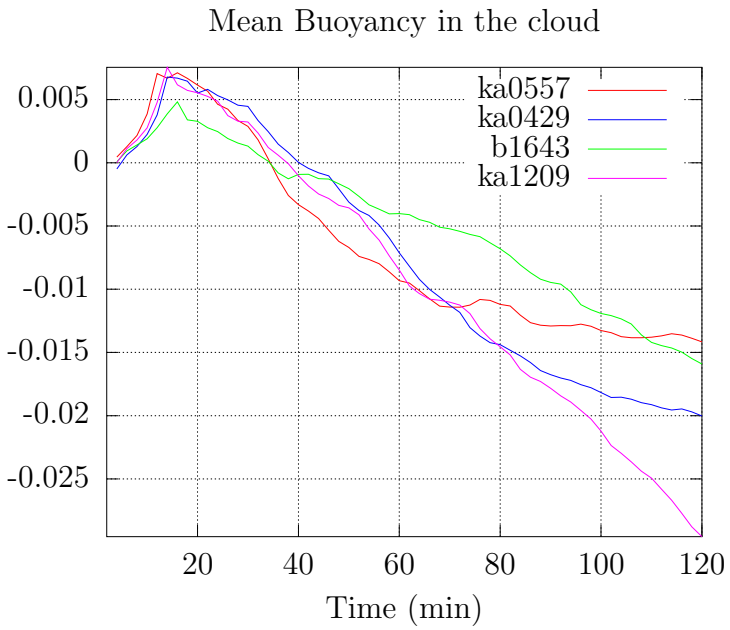

Figure 6-6: Mean buoyancy in the cloud

mixing ratio. (q_H is not the perturbation, but the actual mixing ratio). Unlike in other classes of clouds, in deep convective clouds, the condensate drag on the vertical motion of the cloud is considerable and is of the scale of the other terms in the buoyancy. Also, the pressure perturbation is also of the same order as temperature perturbations. But the pressure gradient force arising out of these pressure perturbations – usually positive pressure perturbation at the top of the cloud and negative below the strong convective core – comes in to play intrinsically as a response to strong vertical motions.

Because buoyancy is such a key characteristic of deep convection which shapes the microphysical and dynamical evolution of the cloud, any process affecting the generation or dissipation of buoyancy will have serious effect on the cloud.

Figure 6-6 shows the evolution of the mean buoyancy computed using the equation 6.7. The buoyancy at each grid point in the domain which can be defined as cloudy if the total condensate concentration is greater than $0.01g/m^3$ of air is calculated and the mean buoyancy is the mean over the cloudy domain. The plot shows that the mean buoyancy is positive during the initial 40 minutes of evolution and becomes negative from then on. From the expression for buoyancy, it can be inferred that buoyancy is lowered due to

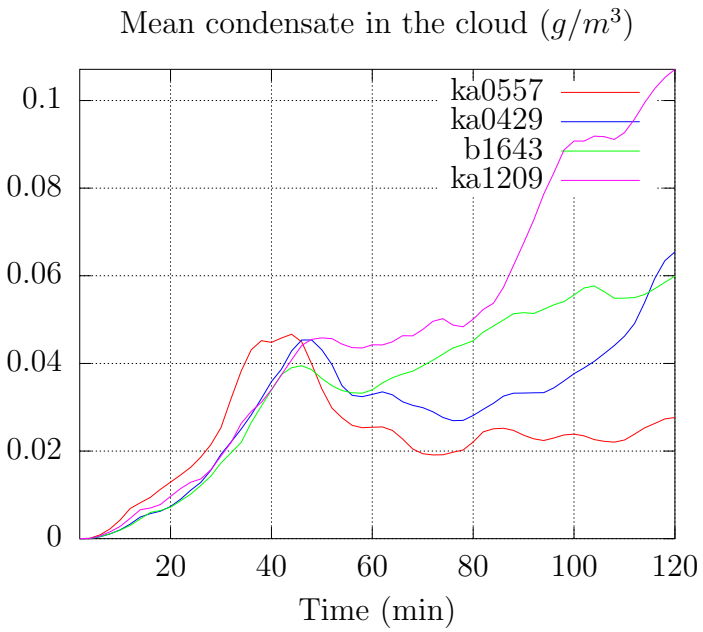

Figure 6-7: Mean condensate mixing ratio

- high pressure gradient which might be a result of strong convergence below the region of strong convection – these high pressure gradients are a consequence of strong vertical motion.

- high condensate (water+ice) which exerts drag on the vertically moving air and retards the motion . In other kinds of clouds, the condensate concentrations are small and as a result, this term is not a dominant sink of buoyancy. In deep convective clouds, because of the large characteristic vertical velocities and the resulting high supersaturations, the condensate loads are more than the stratiform and small cumulus clouds.

In the buoyancy plot 6-6, the buoyancy in the different cases increases initially due to latent heat release and after about 40 minutes when the condensate stops increasing, the latent heat release reaches a steady sate and the condensate drag starts dominating in buoyancy. As a result, the clouds are largely negatively buoyant. The case **b1643** with a CAPE of $1800 J/Kg$ has the least total water content (figure 6-7) during the initial 40 minutes and hence lower latent heat, so, its mean buoyancy is lower. But after 40 minutes, the other cases have accumulated larger amounts of condensate and the resultant drag makes them more negatively buoyant. Also, most of the

condensation happens during the initial 40 minutes in general.

This reversal of buoyancy has important effects on many characteristics of clouds as will be discussed later in this chapter.

6.2.2 Center of Gravity Analysis

The center of gravity of a system is the point in space at which the total mass can be considered to be concentrated, and at which external forces may imagined to be applied. *Koren et al.* [2009] proposed the center of gravity of a cloud as a device to understand the spatial relationships of cloud fields. Also, this is a succinct method to compare different clouds. In this approach, the center of gravity of the cloud is defined as the average position of the cloud fields and the masses are used as weights in averaging. So, in this framework,

$$\text{Center of gravity} = R = \frac{\Sigma r_i m_i}{M} \tag{6.8}$$

where R = coordinates of the center of gravity , r_i = position of each grid point, m_i = mass at each grid point, M = total mass in the domain; and the spread of the cloud is defined as

$$\text{Spread of the cloud} = S = \sqrt{\frac{\Sigma m_i (r_i - R)^2}{M}} \tag{6.9}$$

with the different variables defined as above.

Figure 6-8 shows the center of mas of the four clouds as they evolve. It shows that as deep convective clouds evolve, most of the condensate is in the upper or middle troposphere. Further, because the vertical velocities in the case **b1643** are lower than in the other three cases, it has much of its water in the middle and lower troposphere. It should be noted that **b1643** has more rain water and total condensate than **ka0557** (CAPE = 670 J/Kg) and **ka0429** (CAPE = 1200 J/Kg). But because of lower condensate drag, those cases have higher vertical velocities and hence the cloud droplets and rain drops are lofted to greater heights.

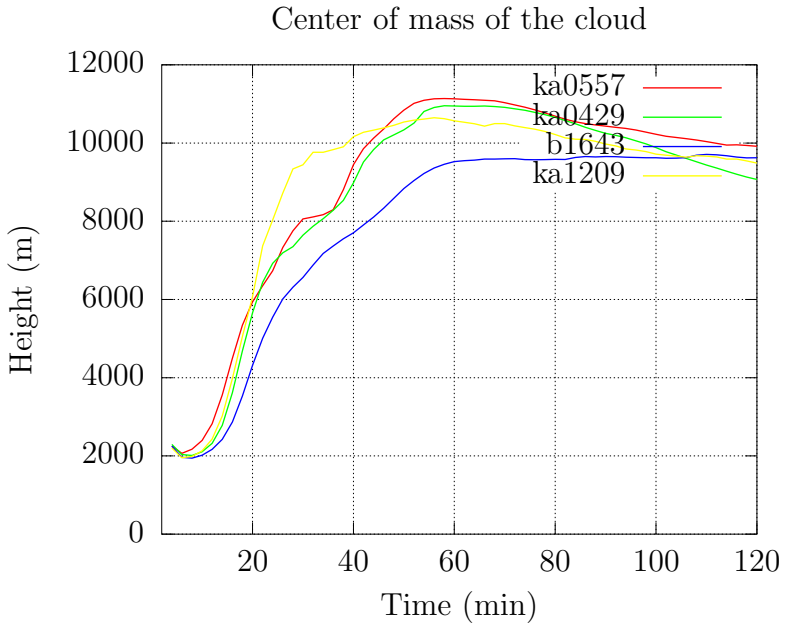

Figure 6-8: Center of mass of the cloud, defined as the height at which the whole condensate can be assumed to be concentrated.

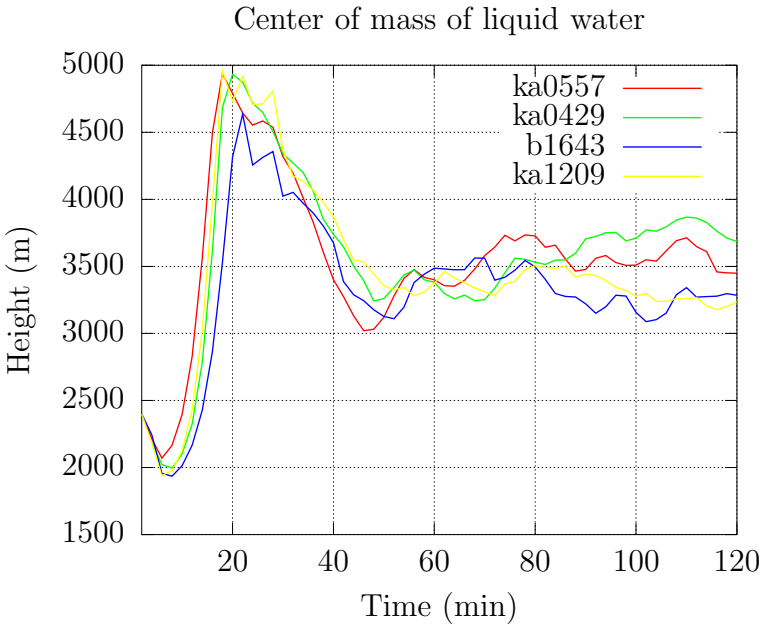

Figure 6-9: Center of mass of the liquid water

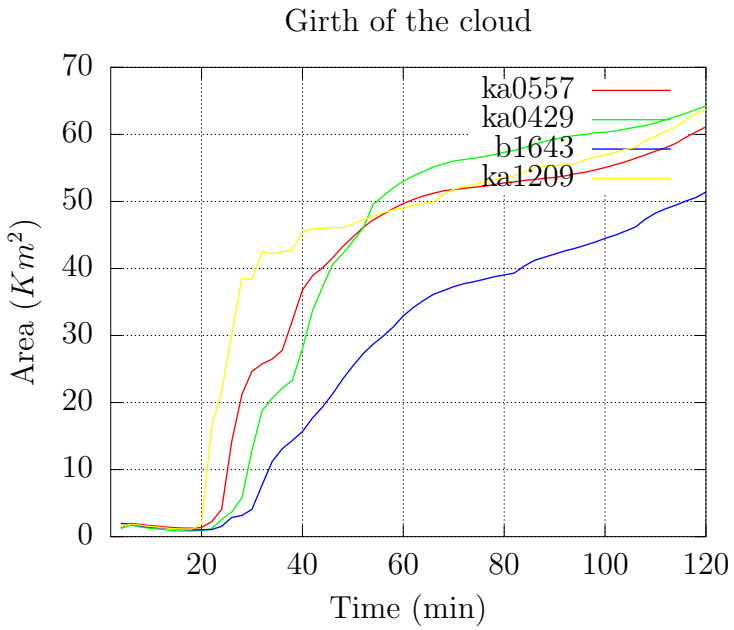

Figure 6-10: Horizontal spread of the cloud

Further, the centers of mass of the total condensate (figure 6-8) and the centers of mass of of liquid water (figure 6-9) show that a large fraction of the cloud mass is in ice phase. The horizontal spreads of the clouds as defined by the spread about the center of gravity (equation 6.9) and as shown in figure 6-10 are larger for the cases **ka0557**,**ka0429** and **ka1209** and **b1643** is leaner in structure. Because the former cases have larger mean updrafts (figure 6-5), they develop larger downdrafts leading to secondary cloud formation and the spread of the cloudy area.

Drop Sizes The cloud droplet sizes in the four different clouds simulated are shown in figure 6-11. The clouds with larger vertical velocities (**ka0557** and **ka0429**) make larger supersaturation and the cloud droplets grow to larger sizes. But as was seen in subsection 6.2.1, these cases do not sustain those large supersaturations longer. But the case **b1643**, which has sustained vertical velocities throughout the simulation time of two hours maintains the supersaturations longer and so, the droplet size is almost constant.

The mean rain drop size (figure 6-12) is larger in the lowest CAPE case **ka0557** and the highest CAPE case **ka1209** during the initial 20 minutes. The mean cloud

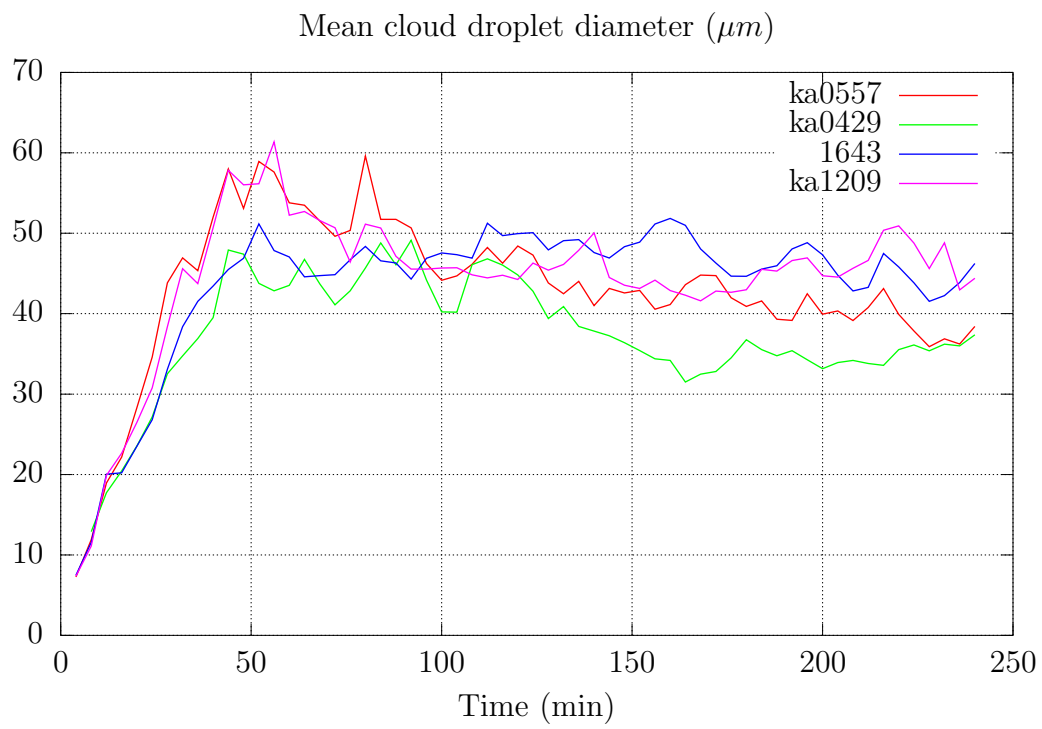

Figure 6-11: Mean cloud droplet radius

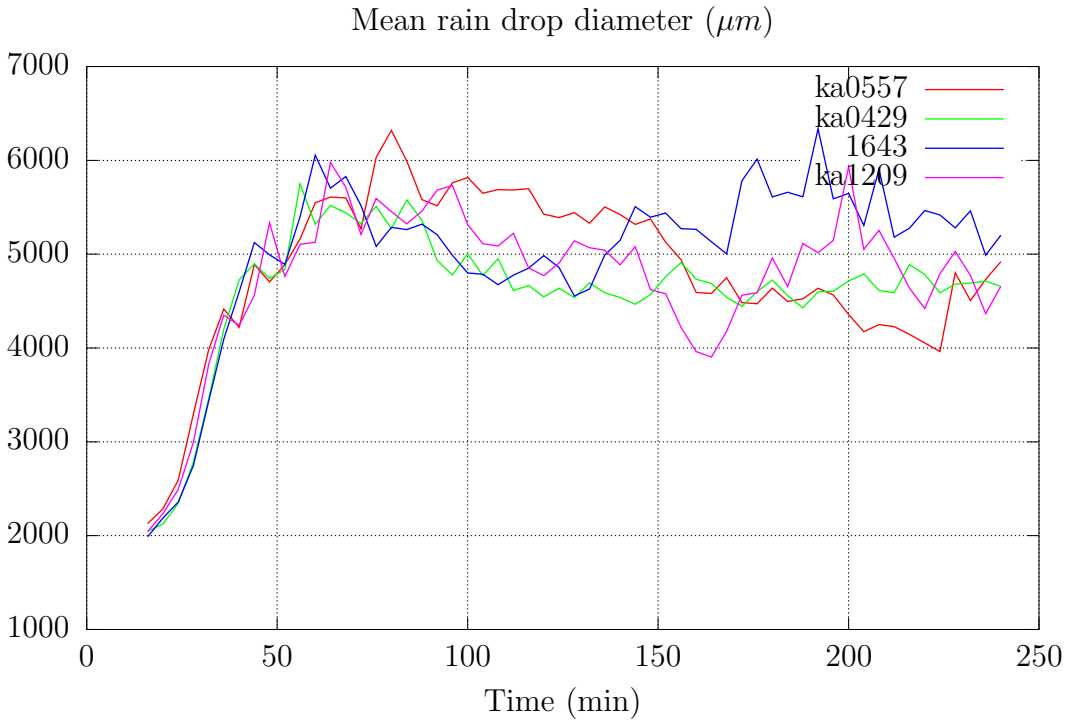

Figure 6-12: Mean rain drop radius

droplet sizes in these two cases are the largest during that time (figure 6-11).In the **ka0557** case, the CAPE is low so, the velocities are small and the aerosols have larger lagrangian times in regions of supersaturation and in the **ka1209** case, with the highest CAPE, the supersaturations are large even though the lagrangian times of the particles might be small. From 40 minutes to 80 minutes too, the larger rain drop size in the lowest and highest CAPE cases continues. But after 80 minutes, collision-coalescence becomes less efficient in the **ka0557** (low CAPE) cloud while at the same time, because of larger cloud drop size in the **b1643** case, collision-coalescence is very efficient and as a result, its rain drop size is the largest.

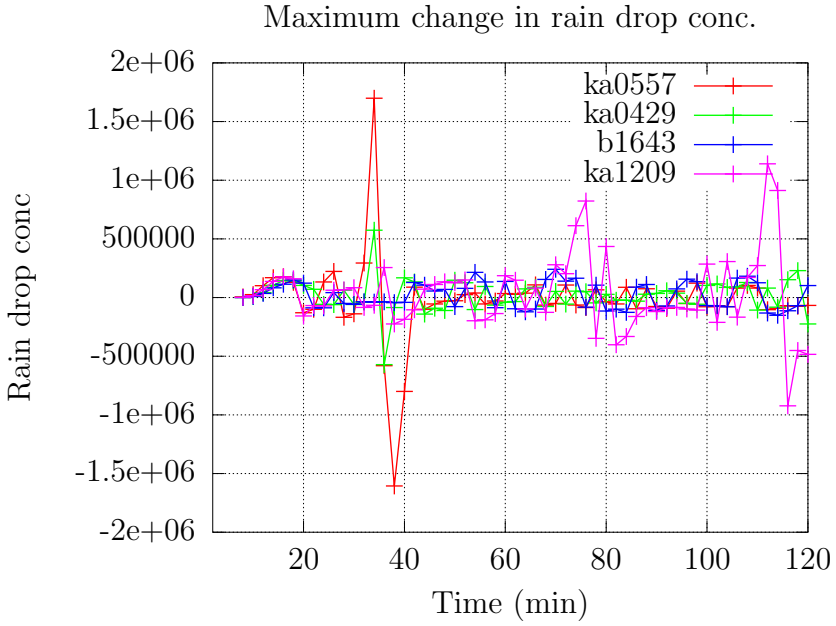

Figure 6-13: Maximum rain drop concentration change. During the initial 60 mins, the case with the lowest CAPE has maximum change in rain drop concentration indicating effective collision-coalescence whereas during the later 60 minutes, the case with the heighest CAPE shows the greatest variations. But the variations in **ka1209** are lower and numerous than those in **ka0557** indicating formation of secondary clouds.

Collision-coalescence is a dominant process in the low-CAPE and high-CAPE cases. The plot of the maximum change in rain drop concentration (figure 6-13) also corroborates. During the initial 40 minutes, **ka0557** case has vigorous collision-coalescence and during the second half of the simulation time, the high-CAPE **ka1209** has stronger rain drop formation as shown in the figure. But in the case of the high-

CAPE cloud, the strong convection results in high downdrafts which cause saturation of air in the boundary layer and lead to secondary clouds.

Precipitation Precipitation cannot form by condensation processes alone in which water vapor condenses to liquid or ice particles [*Rogers and Yau*, 1989]. Precipitation formation in convective clouds essentially involves collection processes: collection of liquid particles by liquid particles, collection of ice particles by ice particles or collection of liquid particles by ice particles. One of the dominant process in which precipitation sized particles are formed in convective clouds is collision-coalescence, that is, the collision between cloud droplets and subsequent sticking together to form a larger drop such that the larger drop has sufficient terminal velocity to reach ground.

The efficiency of collision-coalescence depends on

1. the concentration of the cloud droplets: the larger, the more efficient the process

2. the size of the droplets: the collection efficiency for drop-drop collisions were estimated theoretically and observed in laboratory studies by several researchers. Figure 2-5 shows the field of geometric collection efficiency is defined commonly as

$$E_{LS} = \frac{R^2}{(r_l + r_s)^2} \tag{6.10}$$

where πR_2 is the area swept and $\pi(r_L + r_s)^2$ is the area swept by the collector-collected particles. It is to be noted that $R^2 \sim r_L^2$ as the swept area is impacted by the nature of hydrodynamic motions of the collector particle and the hydrodynamic motion is dependent on the flow field around the drop and the deformation of the drop.

The plot of collision efficiencies (figure 6-14) shows the theoretical collision efficiencies of drops in calm air as functions of the small drop radius and the large drop radius. Some key observations from this plot are:

1. Collision efficiency increases with the small drop radius and the large drop radius.

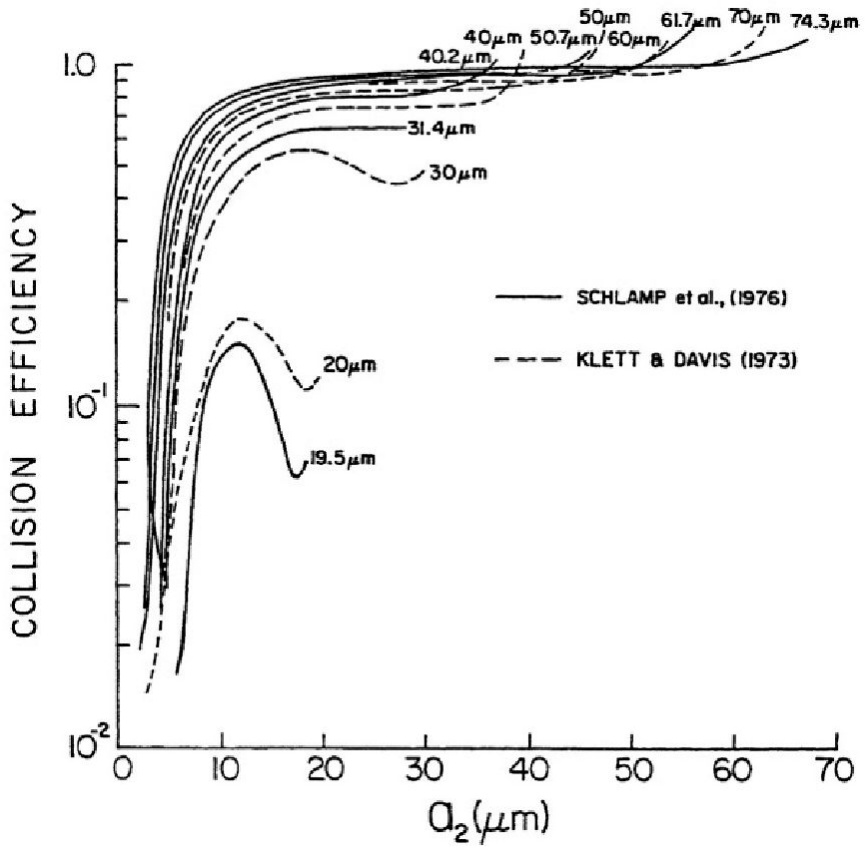

Figure 6-14: Theoretical collision efficiencies of spherical water drops in calm air as a function of collector drop (large drop) radius and the collected drop (small drop) radius. The collector radius is given by label of each curve) [*Pruppacher and Klett*, 1998]

2. For each large drop radius, there is a cut off small drop radius below which the collision efficiency is negligible.

3. As the collector radius increases, the above mentioned cutoff small drop radius decreases, i.e. the larger large drops collide with the smaller small drops more efficiently than the smaller large drops.

4. The collision efficiency for collector drops larger than $40\mu m$ is ~ 1.0 for small drop radii greater than $15\mu m$.

Table 6.3 shows the precipitation from each of the simulated clouds and the relevant mean physical quantities which are important in precipitation formation.

		Simulations			
		ka0557	**ka0429**	**b1643**	ka1029
CAPE	J/Kg	670	1200	1800	2700
Aggregate Condensate	$\times 10^{10} Kg$	2.03	2.67	2.57	3.87
Aggregate Precipitation	$\times 10^{8} Kg$	1.62	1.94	2.60	2.75
Precipitation Efficiency	%	12.51	23.46	28.40	26.80
Cloud droplet diameter	μm	43	38	43	44
Rain drop diameter	mm	4.83	4.61	5.02	4.80
Cloud droplet conc.	$\times 10^{7}/m^{3}$	1.63	1.78	1.80	1.72
Cloud water content	g/m^{3}	0.19	0.18	0.24	0.24
Rain drop concentration	$/L$	4.81	4.30	5.13	7.58
Rain water	g/m^{3}	0.38	0.35	0.47	0.56
Ice content	g/m^{3}	0.04	0.04	0.04	0.05

Table 6.3: Precipitation related mean values for the different cases. The aggregates are the total values summed over the domain for the simulation time. Other quantities are domain mean values averaged over the simulation time.

The aggregate condensate is the total water vapor that has condensed into water or sublimated onto ice. As the convective strength of the cloud increases as indicated by CAPE, the total condensate increases initially, but for **b1643**, which has a CAPE of $1800 J/Kg$, the condensate decreases and again increases for higher CAPE.

The total accumulated precipitation increases from $1.62 \times 10^{8} Kg$ to $2.75 \times 10^{8} Kg$ as the CAPE increases from $670 J/Kg$ to $2700 J/Kg$. But increase in precipitation for an increase in CAPE from $1200 J/Kg$ to $1200 J/Kg$ is large compared to that for an increase in CAPE from $1800 J/Kg$ to $2700 J/Kg$.

Further, it is more interesting that the total condensed water decreases from $2.67 \times 10^{10} Kg$ to $2.57 \times 10^{10} Kg$ when the CAPE increases from $1200 J/Kg$ to $1800 J/Kg$.

The higher rain drop radius in the case of $1800 J/Kg$ CAPE also indicates that precipitation forming processes are very different. In this case, the greater precipitation is not due to enhanced condensation of water vapor because of a larger CAPE

because, in that instance, the total condensed water would increase as CAPE increases from $1200 J/Kg$ to $1800 J/Kg$.

In the case of **ka1209** ($CAPE = 2700 J/Kg$), the total condensate is large which, as discussed earlier, decreased the buoyancy of the cloud, enhanced downdrafts and led to secondary cloud formation. Some of the increased precipitation from **b1643** to **ka1209** is due to the secondary clouds in **ka1209**. Further, the horizontal spread of **b1643** cloud is lower than that of **ka1209**.

Precipitation Efficiency It is defined as the fraction of condensed water reaching the surface as rain [*Emanuel*, 1994]. It is also one of the most ambiguous concept as it is defined in different contexts differently and although being a widely used idea in studies involving precipitation, it does not yet find a place in the Glossary of Meteorology. One of the often used definitions is :

$$\text{Precipitation efficiency} = \frac{\text{Precipitation}}{\text{Water vapor flux at the cloud base}} \tag{6.11}$$

The original definition [*Emanuel*, 1994] is difficult to use in observational studies because it is not possible to measure or estimate the total condensed water in the cloud and the total precipitation reaching the ground. But in a modeling effort like the present one, it is possible to compute the precipitation efficiency as the fraction of total condensate reaching the ground as rain. For the advantages of conformity with other studies and comparison with observations, the definition given by equation 6.11 is used in the present study.

In the table, the mean precipitation efficiency increases with CAPE, reaches a peak for 1800 J/Kg and then for the highest CAPE, decreases slightly. This decrease in high CAPE might be due to the reversal of buoyancy and consequent development of downdrafts which evaporate precipitation sized particles. This result has great significance in explaining the precipitation suppression in events when high aerosol concentration invigorates convection. The pyroconvective clouds observed in the Amazon region where precipitation was suppressed is a case in point [*Andreae et al.*, 2004].

6.3 Conclusions

Although empirically it is known that the maximum vertical velocity in a deep convective cloud is an increasing function of the convective available potential energy, the role of microphysics is also important.

By modulating the total condensate, the microphysical processes control the buoyancy of the cloud and hence the vertical velocities. In fact, the dependence and control is not one way but cyclical and the parameters in the feedback cycle considerably affect the evolution of the cloud and precipitation formation. As is conventionally assumed, precipitation may not be a linear function of the initial thermodynamic condition.

But a larger trend that appears in these results is that larger initial instability does not always translate into larger precipitation efficiency and accumulated precipitation. Most importantly, the initial thermodynamic conditions with moderate CAPE may be more efficient in turning water vapor into precipitation.

These results are very important in the context of aerosol-cloud-precipitation as many studies reported either enhancement or suppression of precipitation and in both instances, the convection was observed to be invigorated. And in the two different instances, the invigorated convection resulted in different precipitation scenarios. This set of experiments is an attempt to understand the effect of such invigoration of convection in an aerosol-cloud interaction.

The discussion in the previous subsection also points to the possibility that in these instances of moderate CAPE, the dominant process of precipitation formation is not collision-coalescence or enhanced deposition of water vapor on to ice and associated ice particle growth, but some process that involves both ice particles and liquid drops. The possible mechanisms of these processes are explored in subsequent chapters.

Chapter 7

Low and High Aerosol Concentrations

One of the most important characteristic of aerosols by virtue of which they affect cloud formation, evolution and formation of precipitation is their number concentration. As the cloud droplets are nucleated on aerosols, the number concentration of aerosols affects the number concentration of cloud droplets, hence the efficiency of collision-coalescence dominantly in the warm region of the atmosphere($< 0°C$) and the course of mixed phase processes in the cold altitudes of the cloud. As noted in an earlier chapter, 2, the precipitation can be enhanced or suppressed by increased aerosol concentration in a deep convective cloud. In this set of experiments, an effort is made to understand the changes in microphysical and dynamical characteristics of a deep convective cloud brought about by change in the initial aerosol concentration. In the first experiment, two contrasting initial aerosol concentrations are considered – $100/cm^3$ and $1500/cm^3$ – and the dynamical evolution and microphysics are studied. This has a two fold objective: one, to check if the model can reproduce some of the well-established knowledge of the response of deep convection to increased aerosol concentration and two, to investigate if the model with such sophisticated aerosol activation module can throw new light.

As noted in an earlier chapter, most of the aerosol-cloud-precipitation experiments by earlier researchers were attempts to understand the scenarios of contrasting

aerosol concentrations – a low and high. In the second experiment, I try to investigate the structure and evolution of a deep convective cloud at a range of aerosol concentrations. This study assumes importance as the aerosol concentrations in most atmospheres are not extremes as in the previous studies, but slowly increasing intermediate concentrations.

7.1 Extreme Concentrations

7.1.1 Initial Conditions

Initial Thermodynamic Condition

The initial thermodynamic condition for this study is taken from the INDOEX Intensive Field Campaign. This sounding is the one taken from the research vessel Ronald V Brown at 16:43 UTC on 18th March, 1999. The skewT-logP plot of this sounding is shown in figure 6-3. The computed convective available potential energy of this atmospheric state is $1800 J/Kg$ and the deep convection can be classified as a moderate thunderstorm.

Aerosol Profile The vertical aerosol profile is shown in the figure 5-6. The aerosols are ammonium sulphate particles. Their sizes are log-normally distributed with mean radius $0.124 \mu m$ and a standard deviation of $0.669 \mu m$ [*Clarke et al.*, 2002].

Model Configuration The model parameters for these simulations are listed in the table 6.2. The simulations are all three dimensional and the basic time step of integration is 5 seconds. The domain is $120km \times 60kms \times 20km$ and has $60 \times 30 \times 50$ grid points in the zonal, meridional and vertical directions.

The thermodynamic structure of the atmosphere was initialized with the atmospheric sounding described in in the figure 6-3. Convection was initiated using a Gaussian bubble of temperature and water vapor perturbation centered at (30,15,3) grid point. The aerosols were distributed into 5 size bins.

7.1.2 Results and Discussion

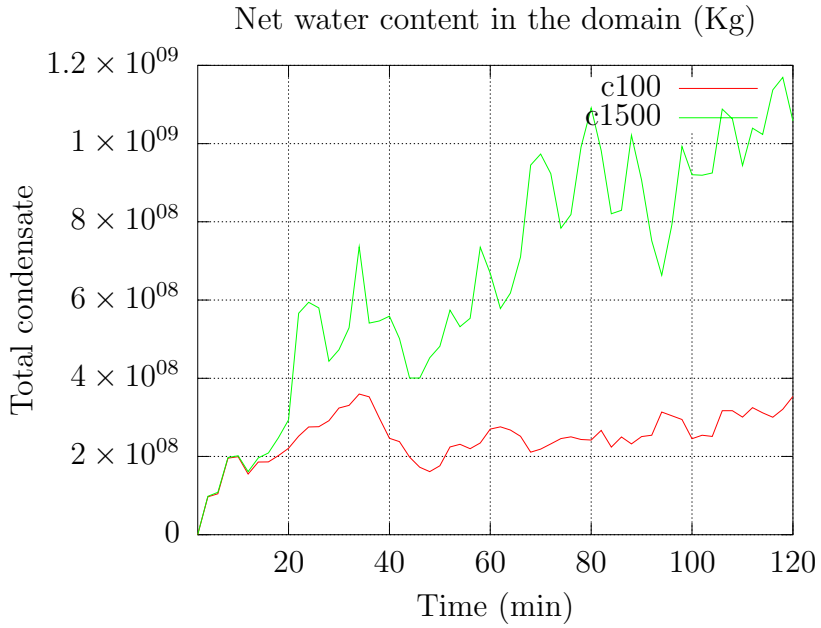

Figure 7-1: Net condensate in the domain with a low aerosol concentration ($100/cm^3$, red) and a high concentration ($1500/cm^3$, green). During the initial 20 minutes, the difference is not considerable but with the initial precipitation onset in both the cases and the high condensation in c1500, the condensate is on rise.

Total Condensed Water One of the most obvious effects of increased aerosol concentration, when other parameters remain same, is that the more numerous aerosols condense more water. Figure 7-1 shows the increased condensation. The resultant latent heat increase invigorates convection and hence the vertical velocities are also large. Figure 7-2 shows that mean vertical velocities are large in the c1500 case which has $1500/cc$ aerosols initially.

The evolution of both the clouds is very similar during the initial 20 minutes (figure 7-1). The aerosols start with the same initial thermodynamic condition, condense almost similar amount of water. But because c1500 has high aerosol concentration, the almost similar condensed water is distributed among more cloud droplets and as a result, the cloud droplet size in the high aerosol cloud is smaller than that in the low aerosol cloud (figure 7-3). Not only are the cloud droplets larger in the c100 case, but also, they grow faster by condensation during the initial 20 minutes as the low aerosol and cloud droplet concentrations can not quench the supersaturations;

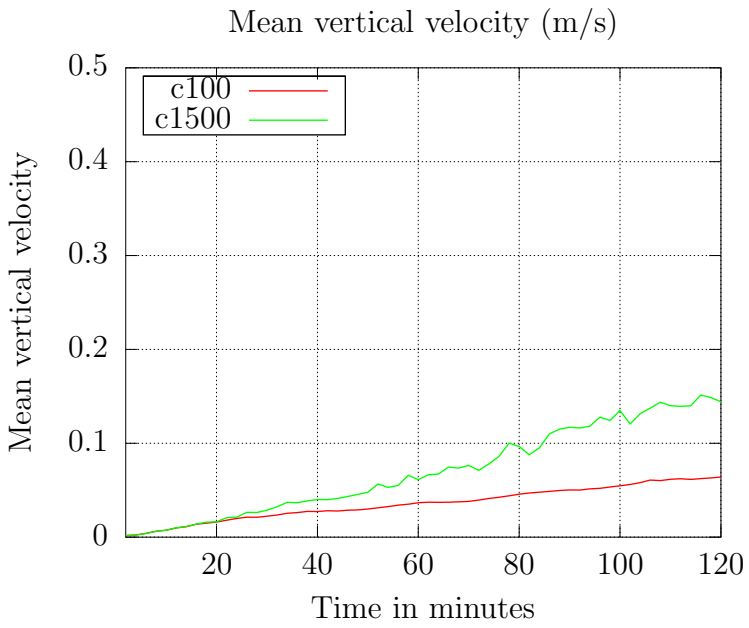

Figure 7-2: Mean vertical velocity

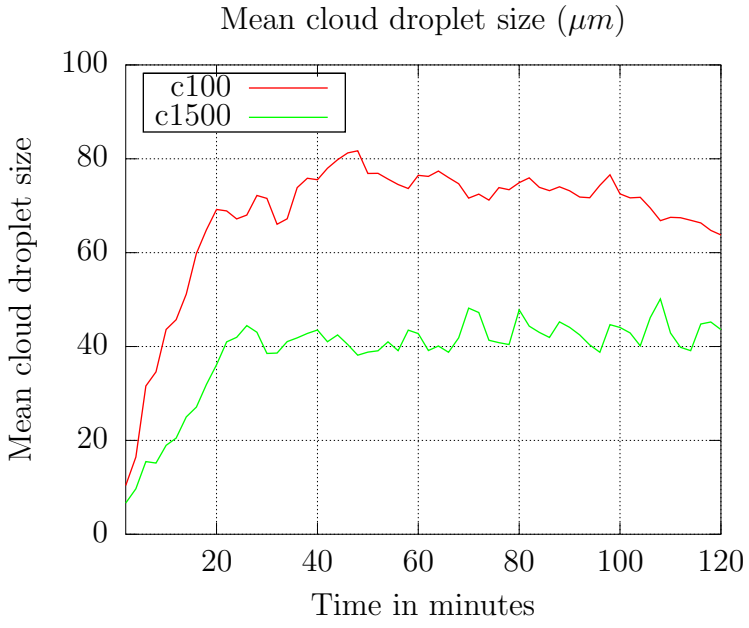

Figure 7-3: Mean cloud droplet size. With aerosol concentration increase, the droplet diameter decrease but not as much to turn off collision-coalescence.

whereas in the high aerosol case, the large number of aerosols and cloud droplets condense water vapor faster and reduce supersaturations quickly.

Another interesting observation from this plot of cloud droplet sizes is that the mean cloud droplet size is set in the initial 20 minutes and the size is almost constant during the rest of the cloud time. The mean cloud droplet concentration also shows a similar trend. Most of the aerosols in the cloud base are activated during the initial 20 minutes if the initial vertical velocities are sufficient to build sustained supersaturations. So, the further growth of these aerosols is contingent upon the equilibration times of the aerosols and cloud droplets and the times for which supersaturations are sustained. In the high aerosol instance, the supersaturations are not sustained longer for two reasons. One, the cloud droplets are smaller and hence they have faster growth rates by condensation and second, there are more cloud droplets which deplete water vapor. Both these effects keep the drop size smaller. The drop size in the high aerosol concentration case is almost half of that in the low aerosol instance.

Collision-coalescence is a strong function of the size of the collector and collected drops. As discussed in the subsection 2.4.1, the efficiency of this process of rain drop formation is strongly dependent on :

- the cloud droplet sizes: The area swept by the collector drop is larger for the larger cloud droplets and so, the low aerosol instance has an advantage.

- the cloud droplet concentration: The collision frequency of the cloud droplets increases linearly with cloud droplet concentration, and so, the high aerosol instance has an advantage.

In stratocumulus and small cumulus clouds, the water contents and supersaturations built are smaller than those in deep convection. So, in those clouds, the cloud droplet sizes are too low making collision-coalescence very inefficient in the high aerosol cases. But as the plot 7-3 shows, the cloud droplet size in the high aerosol case increases to $25\mu m$ when the collision efficiency is appreciable [*Curry and Webster*, 1999]. As a result, the rain drop size in the high aerosol case is larger than that in the low aerosol case during the initial 20 minutes and later, the size advantage

described in (a) above makes the rain drops in the low aerosol case bigger.

Thus, although the conventional wisdom accumulated through a large number of studies, in stratocumulus and other cloud types with less water contents and updrafts, suggests that collision-coalescence is rendered very inefficient, in these kinds of clouds – marine deep convective – which have large water contents and vigorous vertical motions, collision-coalescence might not be too inefficient that precipitation is completely suppressed.

7.1.3 Buoyancy

The evolution of buoyancy of the cloud has important influence on the interaction of microphysics and dynamics in a deep convective cloud.

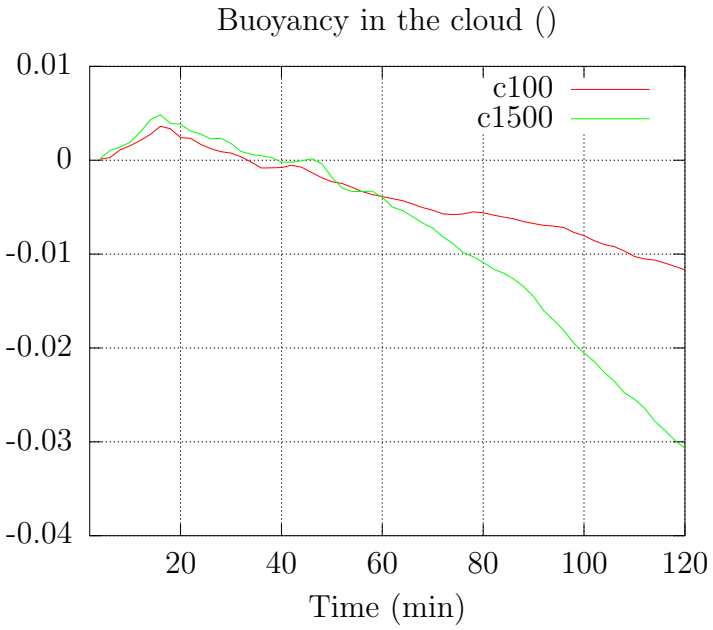

Figure 7-4: Mean buoyancy of the cloud

Figure 7-4 shows the evolution of buoyancy. Buoyancy is calculated using the expression 6.7. During the initial 40 minutes, the latent heat release due to condensation and deposition of water vapor dominates over the condensate drag. But after 40 minutes, both the clouds have large condensates and the drag exerted on vertical motion of air by the condensate makes the clouds negatively buoyant. And the larger condensate in the high aerosol case makes the cloud too negatively buoyant.

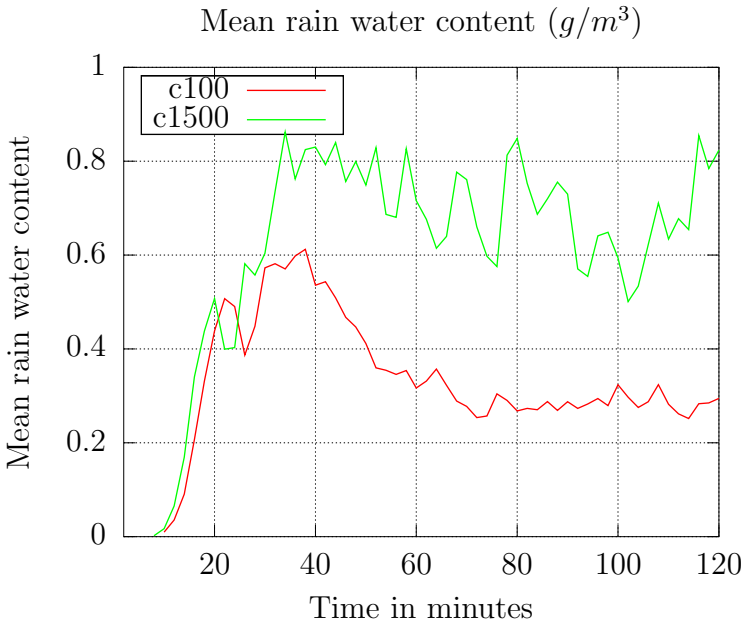

Figure 7-5: Mean rain water in the cloud

Thus the high aerosol cloud has stronger downdrafts which evaporate precipitation particles formed in the upper troposphere and lead to secondary cloud formation.

Albrecht [1989] hypothesized that increased aerosol concentrations suppress precipitation, enhance the colloidal stability of the cloud and hence increase cloud life times. But the large eddy simulations of warm convective clouds by *Jiang and Feingold* [2006] show that the cloud life times are statistically similar. They observed that horizontal gradient of buoyancy increases and the total buoyancy of the cloud decreases. In the present study, the generation of downdrafts due to condensate drag leads to an equivalent conclusion.

Precipitation As discussed above, collision-coalescence may not be very efficient in the high aerosol case. The rain water (figure 7-5) in the high aerosol case is almost double that in the low aerosol case.

But the precipitation formation in a deep convective cloud occurs not only through collision-coalescence but also through the ice phase. The mean ice and graupel contents in the two cases [figures 7-6, 7-7] show that the ice and mixed phase processes are very active in the high aerosol case because of the large condensate loading to

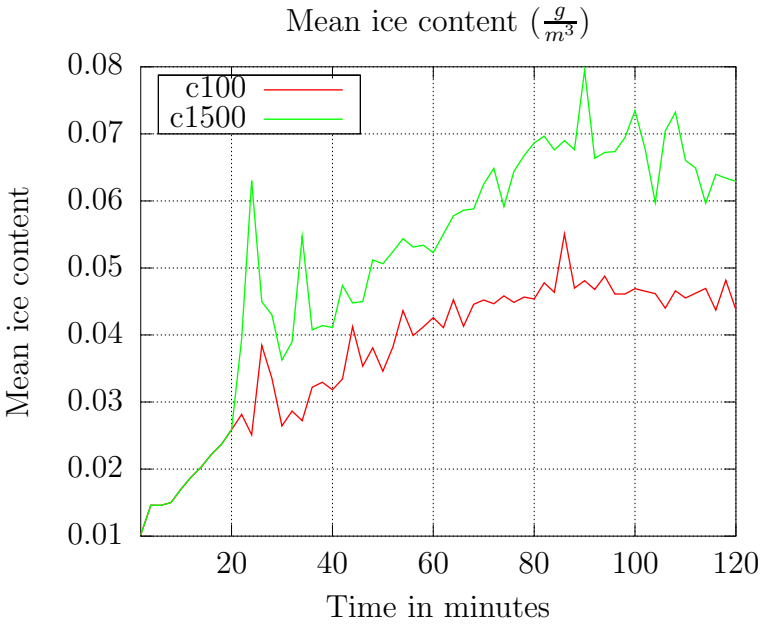

Figure 7-6: Mean ice content in the cloud

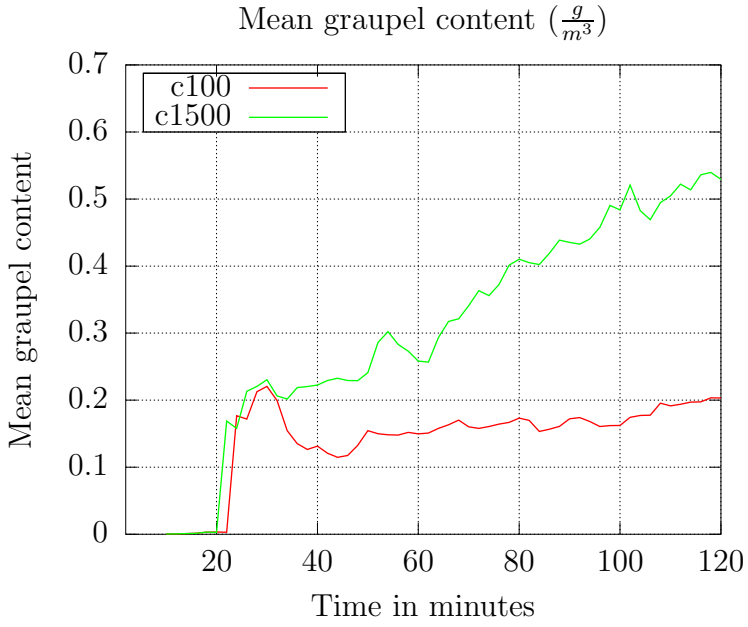

Figure 7-7: Mean graupel content in the cloud

invigorated convection.

The precipitation-sized particles formed in the upper and middle troposphere have the following disadvantages in reaching the ground compared to those formed in the lower troposphere through collision-coalescence:

1. They have long lagrangian times due to the high altitudes they have to traverse and for tow drops that start at different altitudes, the one starting higher will be evaporated longer and so more.

2. The mixed phase/ice particles which form in higher altitudes have lower density than the same sized drops in the lower troposphere and hence, their terminal velocities are low.

3. The invigorated convection creates large updrafts in the middle and upper troposphere and these particles may not have sufficient resultant fall speeds.

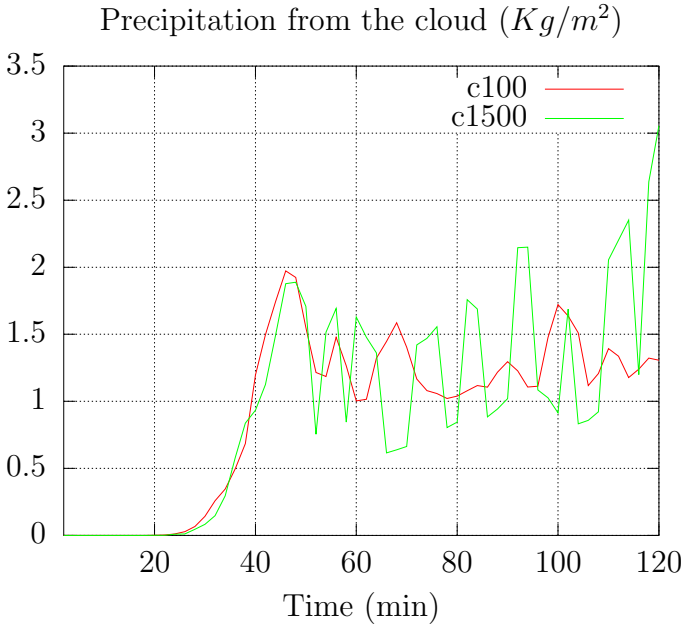

Figure 7-8: Precipitation from the cloud. With increasing aerosol concentration, precipitation is intense and in short periods.

Thus precipitation from increased aerosol concentrations is less efficient as most of these precipitation particles are evaporated in the lower atmosphere as shown in the figure 7-9. But the evaporated precipitation in the lower troposphere and boundary

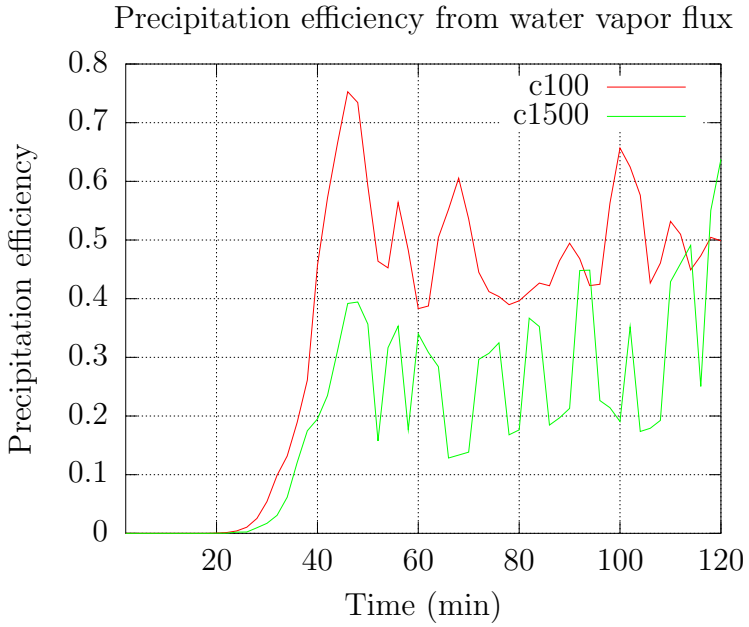

Figure 7-9: Mean precipitation efficiency from water vapor flux at the cloud base

		Simulations	
		c100	c1500
Aggregate Condensate	$\times 10^{10} Kg$	1.48	4.0
Aggregate Precipitation	$\times 10^{8} Kg$	2.26	2.38
Precipitation Efficiency	%	35	20
Cloud droplet diameter	μm	68	39
Rain drop diameter	mm	5.08	4.75
Cloud droplet conc.	$\times 10^{6}/m^{3}$	2.67	3.87
Cloud water content	g/m^{3}	0.17	0.26
Rain drop concentration	$/L$	3.47	7.75
Rain water	g/m^{3}	0.34	0.63
Ice content	g/m^{3}	0.03	0.05

Table 7.1: Summary of the mean cloud microphysical quantities for the low and high aerosol cases. The aggregates are the total values summed over the domain for the simulation time. Other quantities are domain mean values averaged over the simulation time.

layer leads to secondary clouds which may precipitate by collision-coalescence. Thus the total precipitation may increase as shown by the table 7.1.

Figure 7-8 shows the mean precipitation from the two clouds. It is interesting that in the low aerosol instance, the precipitation is mostly steady whereas in the high aerosol case the precipitation occurs in periods of intense rain and low rain.

7.1.4 Conclusions

- The model captures some of the well understood and established aspects of the effect of increased aerosol concentration on deep convective clouds.
- The cloud droplet sizes in high aerosol concentrations are not rendered so small that collision-coalescence is suppressed to a large extent.
- Convection is invigorated during the initial stages of cloud growth but as the total condensate increases, buoyancy is reduced.
- The evaporation of precipitation formed in mixed phase and ice phase processes makes precipitation formation less efficient.
- Precipitation occurs in spells of intense and less intense rain.

Chapter 8

Intermediate Aerosol Concentrations

The concentrations of aerosols in pristine environments are low and those in highly polluted atmospheres are very high. But these are extreme ends of the aerosol concentration distributions around the world. Most of the rest of the world has intermediate concentrations. And these intermediate concentrations are also gradually rising. As discussed in an earlier chapter, it is important to understand the impact of these intermediate concentrations on clouds. Perhaps the earlier researchers were of the opinion that it was easy to detect the signal of impact of the contrasting aerosol concentrations.

In the following subsections, the different characteristics of the clouds evolved in changing aerosol concentrations are discussed. A very interesting aspect is precipitation enhancement in a small range of intermediate aerosol concentrations. A possible mechanism of this new precipitation enhancement is discussed.

8.1 Initial Conditions

Initial Thermodynamic Condition Since in this set of experiments the effect of aerosols is studied, all other parameters and initial conditions are kept constant. The atmospheric sounding to initialize the model is taken from the soundings taken during

the INDOEX Intensive Field Campaign. This sounding was taken from the research ship R/V Ronald V Brown on 18th March, 1999 at 16:43 UTC. The skewT-logP plot of this sounding is shown in figure 6-3. This sounding has a convective available potential energy of 1800 J/Kg and it corresponds to a moderate thunderstorm.

Aerosol Profile Figure 5-6 shows the vertical structure of aerosol concentration. As discussed earlier, this profile was observed in the tropical marine atmosphere in the INDOEX region. The composition of the aerosols is ammonium sulphate. Their sizes are log-normally distributed with mean radius 0.124 μm and a standard deviation of 0.669 μm [*Clarke et al.*, 2002].

Model Configuration Table 6.2 lists the important parameters of the model used for these simulations.

The simulations are all three dimensional, and the basic time step of integration is 5 seconds. The domain is 120 Km $\times$ 60 Km $\times$ 20 Km with 60 $\times$ 30 $\times$ 50 grid points in the zonal, meridional and vertical directions. The thermodynamic structure of the atmosphere was initialized with the atmospheric sounding described in an earlier subsection. Convection was initiated using a Gaussian bubble of temperature and water vapor perturbation centered at (30,15,3) grid point. The aerosols were distributed into 5 size bins. The aerosol concentrations used were 100, 200, 400, 600, 700, 800, 1000 and 1500.

8.2 Results and Discussion

Mean Characteristics

As discussed in the previous experiments,the first clear effect of increasing aerosol concentrations is increased condensation and hence higher total condensed water. Figure 8-1 shows the mean water content in g/m^3 of air in the clouds evolved with different initial aerosol concentrations. During the initial 20 minutes, the condensation in the different cases is roughly an increasing function of the aerosol concentration. The

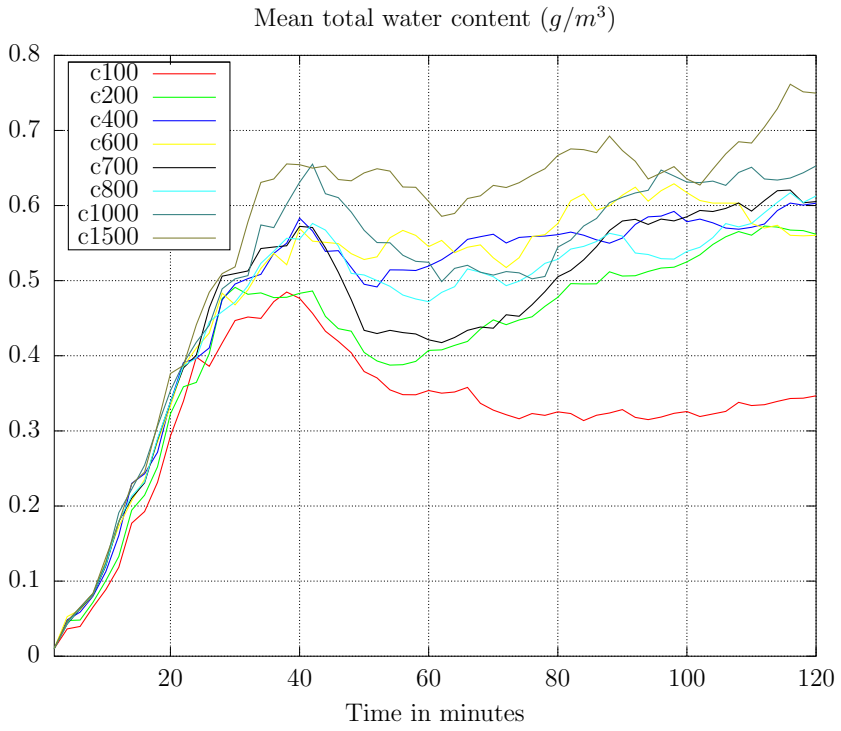

Figure 8-1: Mean condensate

different condensates result in different amounts of latent heat. Thus one effect of increasing aerosol concentration is invigoration of convection. This acts as a positive feedback and the total condensate in all the cases increases up to 40 minutes. As noted earlier, condensate reaches a maximum at about 40 minutes and there is no appreciable increase in the mean condensate later. But the total condensate in the domain (figure 8-2) monotonically increases. Clearly, the mean condensate concentration (figure 8-1) and the total condensate in the domain (figure 8-2) increase with the aerosol concentration. But the increase is not monotonic. They increase in the order 100 $\rightarrow$ 200 $\rightarrow$ 400 $\rightarrow$ 600. But from 600 to 700, they decrease and increase again to 1500.

Since the latent heat generated in condensation drives the vertical motions, the vertical velocities roughly correlate with the total condensate. The mean vertical velocity (figure 8-3) is the minimum for the c700 case except the c100 case which has the lowest aerosol concentration. Also, the vertical velocities increase with aerosol

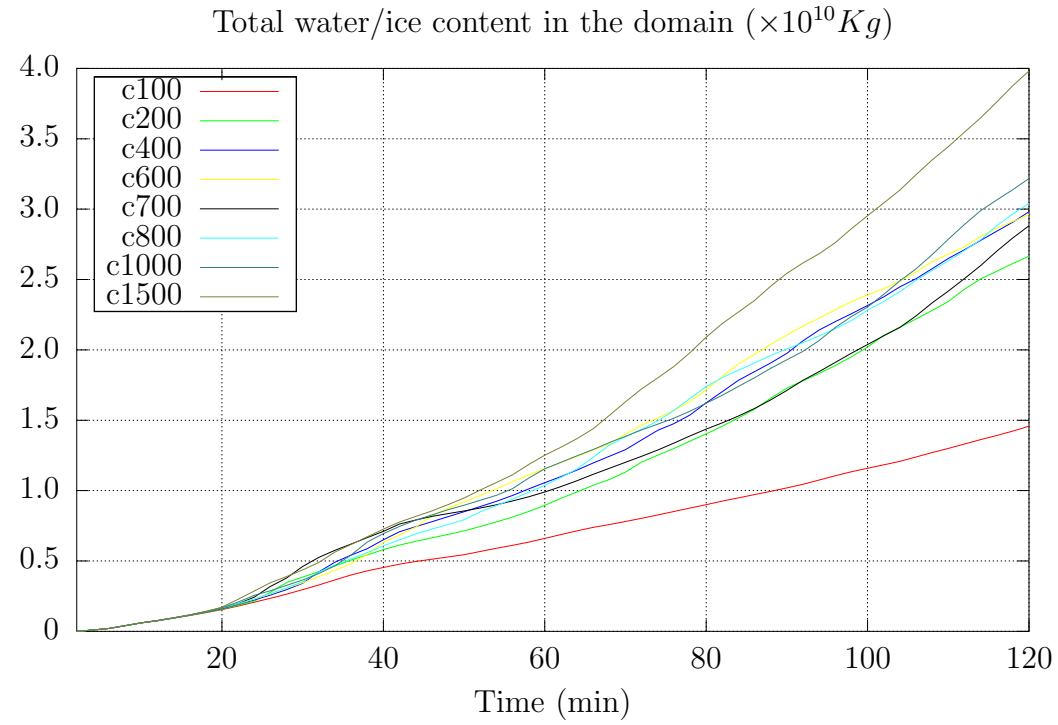

Figure 8-2: Total condensate

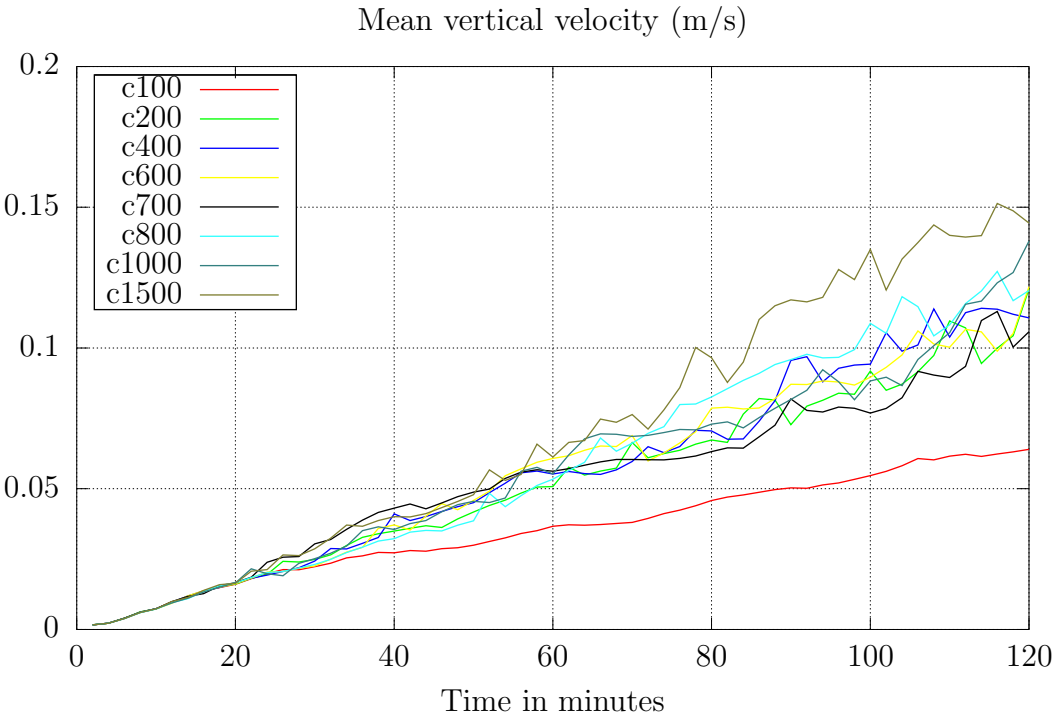

Figure 8-3: Mean vertical velocity

concentration.

The cloud droplet diameter almost monotonously increases with aerosol concentration as observed by Twomey(Twomey effect). But the sizes are still not so small that collision-coalescence is completely shutoff.

8.2.1 Buoyancy

Figure 8-4 shows the mean buoyancy in the cloud for the different aerosol cases. The buoyancy increases or remains positive during the time the latent heat release dominates in the expression for buoyancy (figure 6.7). Once the condensation and sublimation reach a steady state (as much water is condensed as is evaporated) and the condensate drag starts dominating, the mean buoyancy of the cloud starts becoming negative. Because the c100 case, which has 100 aerosols per cubic centimeter initially, has the lowest aerosol concentration, hence the lowest condensed water, has lower buoyancy initially for the first 40 minutes but because it has the lowest condensate, after 40 minutes, has the highest buoyancy.

The mean buoyancy increases with aerosol concentration during the first 40 minutes. But after 40 minutes, the buoyancy decreases with aerosol concentration.

A very interesting feature of this plot is that, even though c700 has $700\,/\mathrm{cm}^3$ aerosols, it has the lowest buoyancy except the c1500 which according to the above argument has the least buoyancy.

The center of gravity analysis as used in the section 5 shows in the present context that the c700 case attains its maximum height sooner than the other cases and also, it spreads in the horizontal direction much earlier than the other clouds.

The total quantities of ice, graupel, rain and total condensate are shown in the figures 8-5, 8-6, 8-7, 8-2. In all of them, the respective quantities increase with aerosol concentrations. Initially, the c700 cloud has greater than the rest of the clouds. Because this cloud reaches higher altitudes earlier than the other clouds, the ice content in this cloud might be greater from 20 minutes to 40 minutes. It also has greater rain water from 80 minutes to 120 minutes. But the graupel content is very low, higher than only c100. And as graupel is the largest fraction of the total

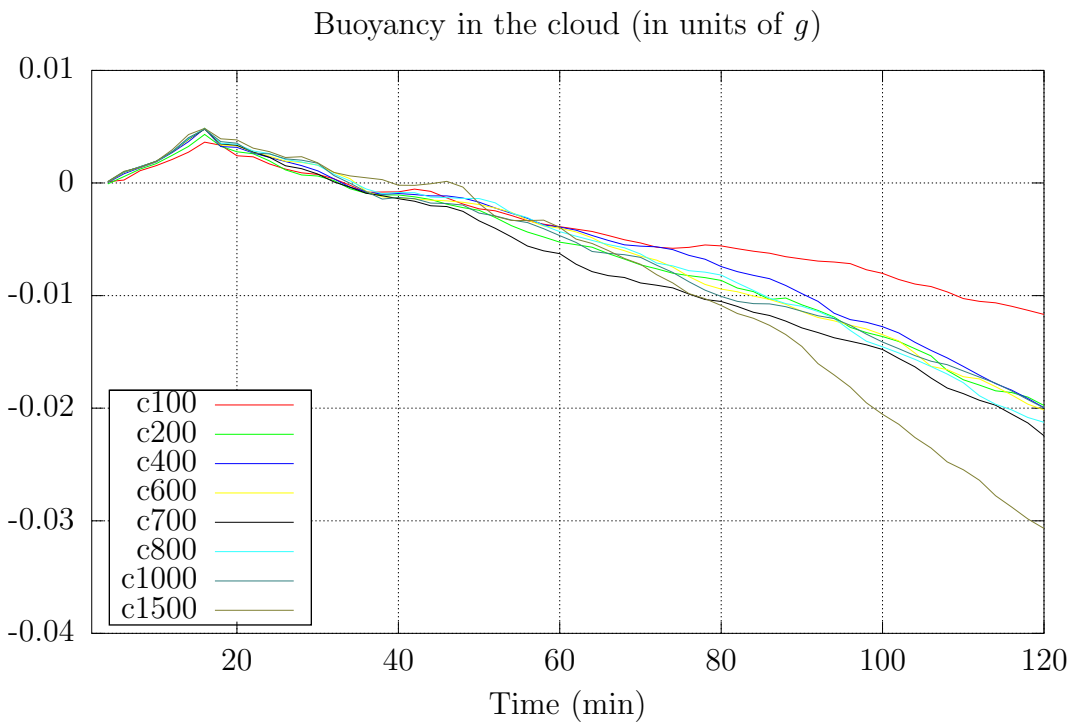

Figure 8-4: Mean buoyancy

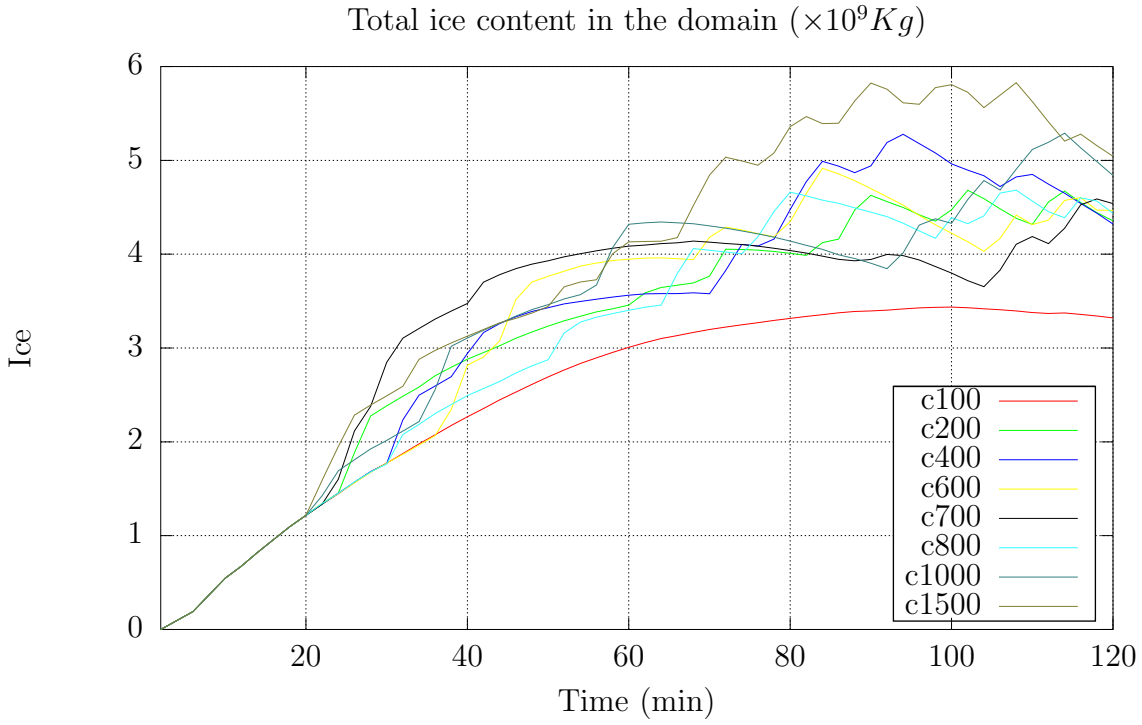

Figure 8-5: Total ice content in the cloud with a range of initial aerosol concentrations

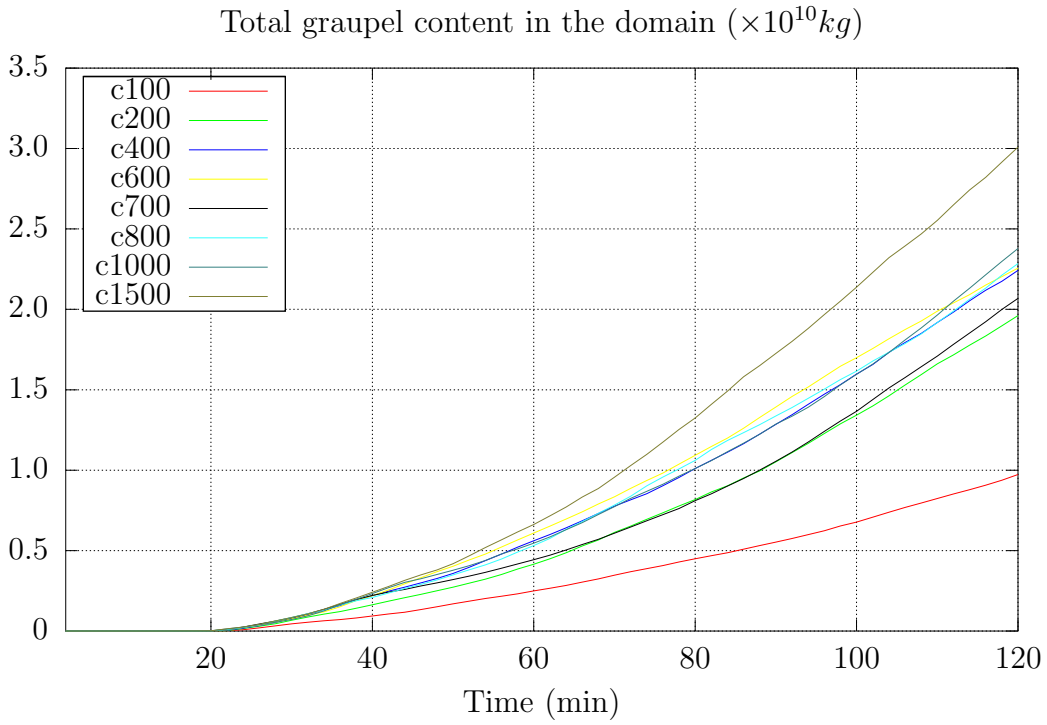

Figure 8-6: Total graupel content in the cloud with a range of initial aerosol concentrations

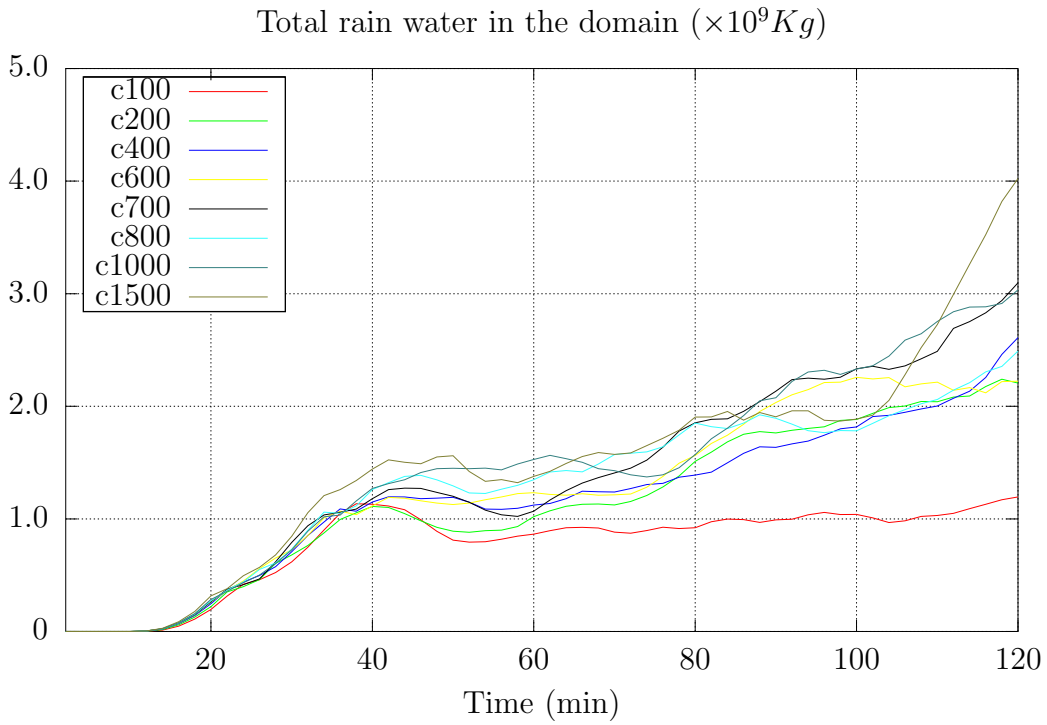

Figure 8-7: Total rain water in the cloud with a range of initial aerosol concentrations

condensate, the total condensate content of c700 is also less.

8.2.2 Precipitation

The table 8.1 shows some of the important cloud fields related to precipitation.

The total condensate during the simulation time (120 minutes) increase with aerosol concentration up to 400 /cm^3 and then there is a decrease – the minimum being for 700 /cm^3. With further increase to 1000 /cm^3 and 1500 /cm^3, the total condensate increases again.

The cumulative precipitation increases with aerosol concentration initially, up to 200 /cm^3 and then decreases because collision-coalescence becomes less efficient due to smaller cloud droplet size. The decrease in the mean drop size can be seen in the cloud droplet size column.

The precipitation efficiency as defined and discussed in 6.2.2 decreases with aerosol concentration up to 600 /cm^3 and then, there is a sudden increase for 700 /cm^3 and 800 /cm^3 and then it monotonically decreases for higher aerosol concentrations. Cloud droplet size, cloud droplet concentration, and cloud water content are monotonic functions of aerosol concentrations. But rain drop size, rain drop concentration and rain water content have jump at 700 /cm^3 and 800 /cm^3. The rain drop size increases, the rain drop concentration and rain water content decrease.

8.2.3 Precipitation Formation

The theory of precipitation formation discussed in subsection 7.1.3 and the mechanisms used to explain precipitation formation reasonably explain the variations in total condensate, precipitation and other dynamical and microphysical fields. But the cases 700 /cm^3 and 800 /cm^3 are anomalous. To bring the deviant characteristics of these cases, I list their anomalous features:

1. While the total condensate in the cloud domain monotonically increases, these two cases have lower condensate than the previous aerosol concentration cases.

		Simulations							
		c100	c200	c400	c600	c700	c800	c1000	c1500
Aerosol conc.	J/Kg	100	200	400	600	700	800	1000	1500
Aggregate Condensate	$\times 10^{10} Kg$	1.48	2.69	3.01	2.99	2.91	3.07	3.24	4.01
Aggregate Precipitation	$\times 10^{8} Kg$	2.24	2.68	2.43	2.35	3.03	2.73	2.65	2.39
Precipitation Efficiency	%	35	33	26	25	30	30	23	20
Cloud droplet diameter	μm	68	56	48	44	43	42	41	38
Rain drop diameter	mm	5.08	5.07	4.98	4.83	4.97	5.01	4.90	4.75
Cloud droplet conc.	$\times 10^{7}/m^{3}$	2.67	5.37	10.90	15.94	18.52	21.27	27.08	38.73
Cloud water content	g/m^{3}	.17	.20	.23	.23	.24	.25	.25	.26
Rain drop concentration	$/L$	3.47	4.55	5.77	6.61	5.27	5.02	6.29	7.75
Rain water	g/m^{3}	.34	.47	.53	.54	.49	.48	.57	.63

Table 8.1: Summary of the microphysical quantities in the cloud with a range of initial aerosol concentrations

2. Vertical velocities in the different cases increase from low aerosol concentration ($100\,/\mathrm{cm}^3$) to the high aerosol concentration ($1500\,/\mathrm{cm}^3$). But these two clouds – $700\,/\mathrm{cm}^3$ and $800\,/\mathrm{cm}^3$ – have lower velocities.

3. The precipitation decreases with aerosol concentration in general, whereas these two clouds have higher accumulated precipitation.

4. Their mean precipitation efficiencies averaged over the whole simulation time are large.

5. With increasing aerosol concentration, the cloud droplet size decreases. As a result, collision-coalescence becomes less efficient. Thus, the rain drop size decreases. But these two cases have larger rain drops than the immediately preceding and succeeding cases.

6. Lastly, the buoyancy of these cases is very low. Particularly, the buoyancy of $700\,/\mathrm{cm}^3$ is higher than only that of $1500\,/\mathrm{cm}^3$ cloud which is the least buoyant due to high condensate load.

Thus it is clear that at the intermediate aerosol concentrations, there is deviant response. If convection invigoration with increased aerosol concentration is assumed, then it would result in larger condensates, high vertical velocities and increased buoyancy. Thus, it is clear that it is not the only mechanism operating.

Analogy Between CAPE and Aerosol Concentration Aerosol concentration increases have been found to result in invigoration of convection in many observations and modeling studies [*Khain et al.*, 2004, 2005; *Wang*, 2005]. Thus in a way the evolution of clouds in atmospheres with increased aerosol concentrations is similar to that in atmospheres with increasing CAPE. Thus the dynamical fields like vertical velocity, buoyancy and precipiation show a similar response with aerosol concentration. In fact, comparison of tables 6.3 and 8.1 shows that the response of the different cloud fields to increasing CAPE is analogous to that to increasing aerosol concentration.

A very interesting observation of this analogy is that the characteristics of the deviant clouds discussed above – 700 /cm^3 and 800 /cm^3 – are very similar to the case with intermediate CAPE – **b1643** ($CAPE = 1800$ J/Kg). Some of their similarities are: less condensate, low vertical velocities, higher precipitation, higher precipitation efficiency and low buoyancy. But still, the mechanisms used to explain precipitation enhancement with convective strength do not explain some of the features listed above. Two common mechanisms used to explain precipitation formation in deep convective clouds are :

1. collision-coalescence of cloud droplets which occurs predominantly in the warm ($> 0°C$) region of the troposphere and

2. deposition/sublimation of water vapor on to ice/graupel and subsequent accretion of ice/graupel particles.

The second mechanism is usually invoked as invigorated convection increases the buoyancy of the cloud and creates supersaturations which are favorable for deposition/sublimation of water vapor on to ice/graupel. A possible mechanism is suggested and discussed in the next section.

8.3 A New Perspective in Precipitation Enhancement

In the absence of an explanation for the response of the precipitation enhancement with 700 /cm^3 and 800 /cm^3 initial aerosol concentrations, it is hypothesized that 'the dominant mechanism for growth of precipitation-sized particles is collection of liquid drops by ice and graupel'.

To elucidate this mechanism, the cloud is divided into three regions as shown in the schematic 8-8.

1. **Warm region** The region in the lower troposphere where the temperature is greater than $0°C$. Most of the cloud droplets form here, go through collision-coalescence to form rain drops.

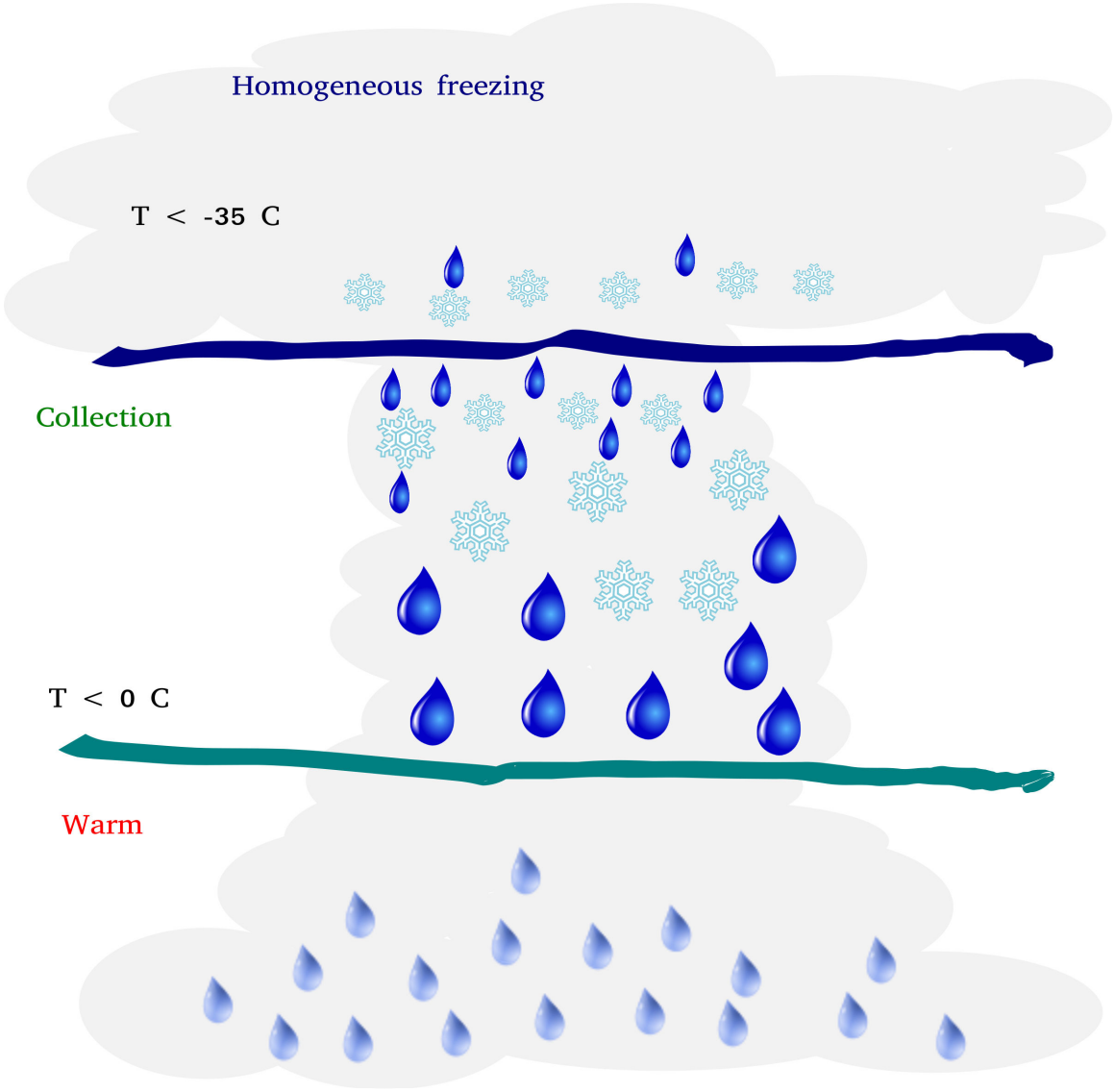

Figure 8-8: A schematic of a deep convective cloud divided in to three levels. The lower warm region has a temperature greater than 0° C. The upper homogeneous freezing region has temperature less than −35° C and the collection region between them has the temperature between 0° C and −35° C.

2. **Homogeneous freezing region** The temperature of this region is less than $-35°C$. At these low temperatures, water drops freeze homogeneously [*Heymsfield et al.*, 2005]. So, any supercooled cloud droplets or rain drops that are transported to this altitude freeze homogeneously and turn in to ice. These ice particles sublimate water vapor, grow larger and start falling when they have appreciable terminal velocities.

3. **Collection region** Ice nuclei present at this level are activated at these temperatures and ice crystals are nucleated heterogeneously. The homogeneously frozen supercooled liquid drops in the homogeneous freezing region also deposit water vapor, grow and fall into this region. Those falling ice crystals collide and stick with other ice particles and also the liquid drops transported up in the convective updrafts.

According to the hypothesis stated at the start of this subsection, it is this collision of liquid drops by ice and graupel particles that leads to the formation of precipitation-sized particles. For this to happen, the collection of liquid drops by ice and graupel has to be an efficient process. In the next subsection, this collection efficiency is discussed.

8.3.1 Collection of Liquid Drops by Ice Crystals

The mechanism of collection of liquid drops by ice particles were theoretically studied in a pioneering study by *Pitter and Pruppacher* [1974]. They solved the hydrodynamic interaction between simple ice plates, assuming them to be oblate spheroids with very small axis ratio (0.05), and spherical water drops for realistic atmospheric conditions. Figure 8-9 shows the collision efficiencies of ice plates with liquid water drops as a function of drop radius a_s. Figure 8-10 shows the collision efficiencies of broad-branched ice crystals with liquid drops as a function of drop radius a_s. Some of the most important results of their study which are relevant to the present context of the thesis are discussed below:

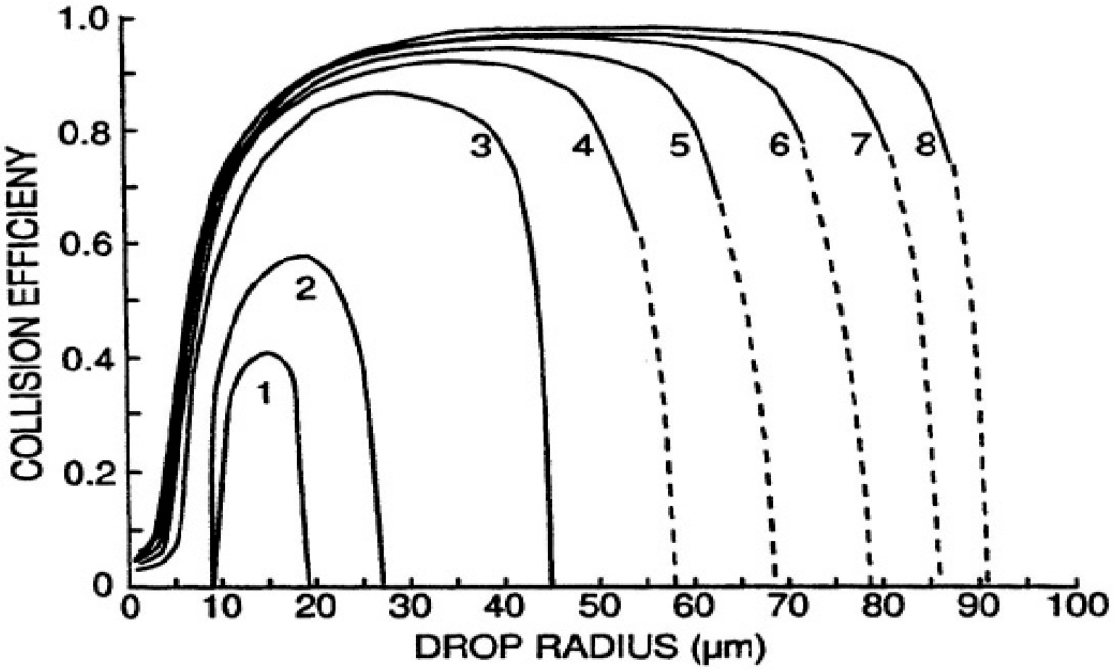

Figure 8-9: Collision efficiency of plate ice particle colliding with liquid drops as a function of drop sizes for various Reynolds numbers of the crystals. d is the diameter of the ice/graupel particle, h is the thickness of the ice crystal, and N_{Re} is the Reynolds number of the crystal. (1) $N_{Re} = 1$, d = 160 μm, h = 18 μm; (2) $N_{Re} = 2$, d = 226.5 μm, h = 20 μm; (3) $N_{Re} = 10$, d = 506.5 μm, h = 32 μm; (4) $N_{Re} = 20$, d = 716.3 μm, h = 37 μm; (5) $N_{Re} = 35$, d = 947.6 μm, h = 41 μm; (6) $N_{Re} = 60$, d = 1240 μm, h = 45 μm; (7) $N_{Re} = 90$, d = 1500 μm, h = 48 μm; (8) $N_{Re} = 120$, d = 1700 μm, h = 49 μm. [*Pruppacher and Klett*, 1998]

1. **The cutoffs** One of the important features of the two figures is that each collecting ice plate collects only within a drop size range and outside this range, the collision efficiency is effectively zero.

2. As the ice crystal size increases, the size of of the drops with which it can collide also increase.

3. **The small drop size cutoff** If a cloud has a narrow drop size spectrum of small drops, the ice particles must grow to relatively larger sizes for the collision efficiency to be appreciable and for riming to start.

4. Apart from the cutoffs on the drop sizes, there is a minimum plate size below

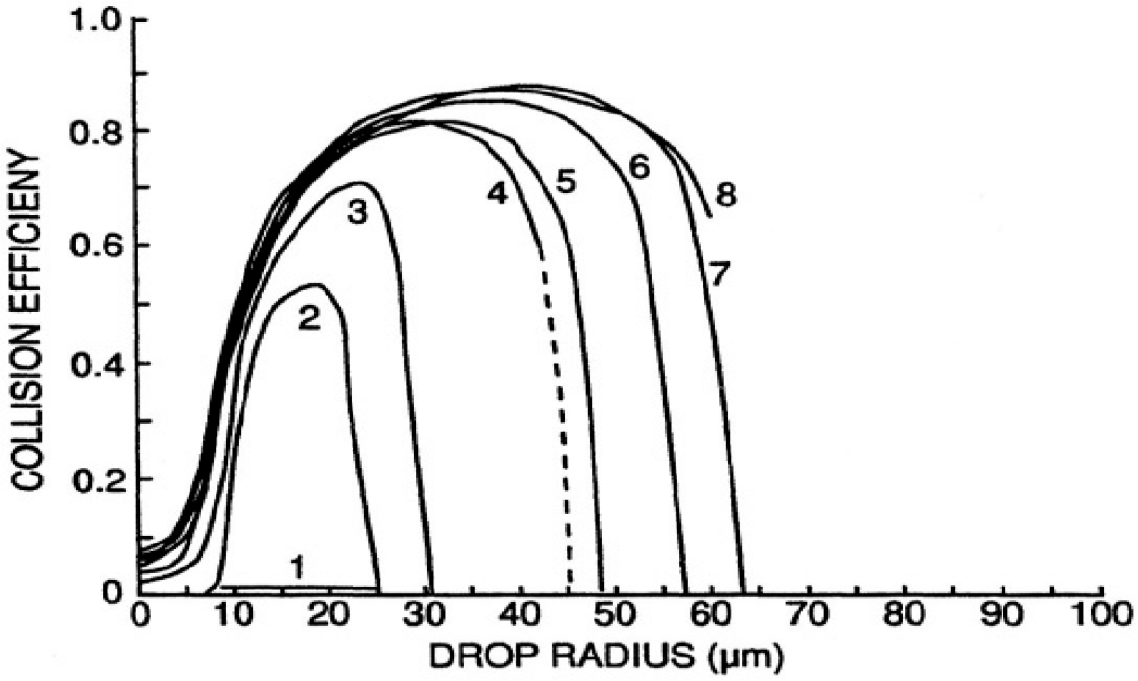

Figure 8-10: Collision efficiency of broad-branched ice particles colliding with liquid drops as a function of drop sizes for various Reynolds numbers of the crystals. d is the diameter of the ice/graupel particle, h is the thickness of the ice crystal, and N_{Re} is the Reynolds number of the crystal. (1) $N_{Re} = 1$, d = 200 μm, h = 15 μm; (2) $N_{Re} = 2$, d = 250 μm, h = 18 μm; (3) $N_{Re} = 10$, d = 700 μm, h = 32 μm; (4) $N_{Re} = 20$, d = 1000 μm, h = 40 μm; (5) $N_{Re} = 35$, d = 1500 μm, h = 50 μm; (6) $N_{Re} = 60$, d = 2000 μm, h = 60 μm; (7) $N_{Re} = 90$, d = 2500 μm, h = 65 μm; (8) $N_{Re} = 120$, d = 3100 μm, h = 73 μm. [*Pruppacher and Klett*, 1998]

which the ice crystal can not collect any drops.

5. The efficiency of colliding with a drop of a given size increases as the ice crystal increases.

Although all the above results are important in determining the variation of collection efficiency with initial aerosol concentration, result 3 is crucial.

One of the important consequence of increased aerosol concentration is that the cloud droplet size spectrum becomes narrow and is shifted towards the lower cloud droplet sizes [*Liu and Daum*, 2002; *Lu and Seinfeld*, 2006]. Thus, result 3 implies that the collision efficiency is very low until the ice crystals grow large enough.

At the left end of lower aerosol concentrations, although the drop sizes are large and the size distribution is broad, the concentrations of cloud and rain drops and ice particles are small for collection to efficiently form precipitation.

Terminal Velocities The terminal velocities and the relative velocity of the collector and collected particles play a very important role in the collection process. Some of the important points regarding the terminal velocities are discussed below.

1. For an ice particle and a water drop of equal mass, because of viscosity of air, the water drop has higher terminal velocity due to its higher density.

2. The updraft speeds, which are usually high in an invigorated convection, reduce the terminal velocities of the ice particles and in some instance, even advect them up. This makes collection less efficient. *Heymsfield et al.* [2005] noted during a study of cloud microphysics in tropical deep convective cores that, collection of liquid drops was rendered inefficient due to high updraft speeds.

8.3.2 The Mechanism

In view of the above discussion of terminal velocities and collection efficiencies, I discuss the mechanism of precipitation enhancement in the following steps. The schematic 8-11 helps in understanding this process.

1. The process starts with sufficiently large ice/graupel particles which have appreciable terminal velocities in the collection region shown in the schematic 8-8.

2. The efficient collection results in large size of the graupel particles. The large graupel particles have greater terminal velocities and hence spend less time in the atmosphere and so less evaporation.

3. Since the precipitation-sized particles evaporate less, the relative humidities created due to evaporation of precipitation are small. As a consequence, the fresh condensation of water vapor is less.

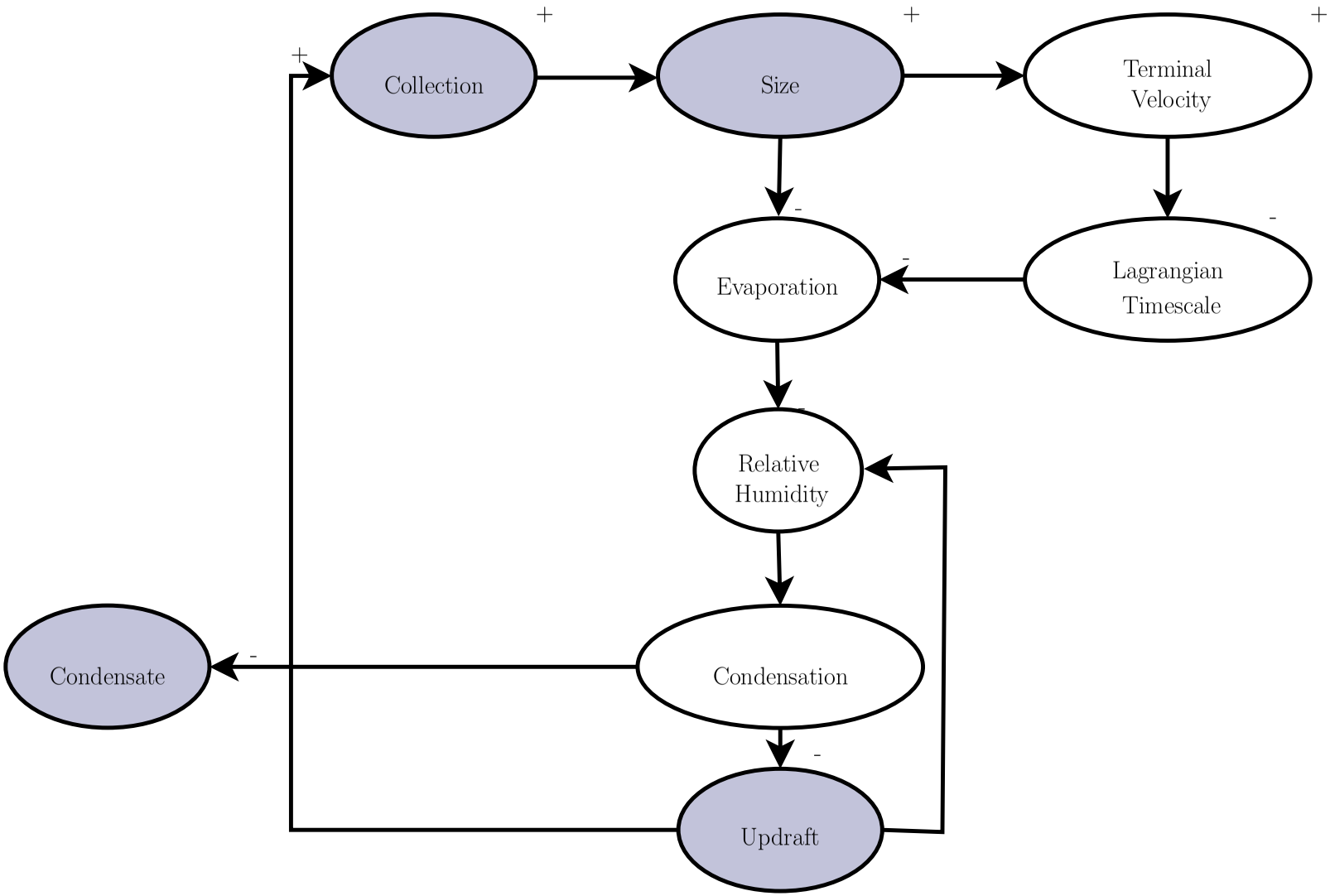

Figure 8-11: New precipitation mechanism. The ovals represent processes. '+' represents an increase as a result of the process and a '-' a decrease.

4. The low condensation means less latent heat release and hence lower updrafts and these lower updrafts keep collection efficient.

   An interesting characteristic of this mechanism is that it is self-sustaining. And that would lead to long living deep convective clouds as opposed to the clouds with high initial aerosol concentrations in which the strong updrafts result in strong downdrafts and the cloud is highly negatively buoyant.

   When the mechanism described above is applied to the $700\,/\mathrm{cm}^3$ case, the deviant characteristics are readily explained.

   - Low condensate
   - Low updrafts
   - Low buoyancy
   - High precipitation
   - High precipitation efficiency

5. If the relative humidities are kept low due to lower evaporation and lower updrafts, it is possible that the atmosphere is just saturated with respect to ice and under-saturated with respect to water. In such a situation, Bergeron process in which the cloud droplets evaporate and the ice crystals in proximity deposit water vapor and growmay be efficient. Even in such case, no new condensate is created but already condensed water is converted in to ice.

8.3.3 Evidence

Some of the facts that provide credence to the theory are:

1. Plot of mean ice particle size (figure 8-12) shows that the ice particle size decreases monotonically with aerosol concentration. But at the intermediate aerosol concentrations, the size increases. The two possible reasons for this increase are Bergeron process and deposition of water vapor.

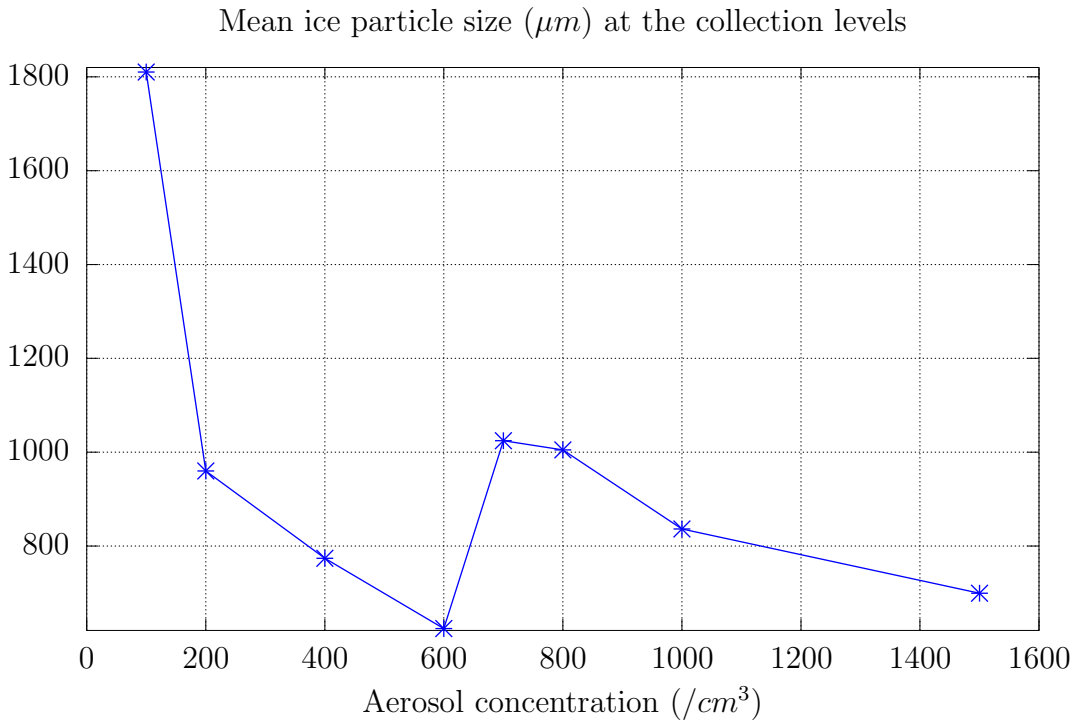

Figure 8-12: Mean ice particle diameter in the collection region

2. Plot of mean rain drop concentration ,figure 8-13, displays the rain drop concentration as a function of the initial aerosol concentration. Because of efficient collection of rain drops by ice crystals and graupel, the rain drop concentration is low in the intermediate range.

3. The graupel size in the collection region shown in the figure 8-14 has a jump at $700 - 1000\ /\mathrm{cm}^3$

4. If the liquid drops are effectively collected in the riming region, then only the small drops which escaped collection would be lofted and reach the homogeneous freezing region. Using the aircraft data collected during CRYSTAL-FACE (Cirrus Regional Study of Tropical Anvils and Cirrus Layers – Florida Area Cirrus Experiment) experiment, *Heymsfield et al.* [2005] observed that the large drops were efficiently collected in the middle troposphere and as a result, the mean size of the cloud drops in the homogeneous freezing region was small. They also found that the efficient collection was facilitated by lower updrafts in the

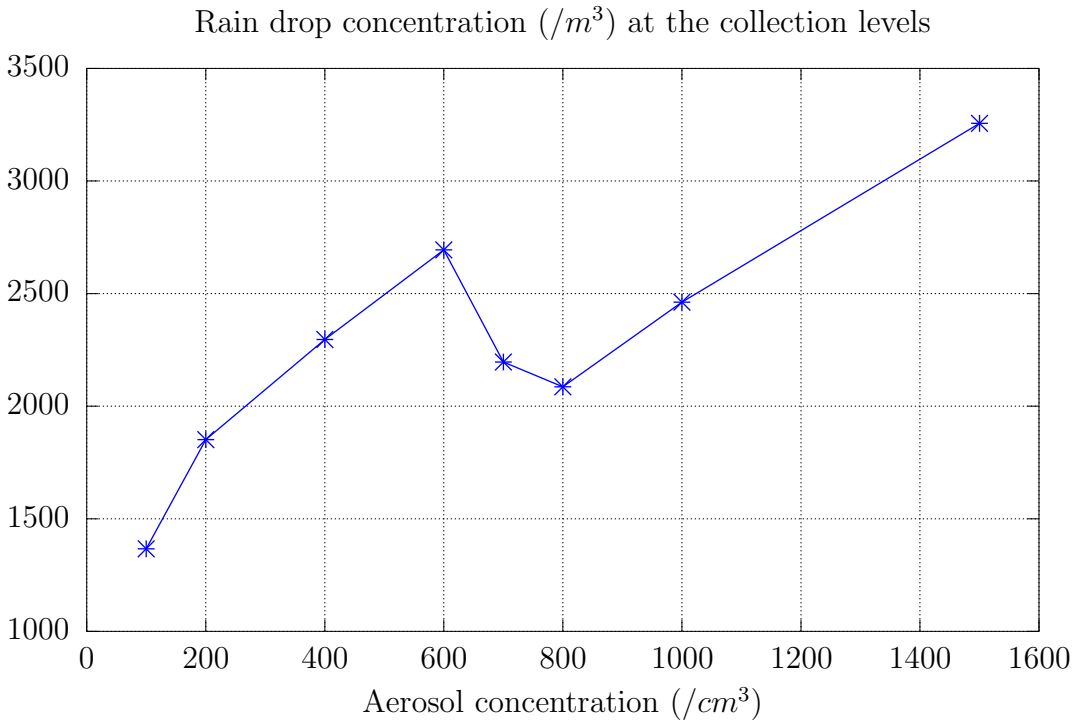

Figure 8-13: Mean rain drop concentration in the collection region

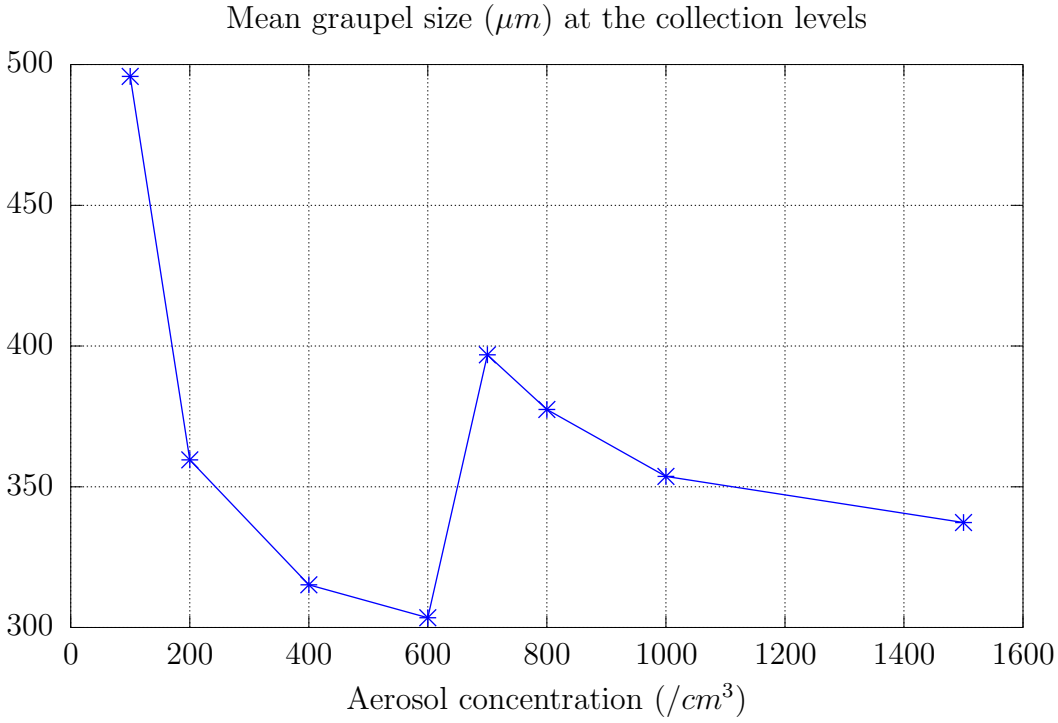

Figure 8-14: Mean graupel particle diameter in the collection region

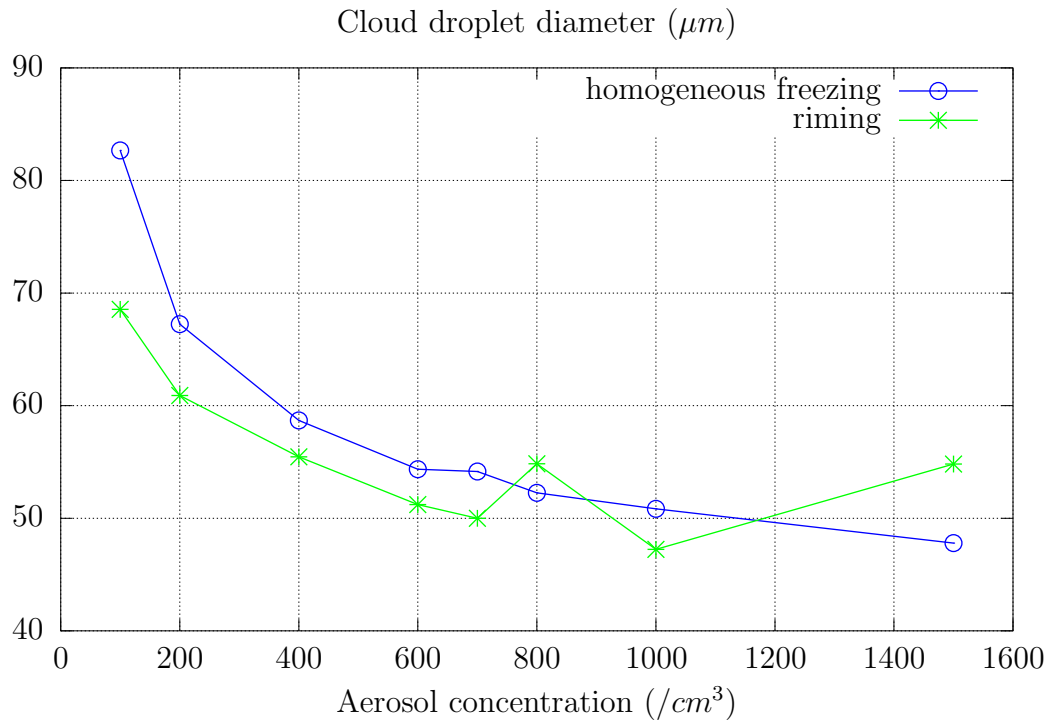

Figure 8-15: Mean cloud droplet diameter in the homogeneous freezing and riming regions

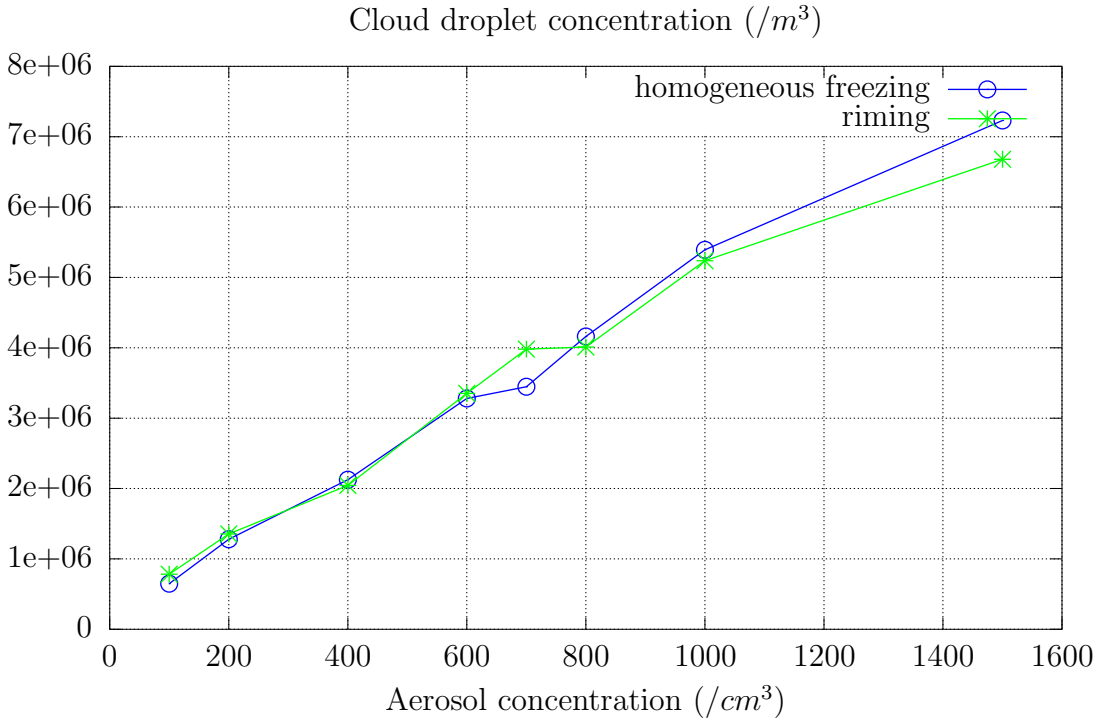

Figure 8-16: Cloud droplet concentration in the homogeneous freezing and riming regions

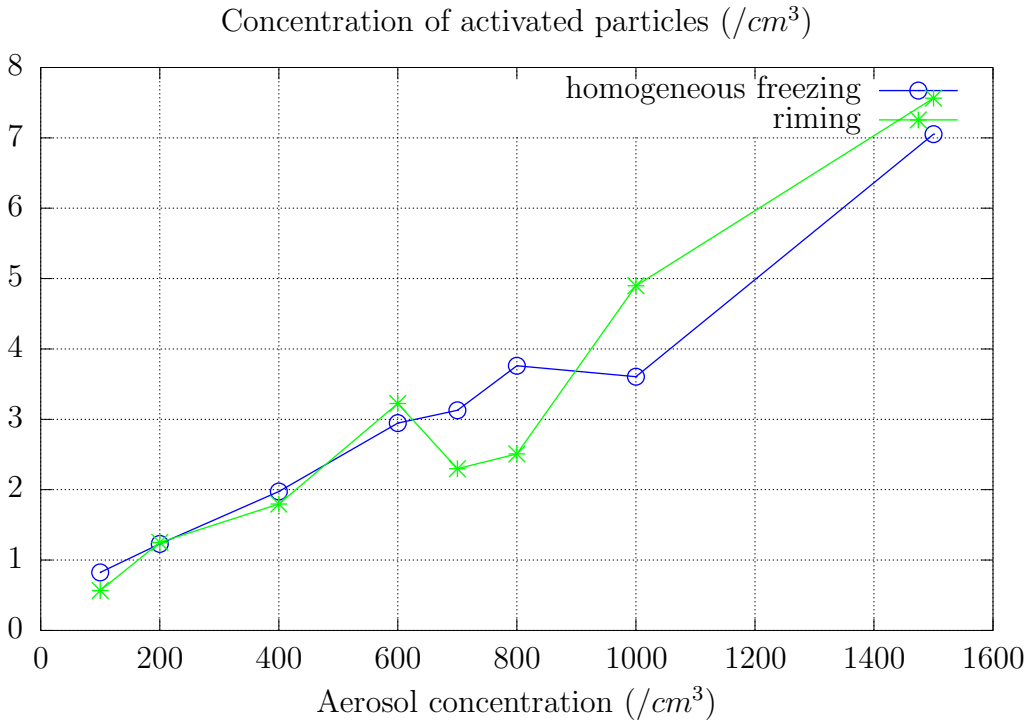

Figure 8-17: Activated particle concentration in the homogeneous freezing and riming regions

riming region.

In the present study, the reduction of mean cloud droplet diameter from riming region to the homogeneous freezing region is not very clear. Figure 8-15 shows the mean cloud droplet diameters in the riming and homogeneous freezing regions. For initial aerosol concentrations up to 700 $/cm^3$, the cloud droplet diameter is greater in the homogeneous freezing region. Figure 8-16 shows the cloud droplet concentration in the homogeneous freezing region and the riming region. In the intermediate aerosol concentration regime, particularly at aerosol concentration at which the anomalous behavior is very prominent, the cloud droplet concentration in the homogeneous freezing region is less than that in the riming region where as for all other concentrations, they are almost same. This, as *Heymsfield et al.* [2005] suggested, may be due to the effective collection in the riming region.

5. In another comprehensive study *Heymsfield et al.* [2009] analyzed aircraft data

collected during seven field campaigns at tropical latitudes. They found large concentrations of small ice crystals, which were generated through homogeneous ice nucleation. They reasoned that the conditions which favor this formation of large numbers of small ice particles are high concentrations of CCN, removal of most of the liquid droplets below homogeneous freezing region and strong updrafts at upper levels.

Figure 8-17 shows the concentration of activated particles in the homogeneous freezing and riming regions. As hypothesized earlier, the collection in the riming region is very efficient at these intermediate aerosol concentrations and the relative humidities are also low. Thus activation of aerosol particles is suppressed in the riming region. These unactivated aerosols are activated at the upper levels and as a result, the concentration of activated particles in the homogeneous freezing region is greater and in the riming region, activation is suppressed.

8.3.4 Observational Evidence

Observations of aerosol effects on clouds in general and precipitation in particular in nature are rendered almost impossible by the vastly diverse atmospheric conditions, different emission sources of gases and aerosols which modulate the aerosol composition, concentration and size distribution and the different cloud types. The vast majority of our understanding of aerosol-precipitation is derived from the deliberate cloud seeding experiments. So, although not studied or described in the detail in this work, the following events/studies/experiments point to some circumstantial evidence to the microphysical processes occurring at intermediate aerosol concentrations.

1. *Silverman* [2003] assessed hygroscopic seeding of convective clouds for rain fall enhancement at several sites around the world (Mexico, South Africa and others). Convective clouds were hygroscopically seeded. As an effect of seeding, precipitation was enhanced and the seeding effect was seen much beyond the initial production of precipitation. Model simulations[*Yin et al.*, 2001] suggested increase in rain fall which were due to increase in graupel number concentrations

and mass which were a result of increased concentration of larger drops. But Yin attributed the enhanced precipitation beyond 30 minutes, which is assumed to be the time of effect of seeding, to problems in radar estimation.

Silverman et al. [1996], cognizant of this problem in the radar estimation of rain fall, performed the same experiment in Thailand and they measured the rain spectra below seeded and unseeded clouds and the spectra were similar in shape. They concluded that the radar estimated rain fall were true. So, this was a puzzle. The mechanism proposed in this work explains the long lasting clouds with heavy precipitation.

2. Very localized cloud bursts with intense precipitation occurred on 26th July, 2005 in and around Mumbai, India. The radar pictures showed that these deep convective clouds had heights of 15 Km. Most of them were single clouds which lasted for several hours and caused record precipitation. The radar pictures showed that the precipitation formed at 10-12 Km height.

   There were several attempts to simulate this event *Vaidya and Kulkarni* [2007]; *Kumar et al.* [2008]. But the mechanism of precipitation formation and other important features like the long life of the cloud could not be explained. This instance also provides circumstantial evidence to the theory of intermediate aerosol concentration on precipitation discussed earlier in this chapter. Some features like the long cloud life time and heavy precipitation can be explained using the mechanism proposed in this thesis.

8.4 Conclusions

The main results of this study are summarized in the following lines.

1. Increasing aerosol concentrations invigorate convection.

2. The mean condensate and the total condensate in the domain increase with aerosol concentration but for intermediate aerosol concentrations, they decrease.

3. The buoyancy of the cloud increases initially with increasing aerosol concentration. At intermediate aerosol concentrations, the mean buoyancy decreases. For a particular intermediate aerosol concentration, the buoyancy is very low, being higher than that of only the highest aerosol concentration case.

4. The mean buoyancy of the cloud is a result of the interplay between the dynamics and microphysics.

5. As aerosol concentration increases, the increasing condensate reduces the buoyancy.

6. Precipitation and precipitation efficiency initially decrease with aerosol concentration. But for intermediate concentrations, both these quantities increase and with further rise in aerosol concentrations, they decrease.

7. At intermediate concentrations, the deep convective clouds respond anomalously.

8. Analysis shows that the precipitation forming mechanism is the collection of rain drops by ice and graupel particles and this is very efficient at these intermediate concentrations.

9. These intermediate concentration clouds have lower buoyancy, longer lifetimes and lower condensates compared to the clouds with low and high aerosol concentrations.

10. With the premise that increased aerosol concentration invigorates convection, a juxtaposition of the response of deep convection to increasing CAPE and that to increasing aerosol concentration show similar behavior. So ,the anomalous behaviour at the intermediate concentratioin is very robust.

11. The effect is also shown with a different initial thermodynamic condition.

12. Circumstantial evidence is shown by observations.

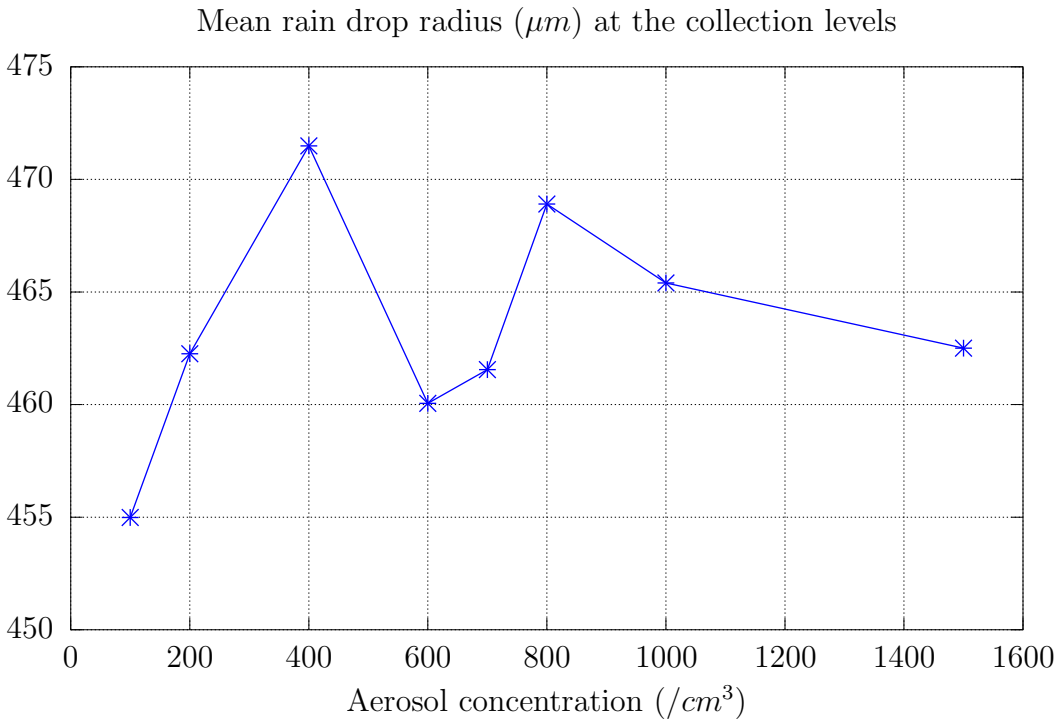

Figure 8-18: Mean rain drop diameter in the collection region

Chapter 9

Summary & Conclusions

In this last chapter of the thesis, the goals, the different chapters, the important results are summarized. In the last sections of the chapter, the limitations of this study are discussed and future directions are proposed.

9.1 Goals of this thesis

Aerosol activation is the weakest link in understanding the impact of aerosols on clouds and hence precipitation. As our understanding of aerosol physics and chemical processes advances through observations, modeling efforts and development of theory, it is expected that our perspective on aerosol-cloud interaction takes into account those advances to understand the processes in aerosol-cloud interactions better. In this work, such an effort is made to bring some of the new techniques of modeling aerosol representation, physics and chemistry in to a cloud model. This is expected to replace some of the parametrization in the cloud model so that a long standing demand of the cloud physics community that aerosol activation be represented in cloud models using more fundamental aerosol physics and chemistry is fulfilled. MELAM, the aerosol activation model used in this thesis is capable of computing activation of very complex aerosol populations with different size distributions, compositions and mixing states. The model is capable of treating gas chemistry and dissolution of gases into the aerosol particles.

One of the primary goal of this work was to develop a coupled model in which the aerosol activation is computed taking into account the full aqueous chemistry and size distribution of the aerosols. To achieve this goal, the aerosol activation model MELAM has been coupled to a cloud resolving model.

The developed model has been used to simulate a deep convective cloud observed during INDOEX observational campaign. This helped understand the strengths and limitations of the coupled model. At the same time, this study also provided perspectives in conducting observational campaigns so that the model and observational data can be used together to better our understanding of aerosol and cloud processes.

The third goal of this work was to use the coupled model to study the sensitivity of the model to different initial thermodynamic conditions. This experiment also helped in understanding how the cloud structure, microphysical evolution and precipitation formation are affected by the initial thermodynamic condition.

The fourth goal of this thesis was to simulate the response of a deep convective cloud to a low aerosol concentration (representing pristine atmospheres) and a high aerosol concentration (representing polluted atmospheres). Since a lot of the research for the last one decade has been in understanding this transition from pristine to polluted clouds, this objective also helped in evaluating the ability of the coupled model in reproducing the well-understood and accepted knowledge.

With the confidence gained from the previous objectives, the model has been used to study the response of a deep convective cloud to a range of aerosol concentrations.

The studies of response of deep convection to increasing aerosol concentrations have particularly looked at the interaction of dynamics and microphysics and the role of this interaction in precipitation formation.

Structure of the thesis In line with the above goals, the thesis is structured as follows.

The theoretical aspects of aerosol activation and formation of cloud droplets and how this process is represented in current cloud models is discussed in the second chapter. Further, the chapter describes the problems with these representations and

points to the need for a new coupled cloud model that computes aerosol activation using aerosol physics and chemistry. A section of the chapter discusses the precipitation formation process and the last part of the chapter gives a critical review of the important efforts in the past one decade understanding aerosol-deep convection-precipitation interactions.

The third chapter describes the models used – aerosol activation model MELAM and the cloud resolving model – to develop the coupled model and looks at the capabilities and assumptions of the new coupled model.

The fourth chapter deals with aircraft observations collected during the INDian Ocean EXperiment of a deep convective cloud. This data has been used to validate the coupled model and for initializing the coupled model in the subsequent experiments.

The fifth chapter describes the simulation of the deep convective cloud that was observed during INDOEX. The conditions of the Indian Ocean region during the deep convection are discussed and they show that the meteorological conditions were conducive for convection. The mean properties of the observed cloud are discussed. The assumptions in sampling the model results to compare with observations, the statistical test used and the results of the statistical test are examined.

In the sixth chapter, the sensitivity of the model to initial thermodynamic conditions is studied. Apart from the experimental conditions, a new technique of analyzing clouds using the concept of center of gravity and the theory of precipitation formation are discussed in the context. The results of the effect of the initial thermodynamic condition on deep convection are analyzed.

In the seventh chapter, the effect of contrasting aerosol concentrations on the dynamics and microphysics of deep convection is studied. The results are discussed in light of previous studies and results. The eighth chapter looks at the effect of a range of aerosol concentrations on the interplay between dynamics and microphysics and their role in forming precipitation.

9.2 Conclusions

In the present section, the conclusions from the results of the four experiments are summarized.

9.2.1 Simulation of a deep convective cloud observed during INDOEX

1. To understand the ability of the model to simulate the observed cloud, the cloud fields at five levels in the observed cloud were compared with the cloud fields at the corresponding levels in the model domain using Mann-Whitney U test with the null hypothesis that the observed and simulated cloud fields have the same underlying distribution at each height level.

2. The vertical velocities and cloud droplet number concentrations are simulated reasonably well.

3. The simulated cloud water and drop sizes compare well with the observations at some levels and there are discrepancies at others.

4. When the updrafts were simulated well, the cloud droplet number concentrations are also simulated with statistical significance. This shows that the aerosol activation model is very accurate in predicting the cloud droplet number concentration.

5. Monte-Carlo resampling technique showed that the results are robust.

6. In spite of the severity of the comparison, several of the simulated cloud fields compare well with the observations. This is significant.

9.2.2 Sensitivity of the Coupled Model to Initial Thermodynamic Condition

1. The mean vertical velocity increases with CAPE. But for an intermediate CAPE value, the mean vertical velocity is the lowest, lower that that of the lowest CAPE.

2. The mean buoyancy in the cloud corroborates the above conclusion: the intermediate CAPE case (CAPE = $1800 J/Kg$) has the lowest mean buoyancy.

3. Generally, it is expected that total condensate, precipitation and precipitation efficiency increase with CAPE. But the results of this experiment show that, these quantities show anomalous behavior at intermediate CAPE. The case in this experiment with an initial CAPE of $1800 J/Kg$ has a lower condensate, highest precipitation efficiency, rain drop size and higher cloud droplet concentration.

4. The intermediate CAPE case also has lower girth and most of the mass of the cloud is at a lower height than in the other cases as shown by the center of gravity analysis.

5. Collision-coalescence is efficient in the lowest CAPE situation during the first half of the simulation time where as it is highest in the second half of the simulation in the highest CAPE case. This is also corroborated by the fact that secondary clouds formed in the highest CAPE case because of its lowered buoyancy and strong downdrafts.

6. The intermediate CAPE case is the most efficient in forming precipitation.

9.2.3 Effect of Low and High Aerosol Concentrations on a Deep Convective Cloud

1. The model simulates some of the well-understood and established aspects of the effect of increased aerosol concentration on deep convective clouds.

2. As aerosol concentration increases from low to high, the cloud droplet size decreases as has been observed and modeled by earlier researchers. The premise for this argument is that the aerosols compete for limited amount of water vapor content. This may not be universally true with tropical marine clouds. This study shows that although the cloud droplet radius decreases with increased aerosol concentration, the droplets do not become so small that collision-coalescence is rendered very inefficient.

3. Increased aerosol concentration invigorates convection but as the total condensate increases, buoyancy is reduced.

4. As aerosol concentration changes from low to high, precipitation formation from ice and mixed phase processes increases. But, their evaporation during fall makes the overall precipitation formation less efficient.

5. As aerosol concentration increases, precipitation occurs in spells of intense and less intense rain.

9.2.4 Effect of a Range of Aerosol Concentrations on a Deep Convective Cloud

1. The mean condensate monotonically increases with increasing aerosol concentration but for intermediate concentrations, the mean condensate decreases.

2. The buoyancy of the cloud decreases with increasing aerosol concentrations due to condensate load but the buoyancy at intermediate concentrations is anomalously low due to precipitation drag.

3. Precipitation shows an anomalous increase at intermediate aerosol concentrations.

4. Precipitation efficiency monotonically decreases except for an anomalous increase at intermediate concentrations.

5. Precipitation forming mechanism at these intermediate aerosol concentrations is the effective collection of rain drops by ice and graupel particles and this mechanism is very efficient at these intermediate aerosol concentrations.

6. Increase of aerosol concentration and increase of CAPE produce similar response in deep convective clouds including the anomalous behavior at the intermediate concentrations. Thus the conclusion about the precipitation forming mechanism is very robust.

7. A similar response is shown with a different initial thermodynamic condition.

8. Observations provide circumstantial evidence for the behavior of the deep convective cloud with intermediate aerosol concentrations.

9.3 Limitations of This Study

Although this study has been as thorough as possible, the following limitations exist.

1. As with most modeling efforts, lack of observational data for initializing model and constraining the model results certainly sets a limitation on this study.

2. The initial thermodynamic conditions that have been used had been measured in tropical marine atmosphere. So, although some of the results can be attributed to continental regions where huge amounts moisture is transported into the lower layers of the atmosphere by circulations like monsoons, the atmospheric conditions in those regions also have to be taken into account while accounting for the different responses.

3. Since the coupled model has been developed out of MELAM and CRM, the limitations of representations inherent in those models and lack of theory translate as limitations of this study.

4. The aerosols and their concentrations considered for this study are the accumulation mode particles. And further, for ease of interpretation and to evaluate

the relationships of the variables in a cause-and-effect paradigm, a single population of accumulation mode ammonium sulphate particles is considered. A more accurate approach would be to include sea salt and insoluble cores.

5. Convection initiation using a temperature and water vapor perturbation bubble in the cloud resolving model is a common practice. But the evolution of the cloud may be sensitive to the size and location of this perturbation.

6. The maze of microphysical transformations in clouds are best represented in models using sections. Although the approach is more accurate, that framework is computationally very expensive.

7. Model resolution is known to have determining effect on the cloud processes. Higher model resolutions being computationally expensive, some of the results may alter at a different resolution.

9.4 Future Directions

For the advancement of our understanding of the processes linking aerosols, clouds and precipitation, the coupled model has great scope as the complete potential of this very sophisticated model is yet to be tapped. The following are some proposals in the short run.

1. Simulation of deep convective clouds with different compositions can help understand the role of the complex aerosol composition and mixing states play in the modulation of the dynamics and microphysics.

2. Simulations with changing aerosol size distributions are helpful in understanding the indirect impact of the source of aerosols and the role of their growth processes in the atmosphere play in impacting deep convection.

3. Observational evidence for some of the interesting results of this work can be sought in observations.

4. It was found that aerosol activation is suppressed in the riming region and, is enhanced in the homogeneous freezing region at the intermediate aerosol concentrations. This is, as suggested by *Heymsfield et al.* [2009], promoted by efficient collection of liquid water below the homogeneous freezing region. In this context, Paluch diagram analysis can be used to examine the source region of these new activations. Further analysis of the vertical profiles of total water content would also help better understand the microphysics involved in these patterns of activation.

In the longer time frame, the following directions are suggested.

1. The coupling between the two models MELAM and CRM has been kept very modular. Thus it is possible to couple the aerosol model to a cloud model that has better representation of the microphysical interactions and transformations, for instance – a sectional model that represents the liquid drops and ice particles using size bins and hence has a better collection kernels. That would help the cause of improving the model physics.

2. If aerosol-cloud observations are taken keeping in view the abilities of the coupled model and if the observations are used to constrain the model, it is expected that the modeling-observation-theory cycle would be accelerated.

Bibliography

Abdul-Razzak, H., and S. Ghan (2000), A parameterization of aerosol activation 2. Multiple aerosol types, *Journal of Geophysical Research–Atmospheres*, *105*(D5), 6837–6844.

Adhikari, M., Y. Ishizaka, H. Minda, R. Kazaoka, J. Jensen, and J. Gras (2005), Vertical distribution of cloud condensation nuclei concentrations and their effect on microphysical properties of clouds over the sea near the southwest islands of Japan, *Journal of Geophysical Research–Atmospheres*, *110*(D10), doi: 10.1029/2004JD004758.

Albrecht, B. A. (1989), Aerosols, Cloud Microphysics, and Fractional Cloudiness, *Science (New York, N.Y.)*, *245*(4923), 1227–1230, doi:10.1126/science.245.4923.1227, PMID: 17747885.

Andreae, M. O., D. Rosenfeld, P. Artaxo, A. A. Costa, G. P. Frank, K. M. Longo, and M. A. F. Silva-Dias (2004), Smoking rain clouds over the Amazon, *Science*, *303*(5662), 1337.

Andrews, E., P. Sheridan, J. Ogren, and R. Ferrare (2004), In-situ aerosol profiles over the Southern Great Plains cloud and radiation test bed site: 1. Aerosol optical properties, *Journal of Geophysical Research–Atmospheres*, *109*(D6), doi:10.1029/2003JD004025.

Ansari, A. S., and S. N. Pandis (2000), Water absorption by secondary organic aerosol and its effect on inorganic aerosol behavior, *Environmental Science and Technology*, *34*(1), 71–77.

Berg, O., E. Swietlicki, and R. Krejci (1998), Hygroscopic growth of aerosol particles in the marine boundary layer over the Pacific and Southern Oceans during the First Aerosol Characterization Experiment (ACE 1), *Journal of Geophysical Research–Atmospheres*, *103*(D13), 16,535–16,545.

Bjerknes, J. (1969), Atmospheric teleconnections from the equatorial Pacific, *Monthly Weather Review*, *97*(3), 163–172.

Borys, R. D., D. H. Lowenthal, and D. L. Mitchell (2000), The relationships among cloud microphysics, chemistry, and precipitation rate in cold mountain clouds, *Atmospheric Environment*, *34*(16), 2593–2602.

Borys, R. D., D. H. Lowenthal, S. A. Cohn, and W. O. Brown (2003), Mountaintop and radar measurements of anthropogenic aerosol effects on snow growth and snowfall rate, *Geophysical Research Letters*, *30*(10), 1538.

Chuang, P. Y., R. J. Charlson, and J. H. Seinfeld (1997), Kinetic limitations on droplet formation in clouds, *Nature(London)*, *390*(6660), 594–596.

Chuang, P. Y., D. R. Collins, H. Pawlowska, J. R. Snider, H. H. Jonsson, J. L. Brenguier, R. C. Flagan, and J. H. Seinfeld (2000), CCN measurements during ACE-2 and their relationship to cloud microphysical properties, *Tellus*, *52*, 843–867.

Clarke, A. D., S. Howell, P. K. Quinn, T. S. Bates, J. A. Ogren, E. Andrews, A. Jefferson, A. Massling, O. Mayol-Bracero, H. Maring, et al. (2002), INDOEX aerosol: A comparison and summary of chemical, microphysical, and optical properties observed from land, ship, and aircraft, *Journal of Geophysical Research – Atmospheres*, *107*(8033).

Colbeck, I. (2008), *Environmental Chemistry of Aerosols*, Blackwell Publishing, Ames, Iowa, USA.

Conant, W., T. VanReken, T. Rissman, V. Varutbangkul, H. Jonsson, A. Nenes, J. Jimenez, A. Delia, R. Bahreini, G. Roberts, R. Flagan, and J. Seinfeld (2004),

Aerosol-cloud drop concentration closure in warm cumulus, *Journal of Geophysical Research–Atmospheres*, *109*(D13), doi:10.1029/2003JD004324.

Crumeyrolle, S., L. Gomes, P. Tulet, A. Matsuki, A. Schwarzenboeck, and K. Crahan (2008), Increase of the aerosol hygroscopicity by cloud processing in a mesoscale convective system: a case study from the AMMA campaign, *Atmospheric Chemistry and Physics*, *8*(23), 6907–6924.

Curry, J., and P. J. Webster (1999), *Thermodynamics of Atmospheres and Oceans*, Academic Press, San Diego.

de Reus, M., R. Krejci, J. Williams, H. Fischer, R. Scheele, and J. Strm (2001), Vertical and horizontal distributions of the aerosol number concentration and size distribution over the northern Indian Ocean, *Journal of Geophysical Research–Atmospheres*, *106*(D22), 28,629–28,641.

Ekman, A., C. Wang, J. Wilson, and J. Ström (2004a), 3-D Simulation of Aerosol Physics and Chemistry Within a Convective Cloud, in *AGU Spring Meeting Abstracts*, p. 05.

Ekman, A. M. L., C. Wang, and J. Ström (2004b), Explicit simulation of aerosol physics in a cloud-resolving model, *Atmospheric Chemistry and Physics Discussion*, *4*, 753–803.

Emanuel, K. A. (1994), *Atmospheric convection*, 598 pp., Oxford University Press, New York, USA.

Engström, A., A. M. Ekman, R. Krejci, J. Ström, M. de Reus, and C. Wang (2008), Observational and modelling evidence of tropical deep convective clouds as a source of mid-tropospheric accumulation mode aerosols, *Geophysical Research Letters*, *35*(23), L23,813.

Fan, J., R. Zhang, G. Li, W.-K. Tao, and X. Li (2007), Simulations of cumulus clouds using a spectral microphysics cloud-resolving model, *Journal of Geophysical Research–Atmospheres*, *112*(D4), doi:10.1029/2006JD007688.

Ferron, G. A., and S. C. Soderholm (1990), Estimation of the times for evaporation of pure water droplets and for stabilization of salt solution particles, *Journal of Aerosol Science*, *21*(3), 415–429.

Fitzgerald, J. W. (1972), A study of the initial phase of cloud droplet growth by condensation, Ph.D. thesis, University of Chicago.

Freud, E., D. Rosenfeld, M. O. Andreae, A. A. Costa, and P. Artaxo (2005), Robust relations between CCN and the vertical evolution of cloud drop size distribution in deep convective clouds, *Atmospheric Chemistry and Physics Discussions*, *5*(5), 10,155–10,195.

Fromm, M., A. Tupper, D. Rosenfeld, R. Servranckx, and R. McRae (2006), Violent pyro-convective storm devastates Australia's capital and pollutes the stratosphere, *Geophysical Research Letters*, *33*(5).

Fukuta, N., and L. A. Walter (1970), Kinetics of hydrometeor growth from a vapor-spherical model, *Journal of Atmospheric Sciences*, *27*(8), 1160–1172.

Gillani, N. V., S. E. Schwartz, W. R. Leaitch, J. W. Strapp, and G. A. Isaac (1995), Field observations in continental stratiform clouds: Partitioning of cloud particles between droplets and unactivated interstitial aerosols, *Journal of Geophysical Research – Atmospheres*, *100*(18), 687–718.

Gorbunov, B., and R. Hamilton (1997), Water nucleation on aerosol particles containing both soluble and insoluble substances, *Journal of Aerosol Science*, *28*(2), 239–248.

Gorbunov, B., R. Hamilton, N. Clegg, and R. Toumi (1998), Water nucleation on aerosol particles containing both organic and soluble inorganic substances, *Atmospheric Research*, *47*, 271–283.

Graham, N. E., J. Michaelsen, and T. P. Barnett (1987), An investigation of the El-Nino-Southern Oscillation cycle with statistical models 2. Model results, *Journal of Geophysical Research–Oceans*, *92*(C13), 14,251–14,270.

Guan, H., S. G. Cober, and G. A. Isaac (2001), Verification of supercooled cloud water forecasts with in-situ aircraft measurements, *Weather and Forecasting*, *16*(1), 145–155.

Guan, H., S. G. Cober, G. A. Isaac, A. Tremblay, and A. Mthot (2002), Comparison of three cloud forecast schemes with in-situ aircraft measurements, *Weather and Forecasting*, *17*(6), 1226–1235.

Gunn, R., and B. B. Phillips (1957), An Experimental Investigation of the Effect of Air Pollution On the Initiation of Rain, *Journal of Meteorology*, *14*(3), 272–280.

Heymsfield, A. J., and G. M. McFarquhar (2001), Microphysics of INDOEX clean and polluted trade cumulus clouds, *Journal of Geophysical Research–Atmospheres*, *106*, 28.

Heymsfield, A. J., L. M. Miloshevich, C. Schmitt, A. Bansemer, C. Twohy, M. R. Poellot, A. Fridlind, and H. Gerber (2005), Homogeneous ice nucleation in subtropical and tropical convection and its influence on cirrus anvil microphysics, *Journal of the Atmospheric Sciences*, *62*(1), 41–64.

Heymsfield, A. J., A. Bansemer, G. Heymsfield, and A. O. Fierro (2009), Microphysics of Maritime Tropical Convective Updrafts at Temperatures from 20 to 60, *Journal of the Atmospheric Sciences*, *66*(12), 3530, doi:10.1175/2009JAS3107.1.

Hobbs, P. V., L. F. Radke, and S. E. Shumway (1970), Cloud condensation nuclei from industrial sources and their apparent influence on precipitation in Washington State, *Journal of the Atmospheric Sciences*, *27*(1), 81–89.

Houghton, J. T., Y. Ding, D. J. Griggs, M. Noguer, P. J. V. der Linden, X. Dai, K. Maskell, and C. A. Johnson (2001), IPCC, 2001: Climate Change 2001: The Scientific Basis. Contribution of Working Group I to the Third Assessment Report of the Intergovernmental Panel on Climate Change, *Cambridge, United Kingdom, New York, USA, Cambridge University Press*, *881*, 9.

Houze, R. (1993), *Cloud Dynamics*, Academic Press, San Diego.

Jacobson, M. Z. (1999), *Fundamentals of Atmospheric Modeling*, 676 pp., Cambridge University Press.

Jiang, H., and G. Feingold (2006), Effect of aerosol on warm convective clouds: Aerosol-cloud-surface flux feedbacks in a new coupled large eddy model, *Journal of Geophysical Research – Atmospheres*, *111*(D1), D01,202.

K., L., and C. Chang (1987), *Monsoon Meteorology*, 544–580 pp., Clarendon Press, London, England, Chap:Planetary scale aspects of the winter monsoon and atmospheric teleconnections.

Khain, A., A. Pokrovsky, M. Pinsky, A. Seifert, and V. Phillips (2004), Simulation of effects of atmospheric aerosols on deep turbulent convective clouds using a spectral microphysics mixed-phase cumulus cloud model. Part II: Sensitivity study, *Journal of the Atmospheric Sciences*, *61*(24), 2963–2982.

Khain, A., D. Rosenfeld, and A. Pokrovsky (2005), Aerosol impact on the dynamics and microphysics of deep convective clouds, *Quarterly Journal of the Royal Meteorological Society*, *131*(611, Part A), 2639–2663, doi:10.1256/qj.04.62.

Klaassen, G., and T. Clark (1985), Dynamics of the cloud-environment interface and entrainment in small cumuli: Two-dimensional simulations in the absence of ambient shear, *Journal of the Atmospheric Sciences*, *42*(23), 2621–2642.

Klemp, J. B., and R. B. Wilhelmson (1978), The simulation of three-dimensional convective storm dynamics, *Journal of the Atmospheric Sciences*, *35*(6), 1070–1096.

Knight, C. A. (1982), The Cooperative Convective Precipitation Experiment (CCOPE), 18 May-7 August 1981, *Bulletin of the American Meteorological Society*, *63*(4), 386–398.

Koren, I., Y. Kaufman, D. Rosenfeld, L. Remer, and Y. Rudich (2005), Aerosol invigoration and restructuring of Atlantic convective clouds, *Geophysical Research Letters*, *32*(14), doi:10.1029/2005GL023187.

Koren, I., O. Altaratz, G. Feingold, Z. Levin, and T. Reisin (2009), Cloud's Center of Gravity - a compact approach to analyze convective cloud development, *Atmospheric Chemistry and Physics*, *9*(1), 155–161.

Koziol, A. S., and H. G. Leighton (1996), The effect of turbulence on the collision rates of small cloud drops, *Journal of the Atmospheric Sciences*, *53*(13), 1910–1920.

Kulmala, M., P. Korhonen, T. Vesala, H. Hansson, K. Noone, and B. Svenningsson (1996), The effect of hygroscopicity on cloud droplet formation, *Tellus Series B-Chemical and Physical Meteorology*, *48*(3), 347–360.

Kumar, A., J. Dudhia, R. Rotunno, D. Niyogi, and U. C. Mohanty (2008), Analysis of the 26 July 2005 heavy rain event over Mumbai, India using the Weather Research and Forecasting (WRF) model, *Quarterly Journal of the Royal Meteorological Society*, *134*(636).

Kusik, C. L., and H. P. Meissner (1978), Electrolyte activity coefficients in inorganic processing, in *Fundamental Aspects of Hydrometallurgical Processesn Proc. Conf.n, Chicago, Ill., U. S. A, Nov.-Dec. 1976(AIChE Symposium Series,*, vol. 74, pp. 14–20.

Langmuir, I. (1918), The Evaporation of Small Spheres, *Physical Review*, *12*(5), 368–370, doi:10.1103/PhysRev.12.368.

Lauer, A., and J. Hendricks (2006), Simulating aerosol microphysics with the ECHAM/MADE GCMPart II: Results from a first multiannual integration, *Atmospheric Chemistry and Physics Discussions*, *6*(4), 7519–7562.

Leaitch, W. R., G. A. Isaac, J. W. Strapp, C. M. Banic, and H. A. Wiebe (1992), The relationship between cloud droplet number concentrations and anthropogenic pollution: Observations and climatic implications, *Journal of Geophysical Research–Atmospheres*, *97*, 2463–2474.

Levin, Z., and W. R. Cotton (2008), *Aerosol pollution impact on precipitation: A scientific Review*, Springer Verlag.

Li, Z., and B. C. Lu (2001), Surface tension of aqueous electrolyte solutions at high concentrations-representation and prediction, *Chemical Engineering Science*, *56*(8), 2879–2888.

Lin, J. C., T. Matsui, R. A. P. Sr, and C. Kummerow (2006), Effects of biomass burning-derived aerosols on precipitation and clouds in the Amazon Basin: a satellite-based empirical study, *Journal of Geophysical Research – Atmospheres*, *111*.

Liu, Y., and P. H. Daum (2002), Anthropogenic aerosols: Indirect warming effect from dispersion forcing, *Nature*, *419*(6907), 580–581, doi:10.1038/419580a.

Lohmann, U., and J. Feichter (2005), Global indirect aerosol effects: a review, *Atmospheric Chemistry and Physics*, *5*(5), 715–737.

Lu, M. L., and J. H. Seinfeld (2006), Effect of aerosol number concentration on cloud droplet dispersion: A large-eddy simulation study and implications for aerosol indirect forcing, *Journal of Geophysical Research-Atmospheres*, *111*(D2), D02,207.

Mason, B. J. (1971), *The physics of clouds*, Clarendon Press.

Maxwell, J. C. (1990), *The Scientific Letters and Papers of James Clerk Maxwell: Volume 1, 1846-1862*, Cambridge University Press.

McFarquhar, G. M., and A. J. Heymsfield (2001), Parameterizations of INDOEX microphysical measurements and calculations of cloud susceptibility- Applications for climate studies, *Journal of Geophysical Research–Atmospheres*, *106*, 28.

McFiggans, G., P. Artaxo, U. Baltensperger, H. Coe, M. C. Facchini, G. Feingold, S. Fuzzi, M. Gysel, A. Laaksonen, U. Lohmann, et al. (2005), The effect of physical and chemical aerosol properties on warm cloud droplet activation, *Atmospheric Chemistry and Physics Discussions*, *5*(5), 8507–8647.

Miller, M. J., and A. J. Thorpe (1981), Radiation conditions for the lateral boundaries of limited-area numerical models, *Quarterly Journal of the Royal Meteorological Society*, *107*, 615–628.

Nenes, A., and J. Seinfeld (2003), Parameterization of cloud droplet formation in global climate models, *Journal of Geophysical Research–Atmospheres*, *108*(D14), doi:10.1029/2002JD002911.

Nenes, A., S. Ghan, H. Abdul-Razzak, P. Y. Chuang, and J. H. Seinfeld (2001), Kinetic limitations on cloud droplet formation and impact on cloud albedo, *Tellus B*, *53*(2), 133–149.

O'Dowd, C., J. Lowe, M. Smith, and A. Kaye (1999), The relative importance of non-sea-salt sulphate and sea-salt aerosol to the marine cloud condensation nuclei population: An improved multi-component aerosol-cloud droplet parametrization, *Quarterly Journal of the Royal Meteorological Society*, *125*(556, Part B), 1295–1313.

Pinsky, M., and A. Khain (1997a), Formation of inhomogeneity in drop concentration induced by the inertia of drops falling in a turbulent flow, and the influence of the inhomogeneity on the drop spectrum broadening, *Quarterly Journal of the Royal Meteorological Society*, *123*(537), 165–186.

Pinsky, M. B., and A. P. Khain (1997b), Turbulence effects on droplet growth and size distribution in clouds: a review, *Journal of Aerosol Science*, *28*(7), 1177i–1214.

Pitter, R. L., and H. R. Pruppacher (1974), A numerical investigation of collision efficiencies of simple ice plates colliding with supercooled water drops, *Journal of the Atmospheric Sciences*, *31*(2), 551–559.

Pruppacher, H. R., and J. D. Klett (1998), *Microphysics of Clouds and Precipitation : Second Revised and Enlarged Edition with an Introduction to Cloud Chemistry and Cloud Electricity*, Kluwer, Dordrecht [u.a.].

Ramanathan, V., P. Crutzen, J. Lelieveld, A. Mitra, D. Althausen, J. Anderson, M. Andreae, W. Cantrell, G. Cass, C. Chung, A. Clarke, J. Coakley, W. Collins, W. Conant, F. Dulac, J. Heintzenberg, A. Heymsfield, B. Holben, S. Howell, J. Hudson, A. Jayaraman, J. Kiehl, T. Krishnamurti, D. Lubin, G. McFarquhar, T. No-

vakov, J. Ogren, I. Podgorny, K. Prather, K. Priestley, J. Prospero, P. Quinn, K. Rajeev, P. Rasch, S. Rupert, R. Sadourny, S. Satheesh, G. Shaw, P. Sheridan, and F. Valero (2001), Indian Ocean Experiment: An integrated analysis of the climate forcing and effects of the great Indo-Asian haze, *Journal of Geophysical Research–Atmospheres*, *106*(D22), 28,371–28,398.

Resch, T. J. (1995), A framework for the modeling of suspended multicomponent particle systems with applications to atmospheric aerosols, Ph.D. thesis, Massachusetts Institute of Technology.

Research Aviation Facility, NCAR-Earth Observing Laboratory (2002), Project Documentation Summary:1999-102 INDOEX, EC-130Q Hercules, http://www.eol.ucar.edu/raf/Projects/INDOEX/, Last accessed: January 22, 2010.

Reynolds, R. W., and T. M. Smith (1994), Improved global sea surface temperature analyses using optimum interpolation, *Journal of Climate*, *7*(6), 929–948.

Robinson, R. A., and R. H. Stokes (1970), Electrolyte Solutions., *Butterworth, London,*, pp. 222–260.

Rogers, R., and M. K. Yau (1989), *A Short Course in Cloud Physics*, Pergamon Press, New York.

Rosenfeld, D. (1999), TRMM observed first direct evidence of smoke from forest fires inhibiting rainfall, *Geophysical Research Letters*, *26*(20), 3105–3108.

Rosenfeld, D., and I. M. Lensky (1998), Satellitebased insights into precipitation formation processes in continental and maritime convective clouds, *Bulletin of the American Meteorological Society*, *79*(11), 2457–2476.

Rosenfeld, D., and W. L. Woodley (2000), Deep convective clouds with sustained supercooled liquid water down to -37.5° C, *Nature*, *405*(6785), 440–442.

Rosenfeld, D., Y. Rudich, and R. Lahav (2001), Desert dust suppressing precipitation: A possible desertification feedback loop, *Proceedings of the National Academy of Sciences*, *98*(11), 5975.

Rosenfeld, D., R. Lahav, A. Khain, and M. Pinsky (2002), The role of sea spray in cleansing air pollution over ocean via cloud processes, *Science*, *297*(5587), 1667.

Rosenfeld, D., U. Lohmann, G. B. Raga, C. D. O'Dowd, M. Kulmala, S. Fuzzi, A. Reissell, and M. O. Andreae (2008), Flood or drought: How do aerosols affect precipitation?, *Science*, *321*(5894), 1309.

Rudich, Y., O. Khersonsky, and D. Rosenfeld (2002), Treating clouds with a grain of salt, *Geophysical Research Letters*, *29*(22), 2060.

Rudich, Y., A. Sagi, and D. Rosenfeld (2003), Influence of the Kuwait oil fires plume (1991) on the microphysical development of clouds, *Journal of Geophysical Research – Atmospheres*, *108*, 4478.

Schumacher, C., and R. A. Houze (2003), Stratiform rain in the Tropics as seen by the TRMM precipitation radar, *Journal of Climate*, *16*(11), 1739–1756.

Seinfeld (1999), IGAC - Measurements and Modeling of Atmospheric Methane Using Stable Carbon Isotopes, http://www.igac.noaa.gov/newsletter/17/cloud.php, Last accessed: Dec 22, 2009.

Seinfeld, J. H., and S. N. Pandis (1998), *Atmospheric Chemistry and Physics*, Wiley.

Shiino, J. (1983), Evolution of raindrops in an axisymmetric cumulus model .1. Comparison of the parameterized with nonparameterized microphysics, *Journal of the Meteorological Society of Japan*, *61*(4), 629–655.

Silverman, B. A. (2003), A Critical Assessment of Hygroscopic Seeding of Convective Clouds for Rainfall Enhancement, *Bulletin of the American Meteorological Society*, *84*(9), 1219, doi:10.1175/BAMS-84-9-1219.

Silverman, B. A., M. Glass, and W. Sukarnjanaset (1996), On the seeding of tropical convective clouds for rain augmentation, in *13th Conf. on Planned and Inadvertent Weather Modification, Atlanta, GA, American Meteorological Society*, pp. 52–59.

Squires, P. (1958), The microstructure and colloidal stability of warm clouds, *Tellus*, *10*, 256–271.

Squires, P., and T. Twomey (1961), The relation between cloud drop numbers and the spectrum of cloud nuclei, *Physics of Precipitation, Monograph*, *5*, 211–219.

Srivastava, R. C. (1978), Parameterization of raindrop size distributions, *Journal of the Atmospheric Sciences*, *35*(1), 108–117.

Steele, H. (2004), Investigations of Cloud Altering Effects of Atmospheric Aerosols using a New Mixed Eulerian-Lagrangian Aerosol Model, Ph.D. thesis, Massachusetts Institute of Technology.

Taylor, J. P., and A. McHaffie (1994), Measurements of cloud susceptibility, *Journal of the Atmospheric Sciences*, *51*(10), 1298–1306.

Teller, A., and Z. Levin (2006), The effects of aerosols on precipitation and dimensions of subtropical clouds: a sensitivity study using a numerical cloud model, *Atmospheric Chemistry and Physics*, *6*(1), 67–80.

Tester, J. W., and M. Modell (1997), *Thermodynamics and its applications*, 936 pp., Prentice Hall PTR.

Tripoli, G. J., and W. R. Cotton (1981), The use of ice-liquid water potential temperature as a thermodynamic variable in deep atmospheric models, *Monthly Weather Review*, *109*(5), 1094–1102.

Twomey, S. (1959), The nuclei of natural cloud formation Part I: The chemical diffusion method and its application to atmospheric nuclei, *Pure and Applied Geophysics*, *43*(1), 227–242.

Twomey, S. (1977), The influence of pollution on the shortwave albedo of clouds, *Journal of the atmospheric sciences*, *34*(7), 1149–1152.

Twomey, S., and J. Warner (1967), Comparison of measurements of cloud droplets and cloud nuclei, *Journal of the Atmospheric Sciences*, *24*(6), 702–703.

Twomey, S., and T. A. Wojciechowski (1969), Observations of the geographical variation of cloud nuclei, *Journal of the Atmospheric Sciences*, *26*(4), 648–651.

Vaidya, S. S., and J. R. Kulkarni (2007), Simulation of heavy precipitation over Santacruz, Mumbai on 26 July 2005, using Mesoscale model, *Meteorology and Atmospheric Physics*, *98*(1), 55–66.

Vaillancourt, P. A., A. Tremblay, S. G. Cober, and G. A. Isaac (2003), Comparison of aircraft observations with mixed-phase cloud simulations, *Monthly Weather Review*, *131*(4), 656–671.

van den Heever, S. C., and W. R. Cotton (2007), Urban aerosol impacts on downwind convective storms, *Journal of Applied Meteorology and Climatology*, *46*(6), 828–850.

Verver, G. H. L., D. R. Sikka, J. M. Lobert, G. Stossmeister, and M. Zachariasse (2001), Overview of the meteorological conditions and atmospheric transport processes during INDOEX 1999, *Journal of Geophysical Research-Atmospheres*, *106*(D22).

Wang, C. (2004), A modeling study on the climate impacts of black carbon aerosols, *Journal of Geophysical Research – Atmospheres*, *109*(D03106).

Wang, C. (2005), A modeling study of the response of tropical deep convection to the increase of cloud condensation nuclei concentration: 1. Dynamics and microphysics, *Journal of Geophysical Research-Atmospheres*, *110*(D21), D21,211.

Wang, C., and J. S. Chang (1993), A Three-Dimensional Numerical Model of Cloud Dynamics, Microphysics, and Chemistry 1. Concepts and Formulation, *Journal of Geophysical Research–Atmospheres*, *98*(D8).

Wang, C., and R. G. Prinn (1998), Impact of the horizontal wind profile on the convective transport of chemical species, *Journal of Geophysical Research–Atmospheres*, *103*(D17).

Wang, C., and R. G. Prinn (2003), On the roles of deep convective clouds in tropospheric chemistry, *Journal of Geophysical Research–Atmospheres*, *105*(D17).

Warner, J. (1968), A Reduction in Rainfall Associated with Smoke from Sugar-Cane FiresAn Inadvertent Weather Modification?, *Journal of Applied Meteorology*, *7*(2), 247–251.

Warner, J., and S. Twomey (1967), The production of cloud nuclei by cane fires and the effect on cloud droplet concentration, *Journal of the Atmospheric Sciences*, *24*(6), 704–706.

Wilks, D. (2006), *Statistical Methods in the Atmospheric Sciences*, 2nd ed. ed., Academic Press, Burlington MA, USA.

Yin, Y., Z. Levin, T. G. Reisin, and S. Tzivion (2001), On the response of radar-derived properties to hygroscopic flare seeding, *Journal of Applied Meteorology*, *40*(9), 1654–1661.